

Institut für Erd- und Umweltwissenschaften, Universität Potsdam
Arbeitsgruppe “Paläohydrologie”
und
DFG Graduiertenkolleg 1364/1

Holocene Variations in the Strength of the Indian Monsoon System: A Combined Biomarker and Stable Isotope Approach

Kumulative Dissertation
zur Erlangung des akademischen Grades
“doctor rerum naturalium”
(Dr. rer. nat.)
in der Wissenschaftsdisziplin “Paläoklimatologie”

eingereicht an der
Mathematisch-Naturwissenschaftlichen Fakultät
der Universität Potsdam

von
Saswati Sarkar

Potsdam, 26. August 2014

Published online at the
Institutional Repository of the University of Potsdam:
URN urn:nbn:de:kobv:517-opus4-74905
<http://nbn-resolving.de/urn:nbn:de:kobv:517-opus4-74905>

Abstract

The monsoon is an important component of the Earth's climate system. It played a vital role in the development and sustenance of the largely agro-based economy in India. A better understanding of past variations in the Indian Summer Monsoon (ISM) is necessary to assess its nature under global warming scenarios. Instead, our knowledge of spatiotemporal patterns of past ISM strength, as inferred from proxy records, is limited due to the lack of high-resolution paleo-hydrological records from the core monsoon domain.

In this thesis I aim to improve our understanding of Holocene ISM variability from the core 'monsoon zone' (CMZ) in India. To achieve this goal, I tried to understand modern and thereafter reconstruct Holocene monsoonal hydrology, by studying surface sediments and a high-resolution sedimentary record from the saline-alkaline Lonar crater lake, central India. My approach relies on analyzing stable carbon and hydrogen isotope ratios from sedimentary lipid biomarkers to track past hydrological changes.

In order to evaluate the relationship of the modern ecosystem and hydrology of the lake I studied the distribution of lipid biomarkers in the modern ecosystem and compared it to lake surface sediments. The major plants from dry deciduous mixed forest type produced a greater amount of leaf wax *n*-alkanes and a greater fraction of *n*-C₃₁ and *n*-C₃₃ alkanes relative to *n*-C₂₇ and *n*-C₂₉. Relatively high average chain length (ACL) values (29.6–32.8) for these plants seem common for vegetation from an arid and warm climate. Additionally I found that human influence and subsequent nutrient supply result in increased lake primary productivity, leading to an unusually high concentration of tetrahymanol, a biomarker for salinity and water column stratification, in the nearshore sediments. Due to this inhomogeneous deposition of tetrahymanol in modern sediments, I hypothesize that lake level fluctuation may potentially affect aquatic lipid biomarker distributions in lacustrine sediments, in addition to source changes.

I reconstructed centennial-scale hydrological variability associated with changes in the intensity of the ISM based on a record of leaf wax and aquatic biomarkers and their stable carbon ($\delta^{13}\text{C}$) and hydrogen (δD) isotopic composition from a 10 m long sediment core from the lake. I identified three main periods of distinct hydrology over the Holocene in central India. The period between 10.1 and 6 cal. ka BP was likely the wettest during the Holocene. Lower ACL index values (29.4 to 28.6) of leaf wax *n*-alkanes and their negative $\delta^{13}\text{C}$ values (–34.8‰ to –27.8‰) indicated the dominance of woody C₃ vegetation in the catchment, and negative $\delta\text{D}_{\text{wax}}$ (average for leaf wax *n*-alkanes) values (–171‰ to –147‰) argue for a wet period due to an intensified monsoon. After 6 cal. ka BP, a gradual shift to less negative $\delta^{13}\text{C}$ values (particularly for the grass derived *n*-C₃₁) and appearance of the triterpene lipid tetrahymanol, generally considered as a marker for salinity and water column stratification, marked the onset of drier conditions. At 5.1 cal. ka BP increasing flux of leaf wax *n*-alkanes along with the highest flux of tetrahymanol indicated proximity of the lakeshore to the center due to a major lake level decrease. Rapid fluctuations in abundance of both terrestrial and aquatic biomarkers between 4.8 and 4 cal. ka BP indicated an unstable lake ecosystem, culminating in a transition to arid conditions. A pronounced shift to less negative $\delta^{13}\text{C}$ values, in particular for *n*-C₃₁ (–25.2‰ to –22.8‰), over this

period indicated a change of dominant vegetation to C₄ grasses. Along with a 40‰ increase in leaf wax *n*-alkane δD values, which likely resulted from less rainfall and/or higher plant evapotranspiration, I interpret this period to reflect the driest conditions in the region during the last 10.1 ka. This transition led to protracted late Holocene arid conditions and the establishment of a permanently saline lake. This is supported by the high abundance of tetrahymanol. A late Holocene peak of cyanobacterial biomarker input at 1.3 cal. ka BP might represent an event of lake eutrophication, possibly due to human impact and the onset of cattle/livestock farming in the catchment.

The most intriguing feature of the mid-Holocene driest period was the high amplitude and rapid fluctuations in δD_{wax} values, probably due to a change in the moisture source and/or precipitation seasonality. I hypothesize that orbital induced weakening of the summer solar insolation and associated reorganization of the general atmospheric circulation were responsible for an unstable hydroclimate in the mid-Holocene in the CMZ.

My findings shed light onto the sequence of changes during mean state changes of the monsoonal system, once an insolation driven threshold has been passed, and show that small changes in solar insolation can be associated to major environmental changes and large fluctuations in moisture source, a scenario that may be relevant with respect to future changes in the ISM system.

Zusammenfassung

Der Monsun ist ein wichtiger Bestandteil des Klimasystems der Erde. Er spielte in der Entwicklung und im Lebensunterhalt der weitgehend agrarisch geprägten Wirtschaft in Indien eine wesentliche Rolle. Ein besseres Verständnis von vergangenen Schwankungen im Indischen Sommermonsun (ISM) ist notwendig, um dessen Wesen unter dem Einfluss globaler Erwärmungsszenarien zu bewerten. Stattdessen ist unser Wissen über räumlich-zeitliche Muster der vergangenen ISM Intensität, wie sie aus Proxydaten abgeleitet wird, aufgrund des Mangels an hochauflösenden paläohydrologischen Datensätzen aus der Kernmonsunregion sehr eingeschränkt.

In dieser Arbeit versuche ich unser Verständnis über die ISM Variabilität im Holozän in der Kernmonsunregion in Indien zu verbessern. Um dieses Ziel zu erreichen habe ich versucht, zunächst die rezente und danach die holozäne monsunale Hydrologie durch das Studium von Oberflächensedimenten und eines hochaufgelösten Sedimentkerns aus dem salzhaltigen-alkalischen Lonar Kratersee, Zentralindien zu verstehen. Mein Ansatz stützt sich auf der Analyse stabiler Wasserstoff- und Kohlenstoffisotopenverhältnisse von sedimentären Lipid Biomarkern, um vergangene hydrologische Veränderungen zu verfolgen.

Um die Beziehung des modernen Ökosystems mit der Hydrologie des Sees zu bewerten, untersuchte ich die Verteilung von Lipid Biomarkern im rezenten Ökosystem und verglich sie mit den Oberflächensedimenten des Sees. Die bedeutendsten Pflanzen aus dem trockenen Laubmischwaldtyp erzeugten eine größere Menge an Blattwachs *n*-Alkanen und einen größeren Anteil von *n*-C₃₁ und *n*-C₃₃ Alkanen im Verhältnis zu *n*-C₂₇ und *n*-C₂₉. Die relativ hohen durchschnittlichen Werte der Kettenlängen (29.6–32.8) für diese Pflanzen scheinen für die Vegetation in einem ariden und warmen Klima weit verbreitet zu sein. Zusätzlich fand ich heraus, dass der menschliche Einfluss und eine nachfolgende Nährstoffzufuhr zu einer Erhöhung der Primärproduktion im See führen, die in einer ungewöhnlich hohen Konzentration von Tetrahymanol, einem Biomarker für Salzgehalt und Schichtung der Wassersäule, in den Sedimenten des Uferbereichs resultiert. Aufgrund dieser inhomogenen Ablagerung von Tetrahymanol in rezenten Sedimenten vermute ich, dass Seespiegelschwankungen möglicherweise aquatische Lipid Biomarker Verteilungen in limnischen Sedimenten, zusätzlich zu Änderungen in deren Herkunft, potentiell beeinflussen.

Ich habe die hundertjährig-lange hydrologische Variabilität, die mit Veränderungen in der Intensität des ISM verbunden ist, auf der Basis von Blattwachs Lipid Biomarkern und ihrer stabilen Kohlenstoff- ($\delta^{13}\text{C}$) und Wasserstoffisotopenzusammensetzung (δD) ausgehend von einem 10 m langen Sedimentkern aus dem See rekonstruiert. Ich habe drei Hauptphasen von signifikanter Hydrologie im Holozän in Zentralindien identifiziert. Die Periode zwischen 10.1 und 6 cal. ka BP war wahrscheinlich die feuchteste während des Holozäns. Geringere durchschnittliche Kettenlängen Indexwerte (29.4 bis 28.6) von Blattwachs *n*-Alkanen und ihre negativen $\delta^{13}\text{C}$ Werte (–34.8‰ bis –27.8‰) wiesen auf die Dominanz von holziger C₃ Vegetation im Einzugsgebiet hin, und negative $\delta\text{D}_{\text{wax}}$ (Durchschnitt für Blattwachs *n*-Alkane) Werte (–171‰ bis –147‰) stehen für eine feuchte Periode in Verbindung mit einem verstärkten Monsun. Nach 6 cal. ka BP führte eine allmähliche Verschiebung zu weniger

negativen $\delta^{13}\text{C}$ Werten (insbesondere für Gras abgeleitete $n\text{-C}_{31}$) und das Vorkommen von Triterpen Lipid Tetrahymanol, allgemein als Indikator für Salzgehalt und Wassersäulenstratifizierung verwendet, zum Beginn von trockeneren Bedingungen. Um 5.1 cal. ka BP deutete ein erhöhter Fluss von Blattwachs n -Alkanen in Zusammenhang mit dem höchsten Fluss von Tetrahymanol auf eine bedeutende Absenkung des Seeufers durch den Rückgang im Seespiegel. Rasche Schwankungen in der Menge von terrestrischen und aquatischen Biomarkern zwischen 4.8 und 4 cal. ka BP wiesen auf ein instabiles Seeökosystem hin, das in einem Übergang zu ariden Bedingungen kulminiert. Eine bedeutende Verschiebung zu weniger negativen $\delta^{13}\text{C}$ Werten in dieser Periode, insbesondere für $n\text{-C}_{31}$ (-25.2% bis -22.8%), zeigte einen Wandel in der dominanten Vegetation hin zu C_4 Gräsern. Zusammen mit einem 40% Anstieg in den δD Werten der Blattwachs n -Alkane, der wahrscheinlich von weniger Niederschlag und/oder höherer Evapotranspiration der Pflanzen ausgelöst wurde, interpretiere ich diese Periode als die trockenste der letzten 10.1 ka. Dieser Übergang führte zu lang anhaltenden spätholozänen ariden Bedingungen und zur Ausbildung eines dauerhaften salzhaltigen Sees. Dies wird durch ein hohes Vorkommen von Tetrahymanol unterstützt. Ein spätholozäner Höchstwert in der Zufuhr blaualgenhaltiger Biomarker um 1.3 cal. ka BP könnte ein Ereignis der Eutrophierung des Sees darstellen, wahrscheinlich in Verbindung mit dem menschlichen Einfluss und dem Beginn der Rinder- und Viehzucht im Einzugsgebiet.

Die faszinierendsten Merkmale der trockensten Periode im mittleren Holozän waren die hohe Amplitude und rasche Fluktuationen in den $\delta\text{D}_{\text{wax}}$ Werten, wahrscheinlich in Verbindung mit einer Veränderung in der Herkunft der Feuchtigkeit und/oder Saisonalität im Niederschlag. Ich vermute, dass eine orbital induzierte Abschwächung der sommerlichen Solarstrahlung und eine damit verbundene Umstellung der allgemeinen atmosphärischen Zirkulation für ein instabiles Hydroklima im mittleren Holozän in der Kernmonsunregion verantwortlich waren. Meine Ergebnisse liefern den Aufschluss über die Abfolge von Veränderungen während der mittleren Zustandsänderungen des Monsunsystems, sobald ein einstrahlungsgetriebener Schwellenwert überschritten ist, und sie zeigen, dass kleine Änderungen in der solaren Einstrahlung mit markanten Umweltveränderungen und großen Schwankungen in der Herkunft der Feuchtigkeit einhergehen, ein Szenario, das in Bezug zu zukünftigen Veränderungen des ISM Systems relevant sein könnte.

Contents

Abstract	i
Zusammenfassung	iii
Acknowledgements	ix
1. Introduction	1
1.1 Climate over the Indian subcontinent: Monsoon and its significance	1
1.2 Monsoon: temporal variability and forcing	2
1.2.1 Tectonic time-scale (10^6 – 10^7 years)	2
1.2.2 Orbital time-scale (10^4 – 10^5 years)	3
1.2.3 Sub-orbital time-scale (10^3 years and less)	3
1.3 Holocene ISM variability	5
1.4 The stable isotopic composition of lipid biomarkers and their use as paleohydrological proxy	7
1.4.1 Factors controlling the stable isotopic composition of water in hydrological cycle	7
1.4.2 Factors controlling the stable isotopic composition in lipid biomarkers	8
1.5 Precipitation characteristics of the study region	11
1.6 Scope of this study	12
1.7 Summary	14
2. Methods	17
2.1 Sample preparation, extraction and SPE fractionation	18
2.2 Gas chromatographic-mass spectrometric (GC-MS) analysis of lipid biomarkers	18
2.3 Compound-specific stable isotope analysis	18
2.3.1 Compound-specific $\delta^{13}\text{C}$ analysis	18
2.3.2 Compound-specific δD analysis	19
3. Spatial heterogeneity of lipid biomarker distributions in the catchment and sediments of a crater lake in central India (own contribution: 80%)	21
3.1 Introduction	22
3.2 Materials and methods	24
3.2.1 Study site, modern environment and hydrology	24
3.2.2 Vegetation mapping and field sampling	25
3.2.2.1 Modern vegetation mapping	25

3.2.2.2	Modern vegetation	26
3.2.2.3	Aquatic plants	26
3.2.2.4	Floating mat and water	26
3.2.2.5	Surface sediments and benthic mats	26
3.2.3	Sample preparation, biomarker identification and quantification	26
3.3	Results	27
3.3.1	Terrigenous biomarkers	27
3.3.1.1	Abundance and distribution of leaf wax <i>n</i> -alkanes in modern vegetation	27
3.3.1.2	Abundance and distribution of leaf wax <i>n</i> -alkanes in lake surface sediments	28
3.3.2	Aquatic biomarkers	28
3.3.2.1	Abundance and distribution of biomarkers in floating and benthic bacterial mats and particulate OM (POM)	28
3.3.2.2	Abundance and distribution of aquatic biomarkers in lake surface sediments	29
3.4	Discussion	32
3.4.1	Terrestrial biomarkers	32
3.4.1.1	Factors influencing biomarker composition in higher terrigenous plants	32
3.4.1.2	Spatial patterns of leaf wax <i>n</i> -alkane abundances in sediments as a consequence of soil erosion	33
3.4.1.3	Spatial patterns of leaf wax <i>n</i> -alkane distributions in sediments as a consequence of distinct plant sources?	34
3.4.1.4	Integration of leaf wax <i>n</i> -alkane abundance and distribution in the deepest part of the lake	35
3.4.2	Aquatic biomarkers	35
3.4.2.1	Bacterial and ciliate communities as the major source of aquatic biomarkers in the lake sediments	35
3.4.2.2	Spatial patterns of aquatic biomarker abundance in sediments reflect nutrient supply	36
3.4.3	General implications for paleolimnological studies	36
3.5	Conclusions	37
3.6	Acknowledgements	38
4.	Monsoon source shifts during the drying mid-Holocene: biomarker isotope based evidence from the core ‘monsoon zone’ (CMZ) of India	39
	<i>(own contribution: 80%)</i>	
4.1	Introduction	40
4.1.1	Organic geochemical proxies as indicators of paleoclimate changes	42

	4.1.1.1	Biomarkers	42
	4.1.1.2	Carbon and hydrogen isotopes	43
	4.1.2	Study site, modern hydrology and vegetation	43
4.2		Material and methods	44
	4.2.1	Sediment core and age model	44
	4.2.2	Sample preparation and lipid biomarker analysis	44
	4.2.3	Compound-specific stable carbon and hydrogen isotope analysis	45
	4.2.4	Precipitation, isotope data and backward trajectory analysis	46
	4.2.5	Pollen analysis	46
4.3		Results	46
	4.3.1	Higher terrestrial plant biomarkers	46
	4.3.1.1	Abundance and distribution of leaf wax <i>n</i> -alkanes in the core	46
	4.3.1.2	Stable carbon isotopic composition ($\delta^{13}\text{C}$) of long chain <i>n</i> -alkanes in the core	47
	4.3.1.3	Stable hydrogen isotopic composition (δD) of long chain <i>n</i> -alkanes in the core	47
	4.3.2	Aquatic biomarkers	49
	4.3.2.1	Abundance of aquatic biomarkers in the core	49
	4.3.2.2	Stable carbon isotope composition ($\delta^{13}\text{C}$) of aquatic biomarkers in the core	49
	4.3.2.3	Stable hydrogen isotope composition (δD) of aquatic biomarkers in the core	50
4.4		Discussion	50
	4.4.1	Environmental sensitivities of stable isotope based proxies	50
	4.4.1.1	$\delta^{13}\text{C}$ values of leaf wax <i>n</i> -alkanes as an indicator of vegetation type and aridity	50
	4.4.1.2	δD values of leaf wax <i>n</i> -alkanes as indicator of P-E balance	50
	4.4.1.3	Variations in $\delta^{13}\text{C}$ values of aquatic biomarkers as a consequence of changes in lake water salinity	51
	4.4.1.4	Variations in δD values of aquatic biomarkers as consequence of change in lake water hydrology	51
	4.4.2	Holocene climate (lake level) changes from biomarkers and their stable isotopes	52
	4.4.2.1	The early Holocene period between 10.1 and 6 cal. ka BP	52
	4.4.2.2	The mid-Holocene period between 6 and 4 cal. ka BP	52
	4.4.2.2.1	Monsoon source shifts during the drying mid-Holocene	54
	4.4.2.3	The late Holocene period from 4 cal. ka BP onwards	56
4.5		Conclusions	57
4.6		Acknowledgements	58

5. Prolonged monsoon droughts and links to Indo-Pacific warm pool: A Holocene record from Lonar Lake, central India	59
<i>(own contribution: 30%)</i>	
5.1 Introduction	60
5.1.1 Study area	61
5.1.1.1 Geology	61
5.1.1.2 Modern climate, hydrology, and hydrochemistry	61
5.1.1.3 Modern vegetation	61
5.2 Sample collection and methodology	62
5.2.1 Coring, documentation and correlation	62
5.2.2 Thin section preparation	63
5.2.3 Chronology	63
5.2.4 Isotope analyses	63
5.2.5 XRF core scanning	64
5.2.6 Lipid biomarker and stable isotope ($\delta^{13}\text{C}$) analysis	64
5.2.7 Pollen analysis	64
5.3 Results	65
5.3.1 Chronology	65
5.3.2 Lithology and evaporitic mineralogy	65
5.3.3 Geochemistry, isotope, and biomarker studies	66
5.3.4 Pollen	67
5.4 Discussion	67
5.4.1 Environmental sensitivity of Lonar core proxies	67
5.4.2 Holocene proxy variability and climate reconstruction	70
5.4.3 Possible climate-culture link?	72
5.4.4 Regional correlation	72
5.4.5 What could have caused the prolonged droughts?	73
5.5 Conclusions	76
5.6 Acknowledgements	76
 6. Future perspectives	 77
 Appendices	 79
 References	 84
 List of Figures and Tables	 106
 List of Publications	 109
 Curriculum Vitae	 110
 Selbstständigkeitserklärung	 114

Acknowledgements

Herewith I would like to thank everyone, who supported me in different stages of my PhD and thus contributed immensely to the successful completion of this dissertation.

This study has been done in the Institute of Earth and Environmental Science at the University of Potsdam within the framework of the DFG Graduate School 1364/1 “The interaction between climate, tectonics and biosphere in the African-Asian monsoon region”, University of Potsdam.

First of all, I would like to thank very much my supervisors Dr. Dirk Sachse, especially Dr. Sushma Prasad, Prof. Dr. Heinz Wilkes, Prof. Dr. Achim Brauer and Prof. Dr. Manfred Strecker for their caring supervision and permanent support throughout my PhD years. I have benefited very much from their work experiences.

Further I would like to acknowledge the financial support I received from the DFG funded Graduate School. In this regard, I want to convey special thanks to Prof. Dr. Manfred Strecker for giving me this academic opportunity to carry out my PhD in Germany and also for supporting my several visits to fieldwork, workshops and conferences to different destinations. I am grateful to the coordinators of the Graduate School Dr. Andreas Bergner and Dr. Henry Wichura for their help in dealing with the administration. I would also like to thank my fellow PhD students from the Graduate School for their friendship (especially Dr. Franziska Wilke and Dr. Lidia Olaka) and providing a stimulating academic environment (Dr. Kathleen Stoof-Leichsenring and Dr. Anoop Ambili).

My sincere thanks also go to my colleagues from the Institute of Earth and Environmental Science, University of Potsdam (Dr. Lidia Romero-Viana, Dr. Yannick Garcin, Antje Musiol, Daniel Vollmer, and Tanja Klaka-Tauscher) and from the Helmholtz Centre Potsdam – German Research Centre for Geosciences (GFZ), especially to Andrea Vieth-Hillebrand, Michael Gabriel, Anke Kaminsky, Cornelia Karger and Sylvia Pinkerneil for helping me in the laboratory work.

I would like to extend my thanks to my colleagues from the Senckenberg Research Institute, Research Station of Quaternary Palaeontology Weimar, from the Indian Institute of Geomagnetism Mumbai (IIGM) and from the University of Hamburg for their encouragement, insightful comments and fruitful scientific discussions, which helped me a lot in developing my scientific ideas. In particular, I am grateful to Dr. Nathani Basavaiah and Dr. K. Deenadayalan from IIGM for their support in various occasions.

Finally I owe my loving thanks to my mother Mrs. Sujala Sarkar and my father Mr. Ajit Kumar Sarkar as well as to my sister Subhasri. I express my thanks to my husband Stefan and his mother Angela Polanski. Without their constant support and encouragement it would have been impossible for me to finish this work. My special gratitude is also due to all my German and Indian friends in Potsdam for enriching my PhD time.

1. Introduction

1.1 Climate over the Indian subcontinent: Monsoon and its significance

The monsoon, a tropospheric low-level wind circulation, is a characteristic climatic feature within the Tropics (Clift and Plumb, 2008) including the Indian subcontinent (Gadgil, 2003). According to the traditional view, this wind system is generated due to large-scale pressure gradients that result from the land-sea thermal contrast (Webster et al., 1998). The alternative hypothesis considers that seasonal changes in maximum insolation and related shifts in the position of the Intertropical Convergence Zone (ITCZ) lead to the reversal of wind directions and thus the word ‘monsoon’ (arabic: ‘mausim’ = season) was used for this wind system (Gadgil, 2003). The monsoon in Asia is the strongest monsoon system of the world, and can be divided into two strongly non-linear interacting subsystems: the East Asian monsoon and the Indian (South Asian) monsoon (P. Wang et al., 2005). The meteorological consequences of the monsoon, leading to rainfall seasonality, directly affect the livelihood of more than 2.5 billion people especially on the Indian subcontinent.

In the summer months of June to September (JJAS) a low-pressure cell is located over the Tibetan Plateau and the ITCZ migrates northwards over the Indian landmass (Fleitmann et al., 2007). Simultaneously high solar radiation over the cloud free subtropical oceans (e.g., over the Indian Ocean basins: Arabian Sea and Bay of Bengal) results in strong convection of moist air leading to vertical ascent of warm water vapour. The water vapour is then transported towards the continents within the near surface, cross-equatorial southwesterly (SW) winds, due to strong pressure gradient between the Tibetan Plateau and Southern Indian Ocean (Fleitmann et al., 2007). Due to different factors such as coastal convergence and orographic uplifting of the moisture, intensive and prevailing rainfall events occur especially over Western Ghats, northeastern India and southern slopes of Himalayas (Fig. 1.1a). During the winter months from December to February (DJF) surface winds are mainly northeasterly (NE) that bring predominantly cold and dry continental air from the interior of Asia originating from the persistent Siberian High. In addition, mid-latitude cyclones steered by the Westerlies can have a major impact mainly on the arid regions of northwestern India (Fig. 1.1b; Prasad and Enzel, 2006).

The most important feature in the meteorology of India is the seasonal rainfall associated with the SW or summer monsoon wind (Gadgil, 2003). Summer monsoon rainfall (ISM: Indian summer monsoon, as used throughout this work) was and still is largely responsible for the development and sustenance of the large agro-based economy in the subcontinent (Gadgil et al., 2005). Thus, knowledge of the timing and magnitude of past variations of monsoonal rainfall is essential to better understand forcing mechanisms and to predict its response to anthropogenic climate change (Anoop et al., 2013a). Apparent changes in the frequency and magnitude of extreme events (such as floods and droughts) (Goswami et al., 2006a; Malik et al.,

2012) and their spatial inhomogeneity in recent decades (Ghosh et al., 2011) have raised concerns about the predictability of regional monsoonal precipitation and its impact on society. Longer, high-resolution paleoclimate records are crucial for understanding monsoon variability over longer timescales (Berkelhammer et al., 2010).

In this thesis I aim to understand modern and thereafter Holocene monsoonal hydrology, by studying a sedimentary record from the saline-alkaline Lonar crater lake, central India. My approach relies on reconstructing stable water isotope ratios from sedimentary proxy data to track past hydrological changes.

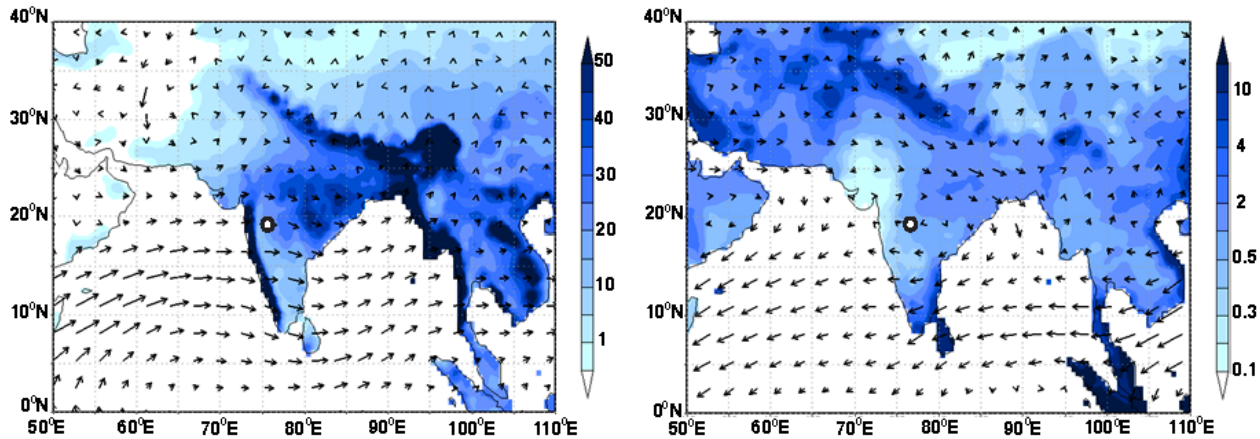


Fig. 1.1. Climatological land surface rainfall for GPCP5^a data set (Becker et al., 2013) from 1901–2009 (mm/day; shaded colours) and lower tropospheric wind vectors at 850 hPa for ERA-Interim reanalysis data set (Dee et al., 2011) from 1989–2011 for summer (JJAS^b) (left) and winter (DJF^c) (right) monsoon. White circles mark the location of Lonar Lake.

^aGlobal Precipitation Climatology Centre Version 5, gridded rainfall reanalysis data set based on monthly global land surface stations (0.5°×0.5° spatial resolution)

^bJune-July-August-September; ^cDecember-January-February

1.2 Monsoon: temporal variability and forcing

Temporal variability of the monsoon can occur over tectonic, orbital and sub-orbital timescales (P. Wang et al., 2005). Assessment of past monsoon variability depends on suitable proxies, which can be related to either monsoon winds (e.g., direction, strength etc.) or monsoonal precipitation. In the following I review the current state of knowledge on past monsoonal variability with a focus on the ISM over these timescales and the possible forcing mechanisms.

1.2.1 Tectonic time-scale (10^6 – 10^7 years)

The longest timescale of monsoon variability is related to the evolution of the monsoon itself forced by tectonically controlled geographic and topographic changes (P. Wang et al., 2005).

Himalayan-Tibetan plateau uplift is the tectonic factor most widely discussed for Asian monsoon evolution. In General Circulation Model (GCM) experiments

orographic features with elevations of at least 50% of today in the Tibet-Himalayan region were necessary for the monsoonal patterns to be induced by solar forcing (Prell and Kutzbach, 1992). Records of monsoon upwelling in Arabian Sea (Prell et al., 1992), dating of faults on Tibetan Plateau uplift/extension (Molnar et al., 1993) as well as modeling studies indicated that intensified uplift of the Tibetan Plateau around 8 Ma was responsible for enhanced aridity in the Asian interior and onset of the Asian monsoon (Prell and Kutzbach, 1997; An et al., 2001). However with subsequent studies, our knowledge of age and the evolution of the monsoon systems remain still deficient and more of long term records are needed (P. Wang et al., 2005).

1.2.2 Orbital time-scale (10^4 – 10^5 years)

Orbital-scale monsoon variability seems mainly to be driven by two primary forcing factors: 1. orbital induced variations in insolation (external) and 2. changes in global ice volume (internal). Analysis of orbital-scale monsoon variability, mainly for the Indian monsoon system, started with the studies on long marine core(s) with proxies as *G. bulloides* from Arabian Sea (Prell, 1984a, b). The author found that within the precession band, summer-monsoon maxima was in phase with $\delta^{18}\text{O}$ minima and lagged northern hemisphere (NH) summer insolation maxima by ca. 5.5 ka, due to the influence of terrestrial ice sheets on albedo and sensible heating over Asia. Solar radiation, modified by albedo feedbacks, is responsible for heating of the continent and therefore creation of the pressure gradient between Asia and the Indian Ocean. More studies on proxy records and modeling followed to understand the relationships between monsoon strength, NH insolation and glacial boundary conditions (Prell and Van Campo, 1986; Prell and Kutzbach 1987). In order to remove the influences of non-monsoon processes from multi-proxy studies had been initiated (Clemens et al., 1991), that found monsoon sharing different variances in precession and obliquity bands. It can be summarized, from the subsequent studies that in addition to glacial boundary conditions monsoon strength can also be influenced by ocean-atmospheric interactions.

1.2.3 Sub-orbital time-scale (10^3 years and less)

Variability on sub-millennial timescales in the monsoonal system was detected as a result of studies on high-resolution archives such as varved marine sediments, ice-cores, speleothems etc. (Schulz et al., 1998; Thompson et al., 2000; Fleitmann et al., 2003). Additionally, the teleconnections to high latitude climate forcings can be studied by comparison of such reconstructions with the Arctic, Antarctic and Greenland ice core records (Gupta et al., 2003; Y. J. Wang et al., 2005). The role of external drivers (e.g., solar flux variability), internal feedbacks among climate components or teleconnections is an active part of current monsoon research (P. Wang et al., 2005).

ISM variability on Dansgaard-Oeschger (DO) timescales (~ 1500 years) during last glaciation was identified from proxy data of marine sediment records from the

Arabian Sea and the Bay of Bengal (Sirocko et al., 1993, 1996; Schulz et al., 1998; Kudrass et al., 2001). These records identified intensified summer monsoons during interstadials, and increased winter monsoons during stadials.

Climate teleconnections such as to North Atlantic SSTs (sea surface temperature) have also been found to influence the ISM variability on interannual to millennial timescales with warm (cold) phases in the North Atlantic linked to increased (reduced) precipitation on the Indian subcontinent (Gupta et al., 2003; Fleitmann et al., 2003; Zhang and Delworth, 2006; Rajeevan and Sridhar, 2008). The teleconnection between North Atlantic and the ISM is hypothesized to be operating through changes in the meridional temperature gradient across the Indian subcontinent, and the subsequent shift in the position of the ITCZ and changes in the intensity of the ISM (Goswami et al., 2006b; Li et al., 2008).

Wintertime snow cover over Eurasia and the Himalaya was found to influence the ISM (Shukla and Mintz, 1982). Since snow cover can affect the thermal contrast between land and ocean by altering surface albedo and the moisture content, stronger (weaker) winter seasons over the Eurasian and Himalayan region tend to be followed by less (more) than average summer monsoon rainfall over India (Dash et al., 2005; Mamgain et al., 2010).

Many studies have identified external factors such as solar flux variability as a driver for small-scale variability of the ISM (Neff et al., 2001; Agnihotri et al., 2002; Burns et al., 2002; Fleitmann et al., 2003). Changes in solar flux influence the vertical temperature gradient in the Tropics leading to enhanced convection in the oceans and an intensified monsoon (Kodera, 2004). Alternatively changes in solar radiation can affect the monsoon through changes in Hadley circulation or El Niño-Southern Oscillation (ENSO) (Haigh, 1996). A combination of both mechanisms (Meehl et al., 2009) has also been suggested for how solar flux variability influences ISM (Berkelhammer et al., 2010).

Among the recurring climate modes with similar periodicities as the ISM, the ENSO phenomenon has received considerable attention. ENSO seems to be linked to ISM variability on inter-annual and also multidecadal timescales (Krishna Kumar et al., 1999; Wang and An, 2002). Instrumental data indicate that a significant reduction (increase) of ISM rainfall and subsequent drought conditions over India are frequently accompanied by an El Niño (La Niña) event over the Pacific due to a shift in the zonal Walker circulation (Goswami, 2005; Ummenhofer et al., 2011). However recent studies reveal the weakening of this inverse relationship between ENSO and ISM rainfall in recent decades (Krishna Kumar et al., 2006).

Similar to SST anomalies over the North Atlantic (AMO: Atlantic Multidecadal Oscillation) or the Pacific Oceans (e.g., ENSO), an inter-annual mode of variability in Indian Ocean SSTs, the Indian Ocean Dipole (IOD) (Saji et al., 1999), can also influence the ISM (Ashok et al., 2004). A positive (negative) mode of IOD is characterized by higher SSTs and precipitation in the western (eastern) Indian Ocean (Krishnan et al., 2011).

The relationship among these different monsoon drivers is still poorly understood. For example the role of ENSO modifying the effect of solar flux variability or the impact of North Atlantic SSTs on the ISM as well as the combined effect of ENSO

and IOD on the ISM (Ashok et al., 2004) is still under discussion.

The intraseasonal ISM variability (from 3–7 days, 10–20 days and 30–60 days) is characterized by intermittent periods of enhanced and deficient precipitation known as “active” and “break” spells respectively (Gadgil, 2003). A “break” like situation is evoked due to intrusion of cold and dry northwesterly (NW) winds from the mid-latitudes and subtropical regions of west-central Asia into the northwestern India (Krishnan and Sugi, 2001). Advection of cold and dry NW winds into the monsoon region leads to abnormal tropospheric cooling, reduces the meridional temperature gradient and therefore weakens the monsoon convective activity. During break cycles large amount of rainfall occur over the central-eastern parts of the Himalayan foothills and a decrease in rainfall in central India (Vellore et al., 2014). Recent studies found that the monsoon can be ‘locked’ with persistent active/break domination over longer timescales as well (Sinha et al., 2011).

1.3 Holocene ISM variability

Paleoclimate studies on Holocene ISM variability from terrestrial as well as marine archives are summarized here. In general, as found in many Arabian Sea marine records and also in terrestrial records from the peripheral domain, ISM started to intensify in the early Holocene (~11–8 cal. ka BP), following increasing temperature in the NH (Sirocko et al., 1993; Overpeck et al., 1996; Jung et al., 2002; Fleitmann et al., 2003; Ivanochko et al., 2005). It is broadly accepted that the monsoonal maximum lagged behind the insolation maximum due to glacial boundary conditions in the NH (Fleitmann et al., 2007; Y. Wang et al., 2010). After the initial phase of intensification, ISM strength weakened. However the nature of the ISM weakening during Holocene is one of the questions that is still under discussion. There remained two contrasting hypotheses regarding the nature of the ISM weakening during Holocene: 1. abrupt weakening of the ISM at ~5–4.5 cal. ka BP 2. gradual weakening of the ISM following the decrease of NH summer insolation (Fleitmann et al., 2007).

The marine records from eastern Arabian Sea showed an opposite trend i.e increase in the monsoon strength during Holocene, as reflected from decreasing salinity/ increased freshwater input at the southern tip of India or increasing P-E balance (Sarkar et al., 2000; Govil and Naidu, 2010) compared to records from western Arabian Sea (Gupta et al., 2003; Fleitmann et al., 2003) and Bay of Bengal marine (Govil and Naidu, 2011) and continental (Berkelhammer et al., 2012) records. This inconsistency among the records points to the variability on regional scale in the temporal development of the ISM over the Holocene.

In addition to the millennial scale changes in the ISM intensity the higher frequency changes in ISM strength during Holocene are linked to solar flux variability or NH temperature changes (Gupta et al., 2003; Fleitmann et al., 2003). A Sr isotope record from a marine core in the Arabian Sea off Somalia reported an unstable transitional period from 8.5 to 6 cal. ka BP, characterized by decadal-scale high-amplitude variations in the evaporation/precipitation balance over the horn of Africa (Jung et al., 2004).

The majority of paleomonsoon reconstruction in India was carried out on lacustrine sediments and lake level studies from northwestern India (Singh et al., 1974; Bryson and Swain, 1981; Wasson et al., 1984; Prasad et al., 1997; Enzel et al., 1999; Dixit et al., 2014). Centennial scale reconstructions of Holocene climate indicated wetter climate during the early and mid-Holocene with highest lake levels at ~7.2–6.0 cal. ka BP, likely as a consequence of more winter rains from the mid-latitude Westerlies, followed by the onset of aridity at ~5.3 cal. ka BP (Prasad and Enzel, 2006).

Recent records from northwestern Himalaya allow us for the assessment of climate variability from the region, receiving precipitation from both the ISM and Westerlies (Demske et al., 2009; Anoop et al., 2013a). In northwestern Himalaya palynological core studies from Tso Kar Lake (Demske et al., 2009) showed a strong ISM period (~11–9 cal. ka BP) followed by a weaker epoch and cooler climate (~9–8 cal. ka BP). A drier interval (~8.7–8.1 cal. ka BP), characterized by reduced hill slope erosion, river discharge, and sediment load has been reported from the Sutlej valley in the northwestern Himalaya (Bookhagen et al., 2006). The reconstruction from Spiti paleolake sediments indicated weaker ISM with cooler conditions during ~7.6–6.8 cal. ka BP (Anoop et al., 2013a) while the Tso Kar record indicated weaker ISM with moderate Westerlies during the same period (Demske et al., 2009). The period (~6.8–6.1 cal. ka BP) in the Spiti region was characterized by warmer climate with intensified ISM, also supported from record from Tso Kar basin (Demske et al., 2009).

Periods of intensified monsoon during the Holocene have been identified from the formation of landslide-dammed lakes in the Sutlej valley region (Bookhagen et al., 2005). Additionally several phases of century-long weak ISM phases during the Holocene have been associated with the formation of fluvial terraces through enhanced incision (Bookhagen et al., 2006).

In northeastern India a pollen record from a swamp from the lower Brahmaputra flood plain of Assam indicated relatively warmer and wetter conditions until 8.3 cal. ka BP (Dixit and Bera, 2012). A speleothem stable isotope record from northeastern India showed abrupt shift (decadal scale) towards century-long drier conditions at ~4 cal. ka BP (Berkelhammer et al., 2012).

Compared to other locations paleoclimate records from central India are scarce. Pollen based reconstructions on centennial scale from a central Indian lake indicated enhanced monsoon and warmer condition between 7.1–4.6 cal. ka BP that was followed by weakening monsoon (Quamar and Chauhan, 2012). A marine record from Bay of Bengal, representing regional climate variability in the Godavari catchment reported a humid early Holocene climate, followed by a gradual increase in aridity-adapted vegetation until 1.7 cal. ka BP and prominent after 4 cal. ka BP (Ponton et al., 2012).

In summary, our knowledge of spatiotemporal patterns of past monsoon strength over the subcontinent remains incomplete, since no high-resolution continuous Holocene record from continental India exists. There remained inhomogeneity on regional scale in the temporal development (over the Holocene) of the ISM but the general trends were similar (except in eastern Arabian Sea) with a significant

decrease in ISM strength in mid-Holocene and protracted arid conditions during the late Holocene (4 ca. BP onwards). Most importantly, the question about the nature of the ISM weakening is still under discussion (i.e., abrupt (at ~5–4.5 cal. ka BP) vs. gradual).

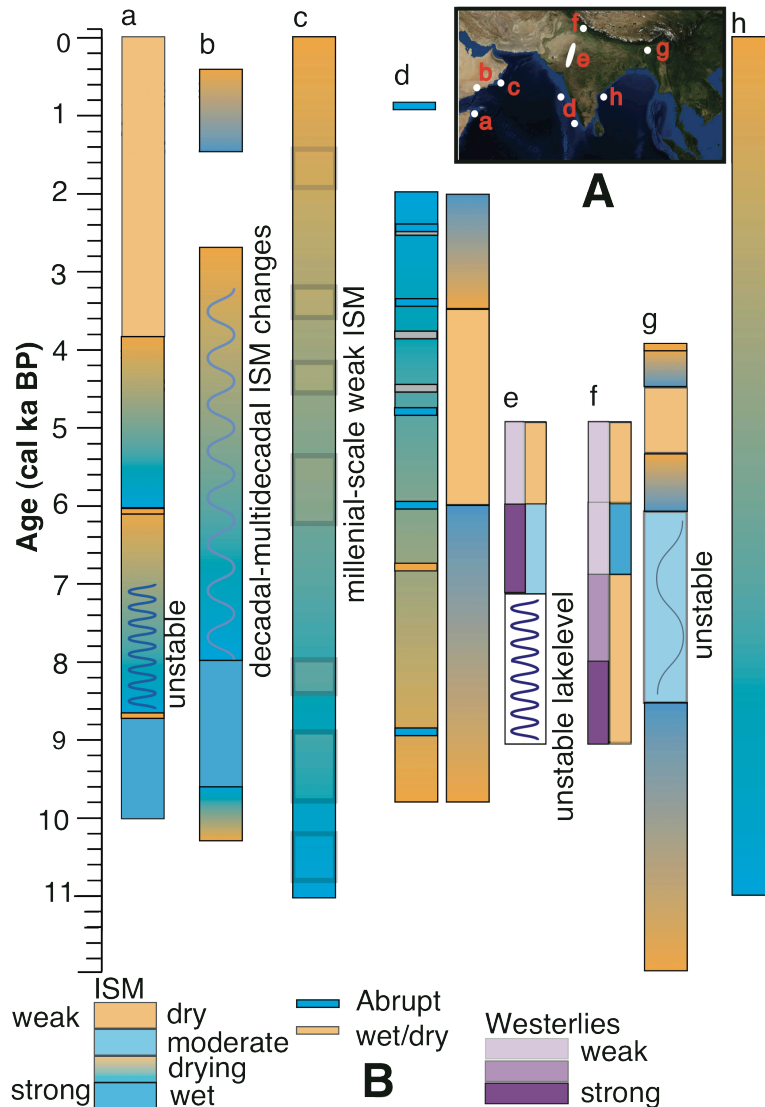


Fig. 1.2. Compilation of Holocene ISM variability from ISM domain. A: Locations of the records, B: Records: a. Jung et al., 2004; b. Gupta et al., 2003; c. Fleitmann et al., 2003; d. Sarkar et al., 2000; e. Prasad and Enzel, 2006; f. Demske et al., 2009; g. Berkelhammer et al., 2012; h. Ponton et al., 2012.

1.4 The stable isotopic composition of lipid biomarkers and their use as paleohydrological proxy

1.4.1 Factors controlling the stable isotopic composition of water in hydrological cycle

The stable isotopic composition of oxygen and hydrogen in water ($\delta^{18}\text{O}$ and δD

values^d) within the hydrological cycle and its spatial distribution has become a powerful tracer for identifying fluxes within the hydrological cycle, and in particular the sources and transport pathways of moisture (Bowen, 2010; Sachse et al., 2012).

Variations in the oxygen and hydrogen isotopic composition of meteoric waters can be explained partly by Rayleigh-type processes during evaporation and condensation (Craig, 1961; Gat, 1996). Briefly, water vapour evaporated from seawater is depleted in the heavy water isotopes due to higher vapour pressure of lighter isotopologues ($^1\text{H}_2^{16}\text{O}$). Heavier isotopologues ($^1\text{H}^{16}\text{O}$) tend to accumulate in liquid than in vapour phase. Therefore precipitation, due to condensation of vapour, is enriched in heavier isotopes relative to the vapour, leaving the remaining vapour depleted in heavier isotopes.

Factors controlling evaporation-condensation and therefore temporal and spatial patterns of stable isotopes in precipitation can result in continental, temperature and amount effects (Dansgaard, 1964). The continental effect would result in the depletion of water isotopes in precipitation, in inland of continents, due to progressive rain out from air masses moving from ocean over the continents. The temperature effect is particularly prominent across regions of strong temperature variability such as polar regions, since isotopic fractionation between vapour and condensate is temperature-dependent. The temperature effect would result in progressive depletion of water isotopes in precipitation with decreasing temperature. In tropical regions a negative correlation was found between isotopes in precipitation and rainfall amount, known as the amount effect. Amount effect is characterized by progressive depletion of water isotopes in precipitation with increasing amount of precipitation. Several physical factors such as convection intensity and cloud height, drop-size of rainfall and re-evaporation of raindrops etc. leading to amount effect have been discussed (Breitenbach et al., 2010). However, the mechanisms behind the amount effect are not completely understood (Kurita et al., 2009; Dayem et al., 2010).

A distinct empirical relationship between $\delta^{18}\text{O}$ and δD in precipitation is observed, known as Global Meteoric Water Line (GMWL, $\delta\text{D} = 8 \times \delta^{18}\text{O} + 10$, $r^2 > 0.95$), first established for fresh surface waters and then for precipitation itself (Craig, 1961; Rozanski et al., 1993). This is due to the fact that the oxygen and hydrogen stable isotopes in water molecules are intimately associated. Since some effects such as moisture recycling or evaporation can cause deviation, a Local Meteoric Water Line (LMWL) better describes rainwater isotopes of a location. Valuable information about the hydrology over a region can be derived from comparison of rainwater isotopes data with the GMWL.

^d(Isotopic composition is expressed as δ (in per mil), $\delta = (R_{\text{sample}} - R_{\text{standard}}) / R_{\text{standard}}$, where R is the ratio between heavier/rare and lighter/common isotopes. δ represents the relative deviation of R in the sample from a standard)

1.4.2 Factors controlling the stable isotopic composition in lipid biomarkers

The stable isotopic composition of meteoric waters from the geological past can be preserved in various archives (e.g., ice-cores, speleothems, tree rings, lake

sediments) (Thompson et al., 2000; Y.J. Wang et al., 2001; Jahren and Sternberg, 2003; Tierney et al., 2008). Among these archives mentioned above, sedimentary records from lakes have become common for studying past changes in terrestrial hydrology. Since bulk sediments from lake represent mixture of components (e.g., carbohydrates, amino acids, lipids etc.), use of elemental and isotopic composition of bulk sediments from lakes as robust proxies are limited (Krishnamurthy et al., 1995).

More recently lipid biomarkers from lake sediments have been analyzed to study terrestrial ecology and environmental change (Castañeda and Schouten, 2011). Lipids produced by all organisms, are ubiquitous in lake sediments and because of their relative stability can be preserved over geological timescales. Since different organisms produce different lipids, the presence of certain lipids in sediments can be used to identify their sources within a lake catchment. In addition to the information about sources of biomarkers the analysis of lipid biomarker distributions in lake sediments can provide insight into changes in lacustrine and catchment ecosystem and hydrology over time (Schwark et al., 2002; Romero-Viana et al., 2012). For example, long chain *n*-alkanes (with 27 to 35 carbon atoms) are produced as leaf wax constituents of terrestrial higher plants (Eglinton and Hamilton, 1967; Cranwell et al., 1987). Changes in the abundance of leaf wax compounds can be used mainly as proxies for transport of terrigenous organic matter (OM) to the lake (Meyers, 2003). However, factors such as surficial erosion in the catchment and vegetation cover may influence flux of leaf wax compounds in the sediments (Sarkar et al., 2014). For the aquatic component, compositional variations in aquatic lipids can be used to assess changes in the lake ecosystem. For example, variations in the abundance of the cyanobacterial biomarkers, such as *n*-heptadecane can be used as proxies for changes in primary productivity. The role of human influence and subsequent nutrient supply in changing lake primary productivity should be considered while assessing changes in lake environment from abundance of aquatic compounds.

Additionally the stable carbon and hydrogen isotopic composition of such biomarker compounds (expressed as $\delta^{13}\text{C}$ and δD values) have emerged as a powerful tool that can provide detailed insights into ecosystem and hydrological change (Castañeda and Schouten, 2011). Since stable carbon isotopic composition of leaf wax compounds clearly differ between C_3 and C_4 plants (Sinninghe Damsté et al., 2011) due to differences in carbon assimilation pathways (Eglinton and Eglinton, 2008), the $\delta^{13}\text{C}$ values of terrestrial biomarkers can provide information about changes in catchment vegetation (e.g., C_3/C_4 vegetation) (Feakins et al., 2005; Eglinton and Eglinton, 2008). C_4 vegetation has an ecological advantage under aridity, high temperature, and low atmospheric pCO_2 conditions over C_3 plants (Eglinton and Eglinton, 2008). Therefore, $\delta^{13}\text{C}$ records are often used as a proxy for aridity (Ponton et al., 2012). However, supply of leaf wax compounds (long chain *n*-alkanes) from different sources can affect $\delta^{13}\text{C}$ values in the sediments, which may not be associated with changes in the vegetation in the catchment. For example, long chain *n*-alkanes (with 27 to 35 carbon atoms) are produced as leaf wax constituents of terrestrial higher plants but also of emerged macrophytes growing in

the lake (Eglinton and Hamilton, 1967; Cranwell et al., 1987; Ficken et al., 2000; Gao et al., 2011). Significant input from emerged macrophytes can affect $\delta^{13}\text{C}$ values in the sediments (Douglas et al., 2012). Therefore an understanding of changes in source/vegetation with other proxies (e.g., pollen) can be useful for interpretation of $\delta^{13}\text{C}$ values in the sediments.

From $\delta^{13}\text{C}$ of aquatic biomarkers the carbon source of individual compounds and carbon cycling through the ecosystem can be assessed. The carbon isotopic composition ($\delta^{13}\text{C}$) of compounds from primary producers, such as cyanobacteria should reflect the carbon isotopic composition of dissolved inorganic carbon (DIC). Lake water DIC can become enriched in ^{13}C as a result of increased primary productivity in an aquatic system, as this would preferentially remove ^{12}C into biomass and thus enrich ^{13}C in the lake water DIC (Meyers, 2003). Another possible origin of the ^{13}C enriched carbon source for organisms producing *n*-heptadecane could be HCO_3^- ions in alkaline lakes that are characterized by less negative $\delta^{13}\text{C}$ values (Meyers, 2003). Therefore possibility of changes in lake water chemistry should be considered for interpretation of $\delta^{13}\text{C}$ values of aquatic compounds in the sediments.

Although relatively new, δD values of lipid biomarkers are increasingly applied as proxy to detect changes in paleohydrology, as the ultimate hydrogen source of any photosynthetic organism is environmental water. As such, δD values of terrestrial biomarkers can be used to detect changes in the processes that affect the isotopic composition of precipitation (see above), such as moisture source or rainfall amount. Recent researches have shown that leaf wax lipid δD values record evapotranspiration in soils (Smith and Freeman, 2006) and higher plants leaves (Kahmen et al., 2013a; Kahmen et al., 2013b). Additionally differences in photosynthetic pathways (C_3 and C_4) used by plants and plant functional types (such as trees, shrubs or grasses) can lead to distinct δD values among plants growing at the same location under the same climatic condition (Hou et al., 2007; Sachse et al., 2012). Therefore it is important to take possible changes in vegetation in to consideration while interpreting leaf wax lipid δD values, as indicator for hydrological changes.

δD values of biomarkers derived from aquatic organisms, such as in algae, in general also record the δD values of the water source used by the organism. δD values of lipids from aquatic organisms can be used to detect changes in the processes that affect the D/H fractionation between environmental and intracellular water, such as temperature, salinity or growth rate (Sachs, 2014). Culture and field experiments indicate that D/H fractionation (1) increases with increasing temperature, (2) decreases with increasing salinity, and (3) changes with changing N-controlled growth rate, differently for different lipids (acetogenic vs. isoprenoid) (Sachs, 2014). However not many studies are available on the role of growth-rate changes on δD values.

1.5 Precipitation characteristics of the study region

Currently no precipitation amount or isotope data are available to assess the precipitation characteristics in Lonar region. However, existing time series from adjacent region, such as Sagar (23°49'N, 78°45'E, 551 m a.s.l.), Madhya Pradesh (ca. 486 km NE of Lonar), allow for an estimation of the main factors controlling precipitation δD and $\delta^{18}O$ values in central India. Lonar is located in the border of the zone referred to as Central India (CI) (Hoyos and Webster, 2007) where oxygen isotopic variability in precipitation is characterized by the amount effect (Bhattacharya et al., 2003; Yadava et al., 2004; Kumar et al., 2010).

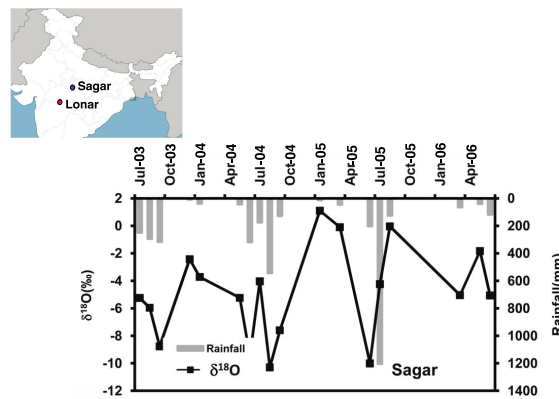


Fig. 1.3. Plot of $\delta^{18}O$ versus rainfall for Sagar, Madhya Pradesh (modified after Kumar et al., 2010).

The Lonar region receives precipitation mainly from the Arabian Sea (AS) branch of the monsoon. It is suggested that transport of moisture from the Bay of Bengal (BoB) can occur, with a longer transport pathway, during post monsoon (September; Sengupta and Sarkar, 2006). The contribution from the BoB branch of the monsoon, as possible for Lonar's central location in peninsular India, has not been assessed yet.

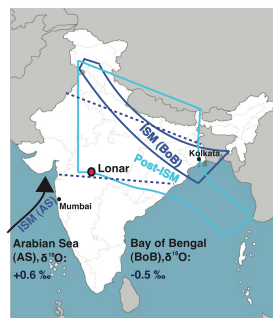


Fig. 1.4. Location of Lonar Lake (red circle) in the 'monsoon zone' (Gadgil, 2003) marked by the blue dashed line. Envelopes in dark and light blue represent storm-tracks from Bay of Bengal (BoB) in monsoon and post monsoon, respectively; the smaller arrow represents the Arabian Sea (AS) branch (modified after Sengupta and Sarkar, 2006). Modern seawater $\delta^{18}O$ values are indicated for Arabian Sea and Bay of Bengal (from Kumar et al., 2010).

In order to determine the moisture source areas for Lonar, an ensemble of backward air mass trajectories has been calculated using the Hybrid Single-Particle Lagrangian Integrated Trajectories (HYSPLIT) ARL trajectory tool database of NOAA (Draxler and Rolph, 2014). Trajectories for time periods of 96 h were computed at the lower troposphere (1500 m a.s.l.) for the pre monsoon, the monsoon (ISM), the post monsoon and the winter monsoon seasons of 2010 and 2013 respectively, with highest amount of rainfall in recent years. These trajectories show that winter monsoon and post monsoon air masses can reach Lonar from the BoB while ISM air masses, which bring 85% of annual precipitation (Sontakke et al., 2008) arrive mainly from AS (Fig. 1.5).

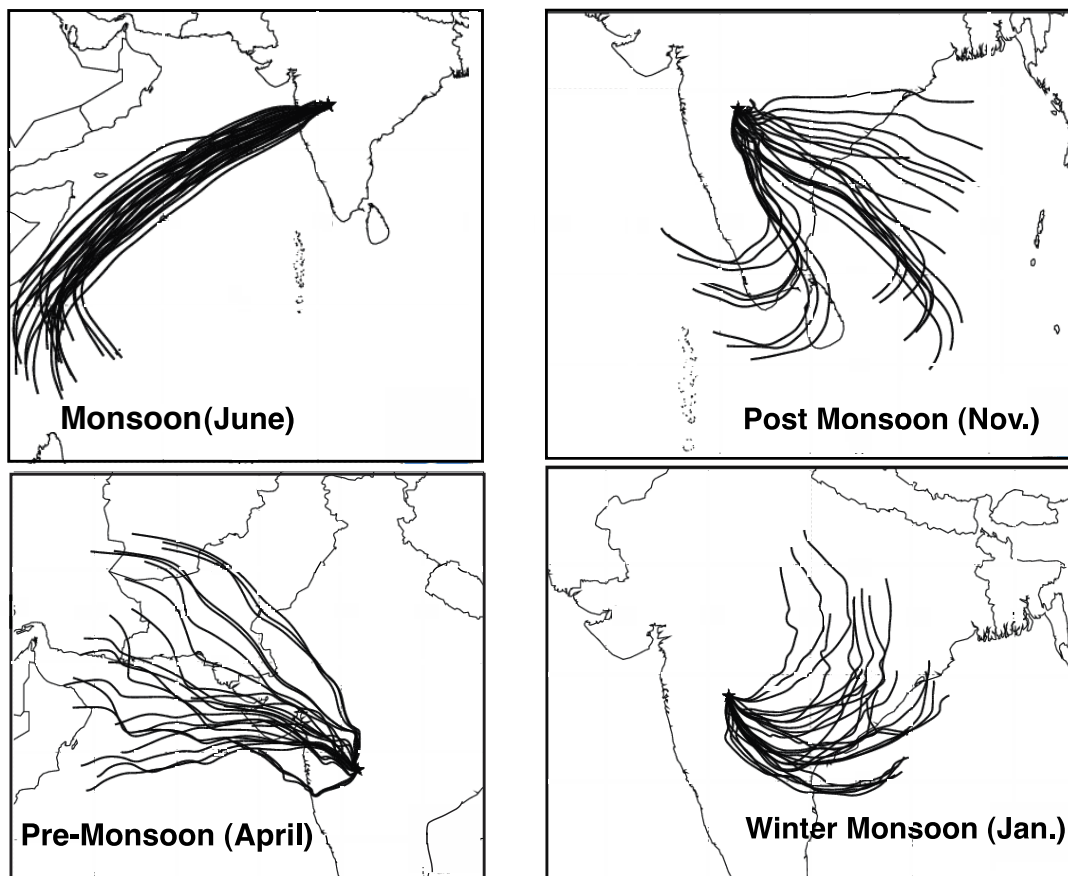


Fig. 1.5. Four day backwards trajectories for air parcels during selected rainfall events affecting Lonar (asterisk) during the monsoon (ISM, 11.6.13), post monsoon (11.11.10), pre monsoon (19.4.13) and winter monsoon (23.1.13) seasons, calculated using an ensemble (24 members) of the Air Resources Lab Hysplit Program, to represent moisture source for the region.

1.6 Scope of this study

Periods of increased monsoon wind strength inferred from marine records did not seem to always coincide with increased precipitation over nearby continental regions (Prasad and Enzel, 2006). Therefore, continental records of paleomonsoon are necessary to evaluate the nature of ISM on land. Further, high-resolution records

would be useful to understand the Holocene monsoon variability on timescales relevant to human societies and to identify the effect of human influence on the environment in the past. This can potentially help in modeling monsoon behaviour in a global warming scenario and better planning the land-use pattern in future. However, few high-resolution Holocene records from continental archives, such as speleothems exist, but these are not continuous and not from the core 'monsoon zone' (CMZ), (MZ: Gadgil, 2003).

Lonar Lake, from where the record studied in this thesis, is situated within the core Indian 'monsoon zone' (CMZ). There, variations in rainfall intensity show a strong correlation with the variations in Indian summer monsoon rainfall intensity as a whole (Gadgil, 2003). Thus a paleohydrological record from that region can be considered as representative for paleomonsoon variability.

There remained several open questions that needed to be addressed before the investigations on Lonar core sediments could be undertaken e.g., what are the biochemical properties of Lonar Lake surface sediments? Are they spatially heterogeneous? What are the controls behind biochemical properties in surface sediments and to what extent organic geochemical proxies represent the modern day ecosystem? Can the link between contemporary processes and biochemical properties of the sediments be identified to select sensitive proxies? Additionally the investigations on Lonar core sediment was undertaken to answer broad research questions. How did the ecosystem and hydrology changed due to change in monsoon strength on the continent during Holocene? What was the nature of this mid-Holocene transition on the continent?

In order to use lipid biomarker abundances and distributions as proxies for paleoenvironmental changes, I performed a detailed analysis of modern day conditions and tested the extent to which organic geochemical proxies represent the modern day ecosystem. Based on this study I attempt to assess the processes that control the distribution of leaf wax and aquatic biomarkers in modern surface sediments. High aquatic and bacterial productivity, and the detailed study about catchment vegetation in the modern lake sediments, helped me to better understand stable isotope and biomarker sources in the lake sediments. The potential of lipid biomarkers and their stable isotope ratios as suitable hydrological proxies, and Lonar Lake sediment as a suitable climate archive will be discussed in detail in this thesis. Then I attempt to document the change in hydrology and ecosystem of the lake and its catchment area over Holocene, as a response to climate (monsoon) change, by determining the change in biomarker concentration and their stable isotope composition (C, H).

Few marine as well as continental records, mainly from the peripheral areas of the ISM realm, have indicated a largely insolation driven, gradual transition from early Holocene wet to late Holocene arid conditions (Gupta et al., 2003; Fleitmann et al., 2003). The nature and the timing of the onset of this transition (abrupt or gradual) are still under discussion (Fleitmann et al., 2007). It was also suggested that the shift of mean latitudinal position of ITCZ (due to a change in insolation) over the Holocene was associated with significant changes in hydrological cycle (Fleitmann et al., 2007 and the references therein). However the associated changes

in continental hydrology and ecosystem changes were not studied. As such, it is difficult to evaluate the nature of this mid-Holocene transition on land.

The new high-resolution Holocene record from Lonar Lake, which is presented in this thesis, will shed light on the nature of this transition, along with its onset, in the core monsoon zone. In addition, the application of a combination of isotope proxies ($\delta^{13}\text{C}$ and δD) of terrestrial and aquatic biomarkers will deliver new insights into changes in the lake as well as the catchment environment along with the effect of human influence on the lake environment.

Specifically, the focuses of my study discussed in the following chapters were:

- (i) Methodology for lipid biomarker and stable isotope analysis of Lonar Lake sediment (chapter 2)
- (ii) Exploring the spatial variability of lipid biomarker distributions in the catchment and the sediments of Lonar Lake (chapter 3)
- (iii) Reconstructing changes in hydrology and monsoon over the Holocene from concentration as well as isotopic composition ($\delta^{13}\text{C}$, δD) of terrestrial and aquatic biomarkers (chapter 4)
- (iv) Comparison of results from lipid biomarker and isotope based reconstructions with other multi-proxy approaches (chapter 5)

1.7 Summary

My thesis comprises of three separate manuscripts dealing with the relationship of ecosystem and hydrology in modern times and a hydrological reconstruction for these relationships during the Holocene from Lonar Lake in the CMZ, India. The key findings from my thesis are summarized below.

Studies based on geochemical proxies, both from surface and core sediments, found Lonar Lake a sensitive continental archive for ‘monsoonal’ India (Anoop et al., 2013b; Menzel et al., 2013). In order to use lipid biomarker abundances and distributions as proxies for such changes, I performed a detailed analysis of modern day conditions and tested the extent to which organic geochemical proxies represent the modern day ecosystem. Additionally, I evaluated the spatial variability in lipid biomarker distributions in the surface sediments to estimate the fidelity of paleoenvironmental reconstruction based on a single long core.

Aquatic and terrestrial lipid biomarkers in modern lake surface sediments provided a detailed picture of the lake ecosystem and its catchment area. Terrestrial vegetation and lake surface sediments were characterized by relatively high average chain length (ACL) index values (29.6–32.8) of leaf wax *n*-alkanes, consistent with suggestions that plants in drier and warmer climates, as in Lonar today, produce longer chain alkyl lipids than plants in cooler and humid areas. The triterpene tetrahymanol, representative of a specific microbial community, occurred in unusually large amounts in surface sediment and benthic microbial mat samples. I concluded that increased primary productivity related to human influence caused these unusually high concentrations of tetrahymanol, especially in the nearshore lake sediments.

Results indicated that a single core from the depocentre of the lake best represents the average variability in terrigenous biomarkers in the lake basin. However, this study also showed that other factors, such as lake level fluctuation might affect the abundance of aquatic biomarkers such as tetrahymanol in a core from a central location within the lake, since this compound was found in higher concentrations in nearshore modern sediments. This should be taken into account for a valid paleolimnological interpretation of sediment core data.

Along with the understanding the modern ecosystem, I reconstructed centennial-scale hydrological variability associated with changes in the intensity of the ISM based on a record of lipid biomarkers (terrigenous and aquatic) and their stable carbon ($\delta^{13}\text{C}$) and hydrogen (δD) isotopic composition from a 10 m long sediment core from the lake. The period between 10.1 and 6 cal. ka BP was likely the wettest during the Holocene: lower ACL index values (29.4 to 28.6) of leaf wax *n*-alkanes and their negative $\delta^{13}\text{C}$ values (-34.8% to -27.8%) indicated the dominance of woody C_3 vegetation in the catchment, and negative $\delta\text{D}_{\text{wax}}$ values (-171% to -147%) argue for a wet period due to an intensified monsoon. After 6 cal. ka BP, a gradual shift to less negative $\delta^{13}\text{C}$ values for *n*-alkanes (particularly for the grass derived *n*- C_{31}) and appearance of the triterpene lipid tetrahymanol, generally considered as a marker for salinity and water column stratification, marked the onset of drier condition. At 5.1 cal. ka BP increasing flux of leaf wax *n*-alkanes along with the highest flux of tetrahymanol indicated proximity of the lakeshore to the lakecenter due to major lake level decrease. Rapid fluctuations in abundance of both terrestrial and aquatic biomarkers between 4.8 and 4 cal. ka BP indicated an unstable lake ecosystem, culminating in a transition to arid conditions. A pronounced shift to less negative *n*-alkane $\delta^{13}\text{C}$ values, in particular for *n*- C_{31} (-25.2% to -22.8%), over this period indicated a change of dominant vegetation to C_4 grasses. Along with a 40% increase in leaf wax *n*-alkane δD values, which likely resulted from less rainfall and/or higher plant evapotranspiration, we interpreted this period to reflect the driest conditions in the region during the last 10.1 ka. This transition led to protracted late Holocene arid conditions and a permanent saline lake. This is supported by the high abundance of tetrahymanol. A late Holocene peak of cyanobacterial biomarker input at 1.3 cal. ka BP might represent an event of lake eutrophication, possibly due to human impact and the onset of cattle/livestock farming in the catchment.

A unique feature of this record was the presence of a distinct transitional period between the wet early Holocene and the dry late Holocene. The mid-Holocene period was characterized by high amplitude and rapid fluctuations in $\delta\text{D}_{\text{wax}}$ values, probably due to a change in the moisture source and/or precipitation tracks. We suggest that the mid-Holocene weakening of the ISM was not gradual, but highly variable. We hypothesized that orbital induced weakening of the summer solar insolation and associated reorganization of the general atmospheric circulation were responsible for an unstable hydroclimate in the mid-Holocene in the CMZ. Only after a certain threshold in the intensity of solar insolation was passed, hydrological conditions stabilized. As such transitions from one hydrological state into another due to small changes in solar insolation can be associated with major environmental

changes/large fluctuations in moisture source, a scenario that may be relevant with respect to future changes in the ISM system.

From multi-proxy investigations (inorganic geochemical and pollen) on the same sediment core from Lonar Lake, two phases of severe aridity (between 4.6–3.9 and 1.5–0.6 cal. ka BP) have been identified following an early Holocene wet phase. These periods of severe aridity coincided with intervals of higher solar irradiance. Possibly the regional warming in the Indo-Pacific Warm Pool (IPWP) played an important role in causing aridity through changes in meridional overturning circulation and position of the anomalous Walker cell. Further, the first settlements in central India coincided with the onset of the first phase of aridity and agricultural populations flourished between those two phases of aridity.

2. Methods

In this chapter the methodology used for lipid biomarker and stable isotope analysis will be presented. An overview of the applied workflow is shown in Fig. 2.1. The discussed methods have been employed to obtain the data discussed in the following chapters.

In order to analyze lipid biomarkers in samples (leaves, microbial mats, particulate organic matter (POM) or sediment samples), total lipids (TLE: total lipid extracts) were extracted with organic solvents. All samples, except sediment samples, were extracted by ultrasonication, while sediment samples were extracted using an accelerated solvent extractor (ASE).

TLEs obtained after extraction consist of a complex mixture of compounds belonging to different compound classes. Prior to instrumental analysis they were separated into compound classes using a solid-phase extraction (SPE) technique, which separated TLEs into fractions of compounds with different polarity, namely an aliphatic hydrocarbon fraction, an alcohol fraction and a fatty acid fraction.

Individual compounds in these fractions were identified and quantified using gas chromatography (GC). The GC system used in this work was connected to two detectors, namely a flame ionization detector (FID) and a mass selective detector (MSD) via a splitter. Identification of compounds was based on comparison of mass spectra with published data.

The stable carbon and hydrogen isotopic compositions of organic compounds (lipid biomarkers) were determined using a GC, which was connected to an isotope ratio monitoring mass spectrometer (IRMS) via a chemical reaction interface. Different chemical reaction surfaces and their operating temperatures were used according to the element of interest, i.e., a pyrolysis interface for hydrogen and a combustion interface for carbon. Thus, the organic compounds were converted to gases, namely CO_2 and H_2 for $\delta^{13}\text{C}$ and δD determination, respectively, which then were analyzed for their isotope ratios.

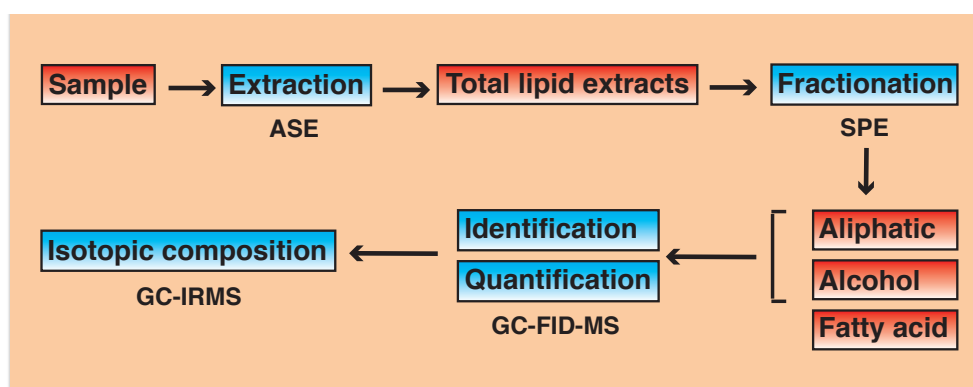


Fig. 2.1. Schematic workflow used for lipid biomarker and stable isotope analysis.

2.1 Sample preparation, extraction and SPE fractionation

In this study leaf, bacterial mat, particulate organic matter (POM), surface and core sediment samples were extracted for lipid biomarker analysis. Prior to extraction, 2–4 g of each mat or sediment samples was freeze-dried. Filters containing POM were also freeze-dried. Leaves were air-dried and cut into small pieces using an electric grinding system. Mat and sediment samples were homogenized in a mortar before lipid extraction.

All samples, except surface sediment samples, were extracted by ultrasonication, with 30 ml (leaves) and 50–100 ml (mat) of dichloromethane (DCM)/MeOH, 9:1 for 30 min. Sediment samples were extracted using an accelerated solvent extractor (Dionex ASE 350) with a mixture of dichloromethane (DCM)/methanol, 9:1 at 100 °C and 103 bar (1500 psi) for 15 min in 2 cycles. Total lipid extracts (TLEs) were passed through activated copper pipette columns to remove elemental sulphur.

After addition of internal standards (5 α -androstan-3 β -ol and erucic acid) the TLEs were separated on SPE silica gel columns (ca. 2 g of silica gel 60, 230–400 mesh) into three fractions of different polarity, namely an aliphatic hydrocarbon (eluted with 10 ml of *n*-hexane), an alcohol (eluted with 15 ml of DCM/acetone (9:1)) and a fatty acid fraction (eluted with 10 ml of DCM/methanol (5:1)).

2.2 Gas chromatographic-mass spectrometric (GC-MS) analysis of lipid biomarkers

Major alcohol compounds, like tetrahymanol, were present in very high concentrations and could be detected without derivatization on the used GC-MS system. Fraction one and two (containing aliphatic hydrocarbons and alcohols, respectively) were measured on a GC-FID/MSD system for compound identification and quantification. The GC-FID/MSD system consisted of an Agilent 7890A gas chromatograph equipped with a flame ionization detector (FID) and an Agilent 5975C mass selective detector. The system used a programmable temperature vaporization (PTV) inlet with split injection (5:1), a fused silica capillary column (Agilent DB-5MS) (length 30 m, inner diameter 0.25 mm and film thickness 0.25 μ m) with helium as carrier gas. 1 μ l of the sample was injected into the GC. The temperature of the injector was 70 °C while the temperature of the oven was kept constant for 2 min at 70 °C. Subsequently the oven was heated to 280 °C at 7 °C/min and then to 320 °C at 3 °C/min (15 min isothermal). Identification of compounds was based on comparison of mass spectra with published data.

2.3 Compound-specific stable isotope analysis

2.3.1 Compound-specific $\delta^{13}C$ analysis

The stable carbon isotope composition ($\delta^{13}C$) of biomarkers was measured on a GC system (Agilent 6890N) coupled via a combustion interface (GC-C III), to a

ThermoFisher Scientific (model 253) isotope ratio mass spectrometer (GC-irm-MS) at GFZ Potsdam. The system used a PTV inlet with split injection (1:1), a fused silica capillary column (Agilent Ultra1) (length 50 m, inner diameter 0.2 mm and film thickness 0.33 μm) with helium as carrier gas. 1–3 μl of the sample was injected into the GC. The temperature (T) programs for the injection and GC oven/column are as follows: Injector T-program: 230 $^{\circ}\text{C}$ (Start-T), with 700 $^{\circ}\text{C}/\text{min}$ up to 300 $^{\circ}\text{C}$ (hold for the complete run); Oven T-program: 40 $^{\circ}\text{C}$ (Start-T) hold for 2 min with 4 $^{\circ}\text{C}/\text{min}$ up to 300 $^{\circ}\text{C}$ (hold for 45 min).

For tetrahymanol analysis, the system used a PTV inlet with split injection (1:1), a capillary column (BPX5) (length 50 m, inner diameter 0.2 mm and film thickness 0.25 μm) with helium as carrier gas. 3 μl of the sample was injected into the GC. The temperature (T) program for the GC oven/column was as follows: Oven T-program: 80 $^{\circ}\text{C}$ (Start-T) hold for 1 min, with 15 $^{\circ}\text{C}/\text{min}$ up to 250 $^{\circ}\text{C}$, 1 $^{\circ}\text{C}/\text{min}$ up to 310 $^{\circ}\text{C}$ (hold for 15 min).

GC-irm-MS analyses were run in triplicate. Calibration of isotope analysis was performed by injecting several pulses of CO_2 at the beginning and at the end of each GC run. Isotopic ratios are expressed as $\delta^{13}\text{C}$ values in per mil. $\delta^{13}\text{C}$ values of compounds measured in laboratory reference scale were converted to the Vienna Pee Dee Belemnite (V-PDB) scale using a linear regression function derived from the relationship of measured values and known values in V-PDB scale, for the compounds of a certified standard between sample runs. The average standard deviation for standards over sequences was between 0.5 and 1.8‰ and for samples it was 0.5‰.

2.3.2 Compound-specific δD analysis

The stable hydrogen isotope (δD) composition of biomarkers was measured on a GC system (Agilent 6890N) coupled via a pyrolysis interface, to a ThermoFisher Scientific (Delta V Plus) isotope ratio mass spectrometer (GC-irm-MS) at GFZ Potsdam. The system used a PTV inlet with split injection (1:3), a capillary column (Agilent Ultra1) (length 50 m, inner diameter 0.2 mm and film thickness 0.32 μm) with helium as carrier gas. 1–3 μl of the sample was injected into the GC. The temperature (T) programs for the injection and GC oven/column are as follows: Injector T-program: 230 $^{\circ}\text{C}$ (Start-T), with 700 $^{\circ}\text{C}/\text{min}$ up to 300 $^{\circ}\text{C}$ (hold for the complete run); Oven T-program: 40 $^{\circ}\text{C}$ (Start-T) hold for 2 min with 4 $^{\circ}\text{C}/\text{min}$ up to 300 $^{\circ}\text{C}$ (hold for 45 min).

For tetrahymanol analysis, the system used a PTV inlet with split injection (1:1), a capillary column (DB-FFAP) (length 60 m, inner diameter 0.25 mm and film thickness 0.25 μm) with helium as carrier gas. 3 μl of the sample was injected into the GC. The temperature (T) program for GC oven/column is as follows: Oven T-program: 80 $^{\circ}\text{C}$ (Start-T) hold for 1 min, with 15 $^{\circ}\text{C}/\text{min}$ up to 250 $^{\circ}\text{C}$, 1 $^{\circ}\text{C}/\text{min}$ up to 310 $^{\circ}\text{C}$ (hold for 15 min).

GC-irm-MS analyses were run in triplicate. Calibration of isotope analysis was performed by injecting several pulses of H_2 at the beginning and at the end of each GC run. Isotopic ratios are expressed as δD values in per mil. δD values of

compounds measured in laboratory reference scale were converted to the Vienna Standard mean ocean (VSMOW) scale using a linear regression function derived from the relationship of measured values and known values in VSMOW scale, for the compounds of a certified standard (Mix A obtained from Arndt Schimmelmann, University of Indiana) between sample runs. The average standard deviations for standards and samples were 3‰.

3. Spatial heterogeneity in lipid biomarker distributions in the catchment and sediments of a crater lake in central India

Saswati Sarkar^a, Heinz Wilkes^b, Sushma Prasad^c, Achim Brauer^c, Nils Riedel^d, Martina Stebich^d, Nathani Basavaiah^e, Dirk Sachse^a

^aInstitute for Earth- and Environmental Science, University of Potsdam, Karl-Liebknecht-Straße 24–25, 14476 Potsdam, Germany

^bSection 4.3, Organic Geochemistry, Helmholtz Centre Potsdam GFZ German Research Centre for Geosciences, Telegrafenberg, D-14473 Potsdam, Germany

^cSection 5.2, Climate Variability and Landscape Evolution, Helmholtz Centre Potsdam GFZ German Research Centre for Geosciences, Telegrafenberg, D-14473 Potsdam, Germany

^dSenckenberg Research Institute, Research Station of Quaternary Palaeontology, Am Jakobskirchhof 4, D-99423 Weimar, Germany

^eIndian Institute of Geomagnetism, New Panvel, Navi Mumbai, India

Published in *Organic Geochemistry* 66 (2014) 125–136

Abstract

*The basin-scale spatial variability in lipid biomarker proxies in lacustrine sediments, which are established tools for studying continental environmental change, has rarely been examined. It is often implicitly assumed that a lake sediment core provides an average integral of catchment sources. Here we evaluated the distribution of lipid biomarkers in a modern ecosystem and compared it with the sedimentary record. We analyzed lipid biomarkers in terrestrial and aquatic organisms and in lake surface sediments from 17 locations within the saline-alkaline Lonar crater lake in central India. Terrestrial vegetation and lake surface sediments were characterized by relatively high average chain length (ACL) index values (29.6–32.8) of leaf wax *n*-alkanes, consistent with suggestions that plants in drier and warmer climates produce longer chain alkyl lipids than plants in cooler and humid areas. A heterogeneous spatial distribution of ACL values in lake surface sediments was found: at locations away from the shore, the values were highest (31 or more), possibly indicating different sources and/or transport of terrestrial biomarkers. In floating, benthic microbial mats and surface sediment, *n*-heptadecane, carotenoids, diploptene, phytol and tetrahymanol occurred in large amounts. Interestingly, these biomarkers of a unique bacterial community were found in substantially higher concentrations in nearshore sediment samples. We suggest that human influence and subsequent nutrient supply resulted in increased primary productivity, leading to an unusually high concentration of tetrahymanol in the nearshore sediments.*

*In summary, the data showed that substantial heterogeneity existed within the lake, but leaf wax *n*-alkanes in a core from the center of the lake represented an integral of catchment conditions. However, lake level fluctuation may potentially affect aquatic lipid biomarker distributions in lacustrine sediments, in addition to source changes.*

Keywords: Lonar crater lake, lipid biomarker proxies, spatial variability, *n*-alkanes, tetrahymanol, catchment vegetation, human influence

3.1 Introduction

Lake sediments are exceptional archives of past environmental and climatic changes (Trauth et al., 2005; Martin-Puertas et al., 2012; Melles et al., 2012). Along with other geochemical proxies, such as the elemental and isotopic composition of bulk sediments, the analysis of lipid biomarkers has become an established tool for paleoecological and paleoenvironmental studies (Hanisch et al., 2003; Eglinton and Eglinton, 2008; Xu and Jaffé, 2008; Castañeda and Schouten, 2011). A prerequisite for a robust interpretation of such paleoenvironmental records is a comprehensive understanding of lipid biomarker sources and transport from within the catchment area, and additionally of the effect of human influence on the lake environment in the relatively recent past.

Lipids as natural products of all organisms are ubiquitous in lake sediments and, because of their relative inertness, can be preserved over geological timescales. Since different organisms produce different lipids, the presence of certain lipids in sediments can be used to identify their sources within a lake catchment. For example, aquatic organisms (bacteria, algae and aquatic macrophytes) produce short to mid-chain *n*-alkanes, whereas long chain *n*-alkanes are almost exclusively produced by terrigenous higher plants (Eglinton and Hamilton, 1967; Cranwell et al., 1987; Ficken et al., 2000; Gao et al., 2011). The analysis of lipid biomarker distributions in lake sediments can therefore provide insight into changes in a lake ecosystem and its catchment over time. Changes in the abundance of biomarkers in sediments can be used as a proxy for changes in primary productivity and/or transport of terrestrial organic matter (OM), respectively (Holtvoeth et al., 2010). Since changes in the lake ecosystem and catchment are often driven by environmental and climatic factors, such records can be used to detect paleoclimatic shifts (Schwark et al., 2002; Romero-Viana et al., 2012; Sachse et al., 2006).

In general, changes in a specific proxy over time determined from a single sediment core are used for the reconstruction of past environmental conditions. Use of a single sediment core, mainly from the center of a lake, has been debated (Wang et al., 2009 and references therein) since significant spatial variability in sediment proxies from lake sediments has long been identified (Hilton et al., 1986). Understanding the basin scale variability, especially for sedimentation pattern, has been emphasized (Lamoureux, 1999). Instead of basin scale heterogeneities, proxies related to the amount of materials rather than to their rate of deposition, were found to better represent the mean conditions (Wang et al., 2009).

For lipid biomarkers, two main processes can lead to substantial proxy heterogeneity within a lake basin. First, lipid production may not be equal in all source organisms, leading to over or under representation of certain components in sediments, and secondly transport into the archive may favor certain ecosystem components. These effects have the potential to significantly affect the interpretation of paleoclimatic conditions using these proxies. Despite these important constraints, spatial proxy heterogeneity for lipid biomarkers in lake systems has not been investigated. Hence, can the analysis of a single core be representative of the spatial variability in lipid biomarker proxies within a lake and should paleoclimatic reconstruction using lipid biomarker proxies be based on such a single core?

To evaluate possible variations in lipid biomarker distributions and its causes, we studied sediments from Lonar crater lake (Fig. 3.1) in central India (19°58'N, 76°30'E; Buldhana district, Maharashtra State, India). The lake lies within the Indian 'monsoon zone', the variation in rainfall over the region showing a strong correlation with the variation in the Indian summer monsoon rainfall (Gadgil, 2003). It is an alkaline saline lake characterized by high autochthonous productivity, which is attributed to a unique microbial community (Surakasi et al., 2010; Antony et al., 2013). High aquatic and bacterial productivity, as well as the availability of a detailed study of catchment vegetation, make it an ideal site for understanding biomarker sources in the sediments. In addition, the well-constrained modern seasonality in rainfall is expected to control physical properties of lake water and primary productivity, as well as terrestrial OM transport to the lake. The crater basin has a small catchment area, so predominantly local/site-specific signals were expected to be recorded in the sediments.

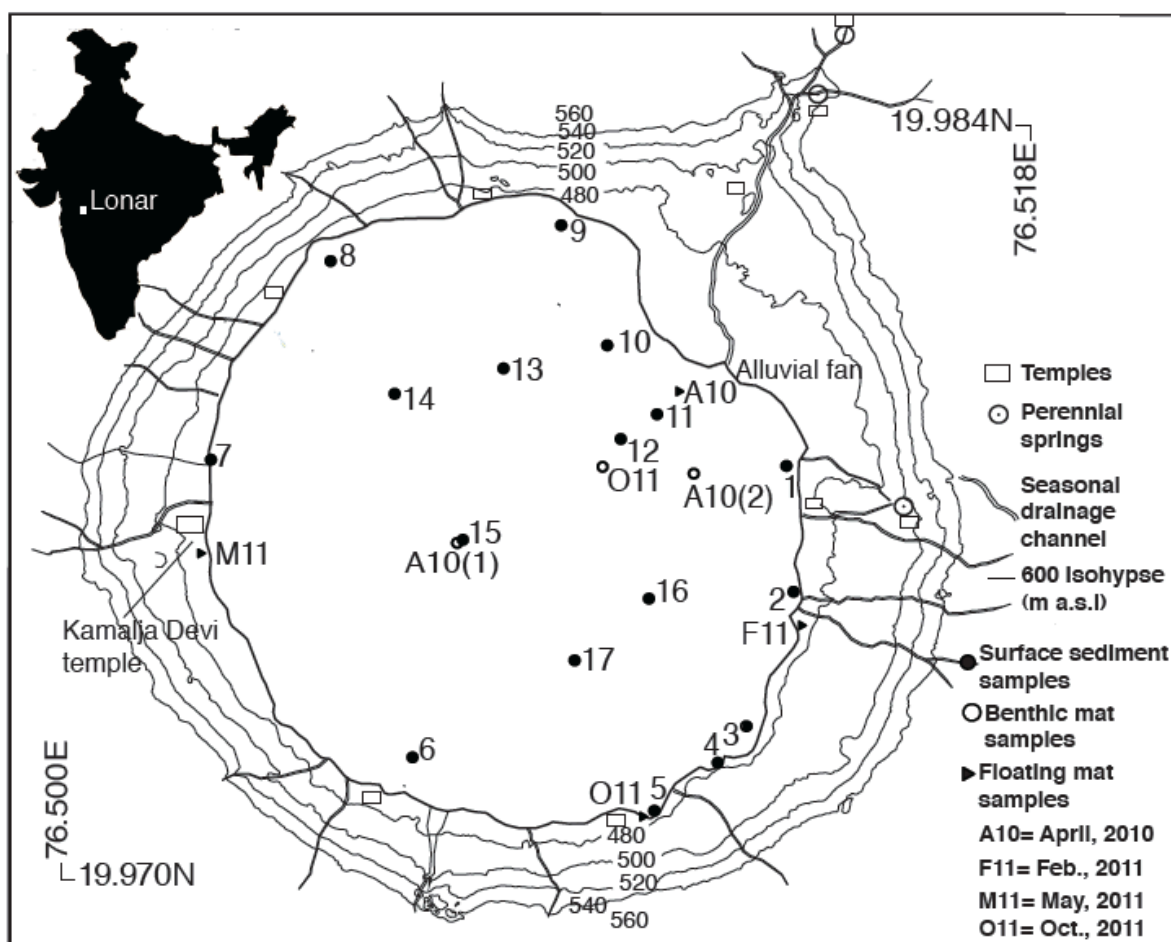


Fig. 3.1. Location of Lonar Lake; map of Lonar crater lake showing sampling locations of floating mat, benthic mat and surface sediment samples.

Changes in physical conditions in the water column and the catchment ecosystem over time, as recorded via geochemical proxies, make Lonar Lake a sensitive continental archive for 'monsoonal' India (Anoop et al., 2013b; Menzel et al., 2013). In order to use lipid biomarker abundances and distributions as

proxies for such changes, we performed a detailed analysis of modern day conditions and tested the extent to which organic geochemical proxies represent the modern day ecosystem. Finally, we evaluated the spatial variability in lipid biomarker distributions in the surface sediments to estimate the fidelity of paleoenvironmental reconstruction based on a single long core.

3.2 Material and methods

3.2.1 Study site, modern environment and hydrology

The lake lies within a crater formed by a meteorite impact on the Deccan trap basalts (Fredriksson et al., 1973). The near-circular crater has a diameter of 1.8 km and a depth of 150 m, with steep sides (Fredriksson et al., 1973). The rim is ca. 30 m above the surrounding plains (Fudali et al., 1980). The crater formation age is debated, 45–67 ka being suggested on the basis of the thermoluminescence of impact glass (Sengupta et al., 1997). Radiocarbon dating of histosol suggested 11.65 ka as a maximum age (Maloof et al., 2010). A significantly older age of 570 ± 47 ka was determined from $^{40}\text{Ar}/^{39}\text{Ar}$ dating of melt rock samples (Jourdan et al., 2011).

The lake is alkaline and saline (pH 10.5, salinity 10.5; La Touche, 1912; Jhingran and Rao, 1958; Nandy and Deo, 1961). It has a mean diameter of 1.2 km and is 5 m deep. The alkalinity is attributed to Na_2CO_3 and NaHCO_3 , formed by evaporative enrichment (Nandy and Deo, 1961). The lake is in the semi-arid region of central India, with an average annual rainfall of 760 ± 50 mm. In the region, the seasonality in the monsoon system results in two general climatic periods: (i) a wet season from June to the end of September (summer monsoon/southwest monsoon), with an average rainfall of 670 ± 40 mm and (ii) a dry season from early October to June. The temperature during summer is around 31 °C, but may increase up to 45 °C; summer monsoon and winter temperatures average 27 °C and 23 °C, respectively (Anoop et al., 2013b). Summer monsoonal rainfall is the major contributor of fresh water to the closed basin lake, although two springs supply fresh water throughout the year. Currently, water from these springs is diverted to agricultural fields. Tritium dating indicated modern to sub-modern age for ground water (Anoop et al., 2013b). There are reports of complete drying out of the lake and formation of thick salt crusts on the lake bed during exceptionally dry years in the mid-1980s (Badve et al., 1993). The seasonal influx of water and evaporation control the chemical properties of the lake water, such as alkalinity and salinity, which in turn affect the autochthonous OM production by thriving cyanobacterial blooms (Surakasi et al., 2010). In recent years, the lake has become increasingly eutrophic, which has been attributed to climatic factors, such as an increase in rainfall amount (Badve et al., 1993). However, agricultural activity and the presence of ca. 800 years old temples at the lake shore suggest that anthropogenic activity may also have been a factor in the eutrophication.

The crater rim is characterized (Fig. 3.2a) by belts of thornshrub (TS) and dry deciduous mixed forest (DDM), which is also a common vegetation type in the Buldhana district (Champion and Seth, 1968). Like the forest in the Lonar catchment, teak (*Tectona grandis*) is the main tree species of this forest type and occurs in nearly all forest communities (Diwakar and Sharma, 2000). A

permanent delta has developed at the outflow of major springs at the northeastern shore of the crater. The delta is currently used for the farming of a variety of plants, including banana (*Musa x paradisiaca*), maize (*Zea mays*) and millet (*Sorghum halepense*; *Setaria italica*).

Aquatic vegetation consisting of the emerged macrophytes Cyperaceae and a *Typha* sp. is abundant mainly near the alluvial fan and with sporadic occurrence (for e.g., Juncaceae) near the shore of other parts of the lake.

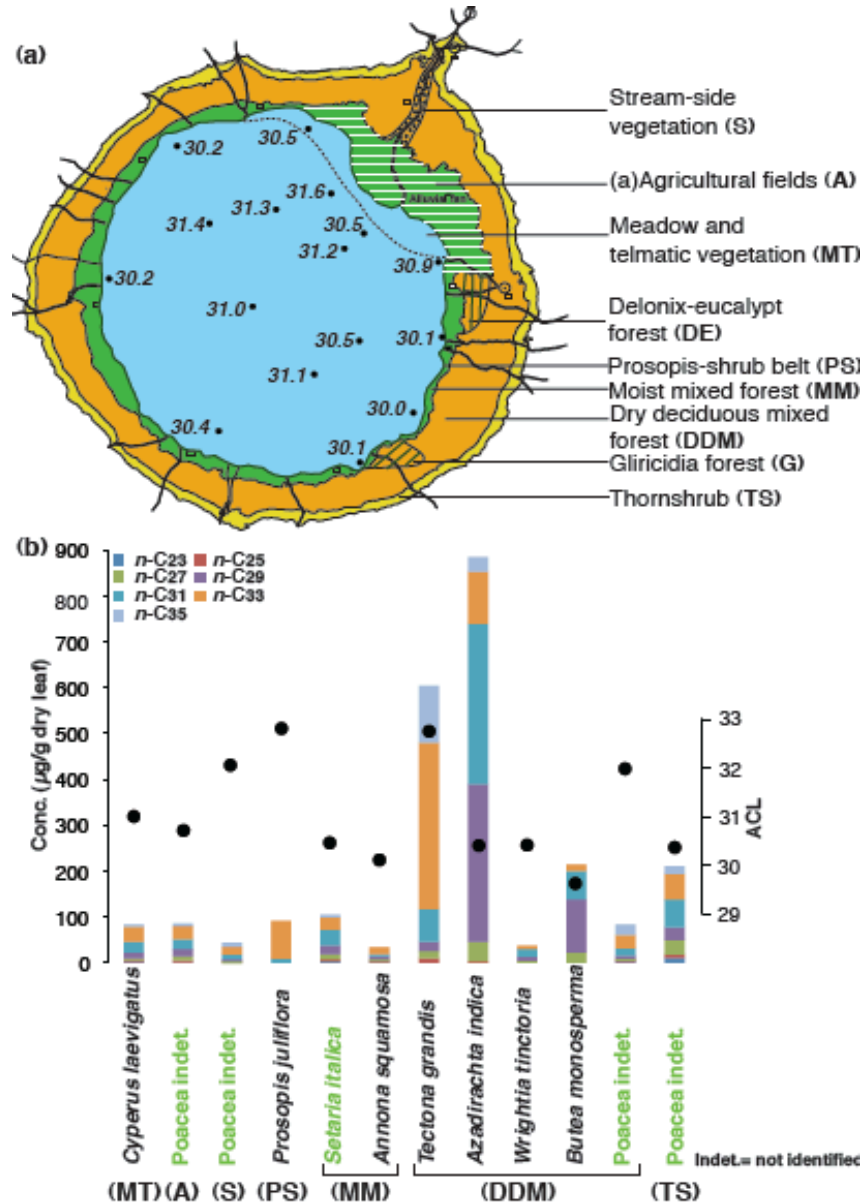


Fig. 3.2. (a) Map of Lonar Lake showing crater vegetation belts and ACL (in oblique numbers) in surface sediment samples. (b) Leaf wax *n*-alkane composition [both concentration of individual *n*-alkanes and distribution (ACL)] in representative vegetation samples from in trees and grasses (name in green).

3.2.2 Vegetation mapping and field sampling

3.2.2.1 Modern vegetation mapping

To map the crater vegetation, 16 line transects from the lake shore to the

crater rim at randomly selected parts in the crater were laid during three field surveys in 2011 and 2012. Along these transects, individual coverage (%) of arboreal plants was measured using visual estimation of vegetation cover (Floyd and Anderson, 1987). A relatively uniform vegetation structure and species composition within the different vegetation types was observed. From this, vegetation was extrapolated to the whole crater and mapped using high resolution aerial pictures.

3.2.2.2 Modern vegetation

Vegetation samples (leaves) from the dominant vegetation were collected during two field campaigns in 2011 and 2012. Plant samples, representative of catchment vegetation, were selected on the basis of the results from the vegetation survey conducted during the same field campaigns (Fig. 3.2a and Tab. A.1). We sampled ca. 10 leaves from each single specimen and pooled them. All the leaves collected had been exposed to the sun, except for the plants like *Prosopis* and *Annona*, which were growing under shady conditions.

3.2.2.3 Aquatic plants

The major aquatic plant was the emerged macrophyte *Cyperus laevigatus*, which was abundant near the alluvial fan. We sampled leaves from several plants and discuss these under “terrigenous lipids” due to the similarity in their leaf wax distributions with those of land plants.

3.2.2.4 Floating mat and water

Nearshore floating microbial mats were collected from different locations (Fig. 3.1 and Tab. A.2) with a phytoplankton net (mesh size 125 μm) during different seasons (April, 2010 and February, May and October, 2011). Water (6 l and 4 l), collected in February 2011 from different depths (above and below the redox boundary at 0.5 and 4 m) was filtered onto pre-combusted glass fiber (GF) Whatman filters with a handheld vacuum pump to collect particulate OM (POM).

3.2.2.5 Surface sediments and benthic mats

Surface sediment samples from 17 locations within the lake (Fig. 3.1 and Tab. A.3) were collected in May 2008 using a Wildco Ponar type grab sampler with a maximum penetration depth of ca. 5–7 cm. Surface sediments from 3 additional locations [A10 (1), A10 (2) and O11] were obtained during collection of lake bottom water using a water sampler. Two of these [A10 (1), A10 (2)] were collected in April 2010 and the other (O11) in October 2010. In the samples a distinct layer of dark green OM was present above the sediment, which most probably represented a benthic microbial mat. We therefore subsampled this layer and discuss it in the following as a benthic microbial mat.

3.2.3 Sample preparation, biomarker identification and quantification

Ca. 2–4 g of dried leaf, microbial mat, POM or surface sediment samples were extracted for lipid biomarkers. Leaves were air-dried and cut into small pieces using an electric grinding system. Mat and sediment samples were freeze-dried and homogenized in a mortar before extraction. All samples, except surface sediment samples, were extracted by ultrasonication, with 30 ml (leaves) and 50–

100 ml (mat) of dichloromethane (DCM)/MeOH, 9:1) for 30 min. Surface sediment samples were extracted using an accelerated solvent extractor (Dionex ASE 350) with DCM/MeOH, 9:1) at 100 °C and 103 bar (1500 psi) for 15 min in 2 cycles. Each total lipid extract (TLE) was passed through an activated Cu pipette column to remove elemental S.

After addition of internal standards (5 α -androstan-3 β -ol and erucic acid) the TLE was separated on an SPE silica gel column (ca. 2 g silica gel 60, 230–400 mesh) into three fractions (1–3) of different polarity, namely an aliphatic hydrocarbon fraction (eluted with 10 ml *n*-hexane), an alcohol fraction (15 ml DCM/Me₂CO, 9:1) and a fatty acid fraction (10 ml DCM/MeOH, 5:1). Major alcohols, like tetrahymanol, were present in high concentration and could be detected without derivatization using gas chromatography-mass spectrometry (GC-MS). Fractions 1 and 2 were measured using GC-flame ionization detection-mass selective detection (GC-FID-MSD) for compound assignment and quantification. The GC-FID-MSD system consisted of an Agilent 7890A gas chromatograph and an Agilent 5975C mass selective detector. The system used a programmable temperature vaporization (PTV) inlet with split injection (5:1), an Agilent DB-5MS column (30 m, inner diameter 0.25 mm and film thickness 0.25 μ m) with He as carrier gas; 1 μ l of sample was injected. The injector temperature was initially held at 70 °C and after 2.5 min the temperature was increased at 720 °C/min to 300 °C; the GC oven temperature program started at 70 °C (held 2 min) and then to 280 °C at 7 °C/min and then to 320 °C (held 15 min) at 3 °C/min. Compound assignment was performed by comparison of mass spectra with our own biomarker database and published data.

3.3 Results

3.3.1 Terrigenous biomarkers

3.3.1.1 Abundance and distribution of leaf wax *n*-alkanes in modern vegetation

Mid-chain and long chain *n*-alkanes (C₂₃ to C₃₅) were found in the aliphatic hydrocarbon fraction of modern vegetation samples (Tab. A.1). Summed concentration of the major (odd numbered) long chain *n*-alkanes in leaves ranged from ca. 30 to 900 μ g/g dry wt., with the highest concentration (Fig. 3.2b) in the leaves of two DDM forest trees (*T. grandis* and *Azadirachta indica* with 600 and 900 μ g/g dry wt., respectively). Among the grasses (Poaceae), the average concentration of *n*-alkanes was significantly lower (avg. 44–210 μ g/g dry wt.) than for trees and shrubs.

The average chain length (ACL) index (concentration weighted average chain length for *n*-alkanes, $\sum n \times C_n / \sum C_n$, where *n* = number of carbons; here *n* = 23–35 and *C_n* = concentration of the *n*-alkane) of the plants varied between 29.6 and 32.8. The highest ACL index value of 32.8 was found in teak and in the prominent shrub *Prosopis juliflora*, which grows all around the lake (Fig. 3.2). The grasses showed ACL values (31.1 \pm 0.3) similar to trees (31.0 \pm 0.3), with the exception of grass from thornshrub vegetation with a value of 30.4). The difference in values between grasses and trees/shrubs was not statistically significant (Students *t*-test), possibly due to the low number of samples. The prominent emerged macrophyte (*C. laevigatus*) analyzed that was abundant near the alluvial fan showed an ACL value of 31.0.

Despite similar ACL values, the distribution of long chain *n*-alkanes was quite variable. For example, several plants [*A. indica*, *Wrightia tinctoria* and the grass from thornshrub (TS) vegetation] showed the same ACL index value of 30.4, but were characterized by strikingly different distributions of *n*-alkanes (Fig. 3.2b). In *A. indica* *n*-C₂₉ and *n*-C₃₁ were present in equal amount, whereas in *W. tinctoria* the concentration of *n*-C₃₁ was higher than that of *n*-C₂₉. Furthermore, other plants, such as *P. juliflora* and *T. grandis*, produced almost exclusively *n*-C₃₃, whereas plants like *S. italica* showed a broader distribution, with the highest abundance of *n*-C₃₁ (Fig. 3.2b).

3.3.1.2 Abundance and distribution of leaf wax *n*-alkanes in lake surface sediments

The most prominent biomarkers of terrestrial origin in the 17 surface sediments were long chain *n*-alkanes with 25 to 35 carbons (Tab. A.3). The major homologues, in order of decreasing abundance, were C₂₉, C₃₁, C₃₃ and C₂₇. They showed a concentration of up to 24 µg/g dry sediment (summed concentrations of major odd long chain *n*-alkanes). Even numbered long chain *n*-alkanes were present, but often in amounts too low for quantification. Overall, the sediment extracts showed a clear predominance of odd long chain *n*-alkanes. For samples from different locations within the lake, substantial variability in absolute concentration was observed. In general, long chain *n*-alkanes showed a higher concentration (17–23 µg/g dry sediment) near the northwestern, eastern and southern shores of the lake (Fig. 3.3a). The maximum amount was in nearshore samples, whereas samples away from the shore were characterized by substantially lower amounts (ca. 50% of nearshore samples; Fig. 3.4). The ACL index (here covering carbon numbers 25 to 35, since *n*-C₂₃ was not present in surface sediments) in the surface samples ranged from 30.0 to 31.6, with a mean of 30.8 and a standard deviation of 0.6 (Fig. 3.4).

The distribution of long chain *n*-alkanes was different between nearshore samples (1 to 9) and samples away from the shore (10 to 17), with the exception of nearshore samples 1 and 6 and sample 11 away from the shore. In summary, nearshore samples showed distributions dominated by *n*-C₂₉ whereas samples away from the shore were dominated by C₃₁ and C₃₃ (Fig. 3.5). The difference in distribution between nearshore and “away-shore” samples was not statistically significant (Students *t*-test), again possibly due to the limited number of samples. At locations away from the shore (such as samples 10–17, except 11) ACL index values were higher than at nearshore (31 or more; Fig. 3.2a), indicating the dominance of C₃₁ and C₃₃ relative to C₂₇ and C₂₉, in “awayshore” samples.

3.3.2 Aquatic biomarkers

3.3.2.1 Abundance and distribution of biomarkers in floating and benthic bacterial mats and particulate OM (POM)

Bacterial mat samples contained mainly *n*-heptadecane (*n*-C₁₇), carotenoids (β-carotene and its homologues/isomers), diploptene [17β,21βhop-22(29)-ene], phytol (3,7,11,15-tetramethylhexadec-2-en-1-ol) and tetrahymanol (gammaceran-3β-ol; Tab. A.2). A high concentration of *n*-heptadecane (up to 1650 µg/g) was found in floating mat samples, especially in one collected in October 2011 (Fig. 3.6). On the other hand, tetrahymanol was the major biomarker in benthic mat samples

(Fig. 3.6), with a concentration >2500 µg/g.

POM contained only *n*-heptadecane at up to 50 µg/l and phytol, whereas tetrahymanol was not detected in the filtered POM from the lake water (Tab. A.2).

3.3.2.2 Abundance and distribution of aquatic biomarkers in lake surface sediments

The most abundant biomarkers in all surface samples were tetrahymanol and the corresponding ketone, gammaceranone (gammaceran-3-one). Total tetrahymanol concentration (summed concentration of tetrahymanol and gammaceranone) was unusually high and varied from ca. 37 to 1000 µg/g dry sediment at various locations (Fig. 3.3d). Gammaceranone was most probably related to tetrahymanol. However, it is not clear, if it was the oxidation product of tetrahymanol or present as such in the source organism (Sinninghe Damsté et al., 1995), so the concentrations were summed. The relative proportion of gammaceranone vs. tetrahymanol did not show any significant spatial variation (Fig. 3.3d). Gammaceranone constituted on average 9.1% of the summed concentration (with a standard deviation 2.9) and was similar to that in the microbial mat samples, where gammaceranone constituted on average 8.7% of the summed concentration. In both benthic microbial mat and surface sediment samples, total tetrahymanol concentration showed the highest values near the eastern shore of the lake, the area of discharge of the two major perennial springs, and also at the western shore (Fig. 3.3d). Total tetrahymanol concentration clearly showed lower values in the center of the lake.

Other major biomarkers of aquatic origin included *n*-heptadecane, phytane (2,6,10,14-tetramethylhexadecane), diploptene, moretene [17β-moret-22(29)-ene; Fig. 3] and fernene (fern-8-ene; Tab. A.3). Although carotenoids were not present in all samples, they showed a wide variability in abundance and were present in high amount in some locations, such as at the eastern and western shore (Fig. 3.3c).

In summary, most of the aquatic biomarkers were present in high concentration in nearshore samples, particularly at the eastern and western shore (tetrahymanol and carotenoids) but also at the southern shore (*n*-heptadecane, diploptene and moretene), but exhibited low concentration in samples away from the shore (Fig. 3.3).

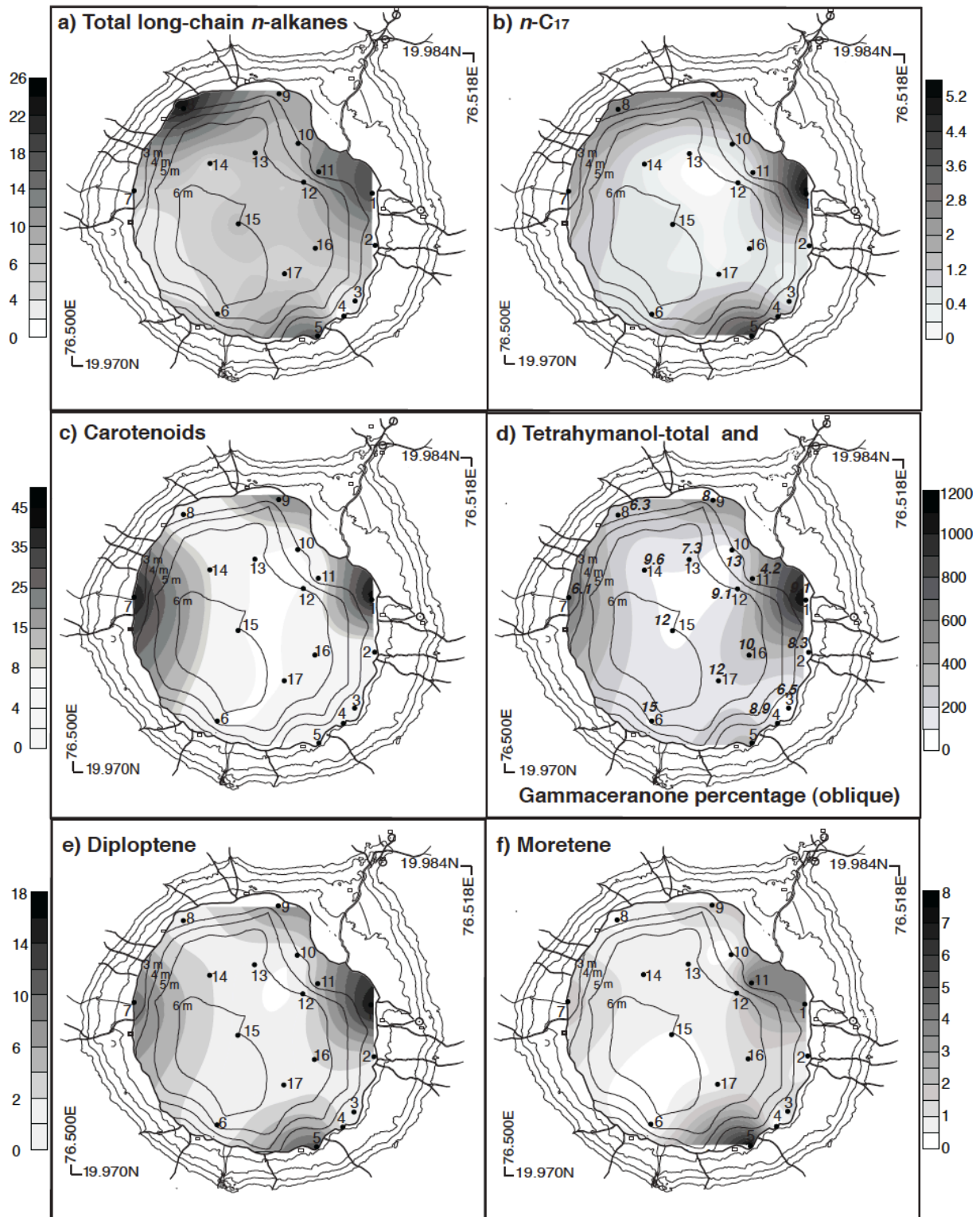


Fig. 3.3. Map of Lomar Lake showing distribution of all major biomarkers in lake sediments ($\mu\text{g/g}$ dry sediment).

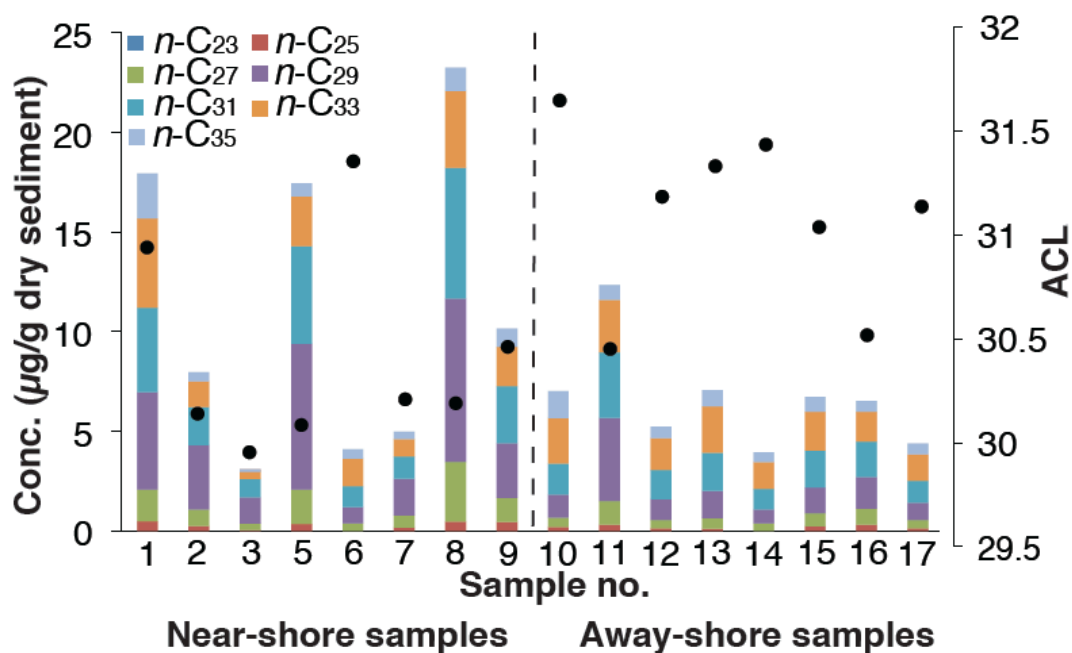


Fig. 3.4. Long chain *n*-alkane composition [both concentration of individual *n*-alkanes and distribution (ACL)] in surface sediment samples.

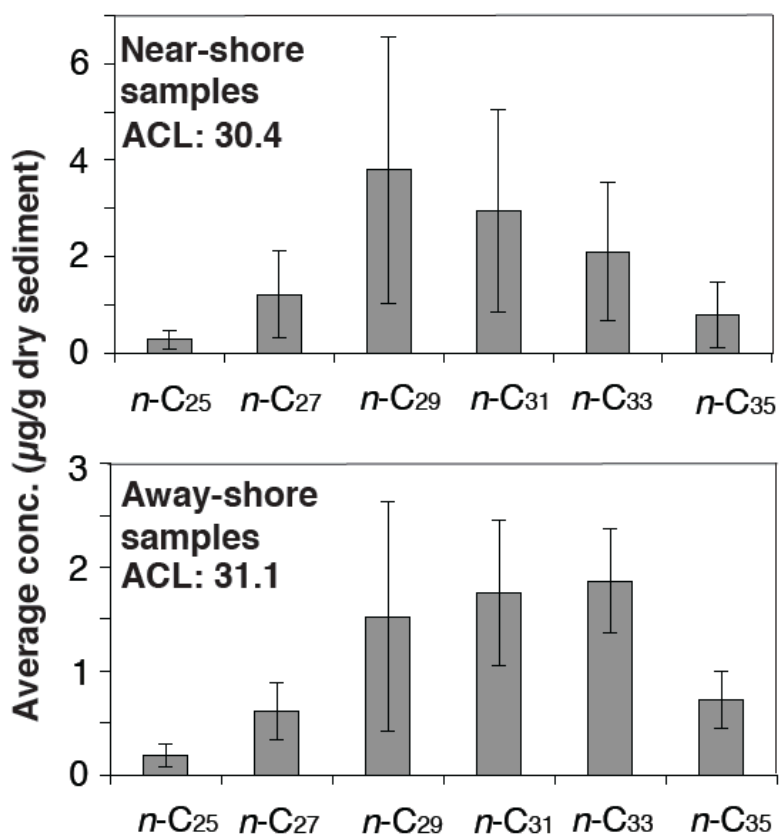


Fig. 3.5. Comparison of composition of long chain *n*-alkanes in nearshore samples and samples away from the shore.

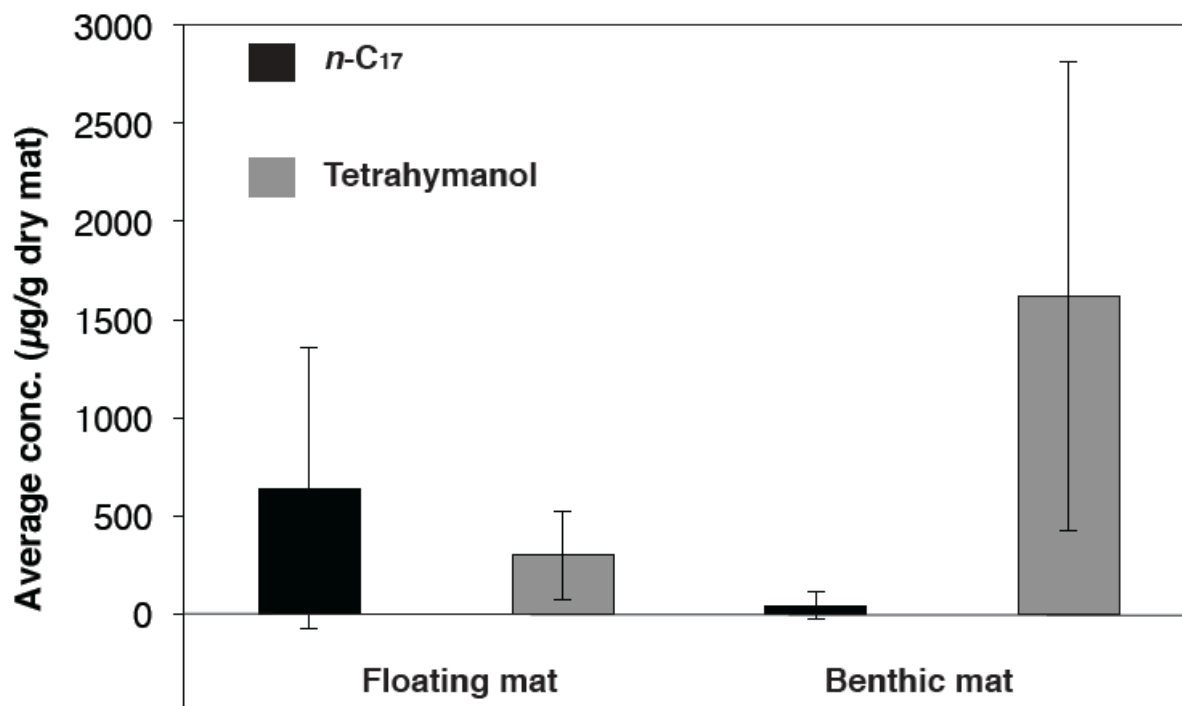


Fig. 3.6. Major lipid biomarker composition of floating and benthic mat samples.

3.4 Discussion

3.4.1 Terrestrial biomarkers

3.4.1.1 Factors influencing biomarker composition in higher terrigenous plants

The ACL index from sediment cores is sometimes applied to detect vegetation or even climate changes over time (Hughen et al., 2004). Surveys of modern plants showed that grasses (C_4) have consistently higher values than trees (C_3) (Rommerskirchen et al., 2006) and that hydrological conditions (Schefuß et al., 2003; Hoffmann et al., 2013) and to a lesser extent temperature (Tipple and Pagani, 2012) can affect ACL values. As such, along with vegetation type, the combined effect of temperature and humidity seems to control the leaf wax composition at most locations, but the direction of that change can be distinct for different plants (Hoffmann et al., 2013).

Due to the relatively low number of sampled plants, we cannot provide a complete discussion about the possible difference of concentration/ ACL index values among trees and grasses (Fig. 3.7a) at the site. Still, the high ACL values (29.6–32.8) of leaf wax *n*-alkanes from modern vegetation sampled at the lake and in its catchment, situated in a drier and warmer environment, corroborate the findings from most studies discussed above.

The ACL index from the lake surface sediments also showed relatively high values, ranging between 31.8 and 30.0 (mean 30.8 ± 0.1), in agreement with our data from modern plants around the lake, although with a lower variability, likely reflecting the integrative character of the lake sediments. Thus ACL values of *n*-alkanes in the lake sediments reflected the range found in modern vegetation and, as being relatively high, seem typical for arid and warm conditions.

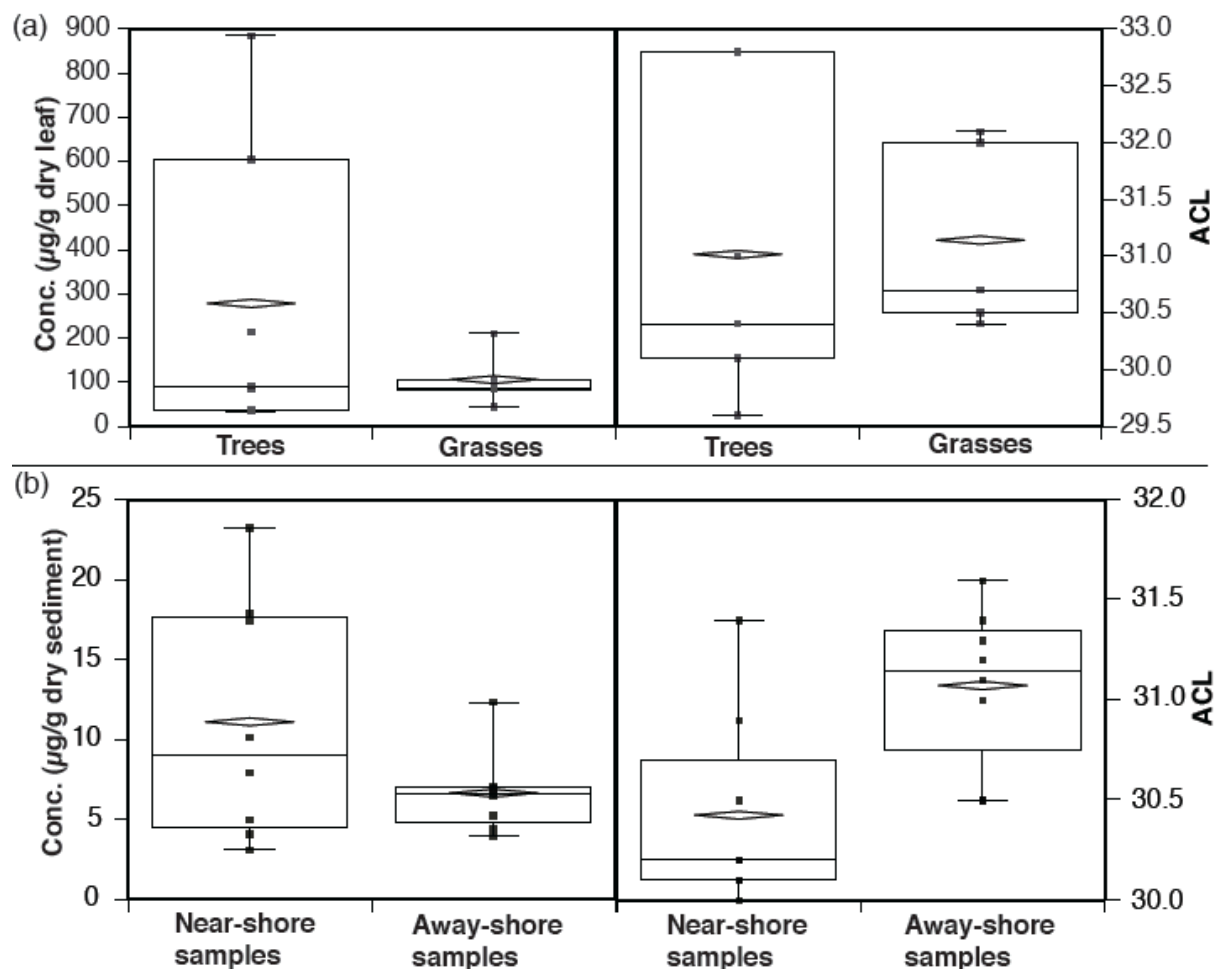


Fig. 3.7. Comparison of *n*-alkane composition [both concentration of total long chain *n*-alkanes and distribution (ACL)] with box and whisker plots, for (a) vegetation samples (b) surface sediment samples. The plots show upper and lower quartiles (boxes), and whiskers extended to extreme data points. They also show median (horizontal lines) and mean (diamond) and the data points (filled squares).

3.4.1.2 Spatial patterns of leaf wax *n*-alkane abundances in sediments as a consequence of soil erosion

In the lake sediments the concentration of individual leaf wax derived long chain *n*-alkanes varied with sampling location, although the vegetation cover was evenly distributed around the lake – with the exception of the agricultural fields and telmatic vegetation near the alluvial fan (Fig. 3.2a). It is thus unlikely that the highest concentration of terrigenous compounds (total terrigenous) near the northwestern shore (sample 8) was due to different vegetation sources. Therefore, higher terrigenous plant input as a result of stronger erosion and less vegetation cover on the steep crater walls in the NW of the crater was likely responsible for the higher than average concentration of long chain *n*-alkanes in this area. Stronger erosion was also supported by higher Al concentration in sediments from this part of the lake (Basavaiah et al., personal communication). On the other hand, terrigenous input from perennial springs may have resulted in a greater input of long chain *n*-alkanes near the eastern shore (sample no. 1). High C/N values in these sediments also implied the presence of a higher amount of

terrestrial than algal material in this part of the lake (Basavaiah et al., personal communication). As such, the delivery of terrigenous OM to the lake seems to be driven mainly by surficial fluvial discharge to the lake and terrestrial OM constitutes the major source in nearshore sediments.

3.4.1.3 Spatial patterns of leaf wax *n*-alkane distributions in sediments as a consequence of distinct plant sources?

The higher abundance of C₃₁ and C₃₃ relative to C₂₇ and C₂₉, as expressed in higher ACL values (≥ 31), for the samples away from the shore (Fig. 3.7b) could indicate different sources and/or transport mechanisms for these *n*-alkanes to the sediment. For example, eolian transport could deliver *n*-alkanes from plants which grow further away in the hinterland to the lake. While the nearshore samples receive plant material from within the crater, overprinting a possible eolian signal, the samples away from the shore could contain a larger fraction of eolian-transported leaf wax. However, an assessment of *n*-alkane distributions and in particular, concentration in plants from the region, as well as in aerosols around the lake would be needed to test this hypothesis. Comparison of *n*-alkane distributions in plants and lake sediments revealed that patterns in nearshore sediments were similar to those from plants like *A. indica* (which produced a high amount of long chain *n*-alkanes) and thus may constitute the major sources in nearshore samples. On the other hand, leaf wax *n*-alkanes of the most abundant plants, like *P. juliflora* and *T. grandis*, which constitute about 15% and 20% of the vegetation in the crater, respectively, and are the major source of C₃₃, could be the origin of *n*-alkanes in sediments away from the shore. By comparing leaf wax lipid distributions with pollen distributions in lake surface sediments (Riedel and Stebich, unpublished results), we tried to test this hypothesis. While pollen from *Azadirachta* was frequently distributed within the lake, pollen from *Tectona* was conspicuously absent from the lake sediments, with the exception of a few nearshore samples. Pollen from *Prosopis* was found mainly in nearshore samples. The apparent mismatch between the distribution of pollen and leaf wax *n*-alkanes within the lake may be due to different transport mechanisms of pollen and leaf wax *n*-alkanes to the sediment.

In addition, emerged macrophytes could also constitute a substantial source of long chain *n*-alkanes in the nearshore samples, as these plants grew especially close to the alluvial fan (Fig. 3.2a). The emerged macrophyte *C. laevigatus* was characterized by ACL values of 31.0, comparable with some of the sediment sample ACL values near the alluvial fan (Fig. 3.2a). Therefore, the concentration of long chain *n*-alkanes in the area closer to the alluvial fan may be significantly influenced by emerged macrophyte input.

While we aimed to sample the most abundant plants to obtain a representative set of samples characterizing the vegetation at Lonar, we may have missed some important species and therefore an important leaf wax *n*-alkane source, during the vegetation sampling. In particular, the large range in *n*-alkane abundance in the sampled plants suggests that only few species may dominate the sedimentary *n*-alkane signal.

3.4.1.4 Integration of leaf wax *n*-alkane abundance and distribution in the deepest part of the lake

In the deepest part of the lake, long chain *n*-alkane concentration (total terrigenous) and ACL values were characterized by values of 6.7 $\mu\text{g/g}$ dry sediment and 31.0 (sample no. 15), respectively. These are similar to the average values for all surface samples (8.3 $\mu\text{g/g}$ dry sediment and ACL value of 30.8). Thus, despite the wide spatial variability in leaf wax *n*-alkane concentration across the lake, the deepest part seemed to integrate the properties from all locations within the lake. Hence, considering the terrigenous biomarkers, the deepest part of the lake did indeed provide an integral over the lake catchment and would be the most suitable location to retrieve a long core for climate reconstruction.

3.4.2 Aquatic biomarkers

3.4.2.1 Bacterial and ciliate communities as the major source of aquatic biomarkers in the lake sediments

Based on the presence of tetrahymanol, diploptene and moretene in the benthic mats, we conclude that these compounds originate from a benthic microbial mat community. The major source of *n*-heptadecane seems to be a cyanobacterial community, as it was found in substantial amount only in floating cyanobacterial mats (Fig 3.6).

Tetrahymanol was by far the most abundant lipid in all the surface sediment samples and benthic mats. It occurs in a variety of environments, widely so in marine sediments (Ten Haven et al., 1989; Venkatesan et al., 1990) and frequently in saline lakes (Thiel et al., 1997; Kristen et al., 2010), but also in freshwater lakes (Xu and Jaffé, 2009; Holtvoeth et al., 2010; Castañeda et al., 2011). It is the primary lipid in marine and freshwater ciliates (Mallory et al., 1963; Harvey and McManus, 1991) and is believed to act as membrane rigidifier in these protozoa (Ourisson et al., 1987). It was also proposed that ciliates, especially in the absence of a supply of dietary sterols, thrive on bacteria and synthesize tetrahymanol (Sinninghe Damsté et al., 1995). The common occurrence and similar distribution of tetrahymanol and *n*-heptadecane in Lonar sediment samples (Fig. 3.3b and d) suggests a common origin, either from the same species or from a microbial community. While there are no reports of a single organism producing both *n*-heptadecane and tetrahymanol, we hypothesize that tetrahymanol-producing ciliates feed on cyanobacteria synthesizing *n*-heptadecane. The absence of algal sterols from sediments and algae in the lake floating mats (Surakasi et al., 2010) also points to bacterivory of the ciliates and their possible dependence on a cyanobacterial food source.

Another possible source of tetrahymanol is the purple non-sulfur bacterium *Rhodopseudomonas palustris* (Kleemann et al., 1990). Gene sequences belonging to purple non-sulfur bacteria have also been detected in mats from Lonar Lake (Surakasi et al., 2010). Purple non-sulfur bacteria could co-occur with cyanobacteria in the mats and as such could also be an additional source of tetrahymanol in the lake sediments. *n*-Heptadecane is produced by a variety of algae and phototrophic bacteria (Cranwell et al., 1987). It occurred in large amount in Lonar Lake floating microbial mats (see Fig. 3.6) and in POM. In addition, β -carotene, the second most abundant compound in the sediments, is

prominent in primary producers such as cyanobacteria (Bullerjahn and Sherman, 1986; Masamoto et al., 1987).

Another bacterial biomarker in the lake sediments and benthic mats was diploptene (Kannenberg and Poralla, 1999), which can be produced by the same organisms synthesizing tetrahymanol (from defunctionation of diplopterol, an isomer of tetrahymanol; Venkatesan, 1989). Diploptene and moretene have also been identified in soils (Prahl et al., 1992) and in soil-bacteria (Rosa-Putra et al., 2001). However, the limited soil development around Lonar Lake due to the arid climate and the high concentrations of these compounds in the benthic mats, make a substantial input from soil in this case unlikely.

Diploptene has also been attributed to a methanotrophic origin (Rohmer et al., 1984). The occurrence of moretene, closely related to diploptene, is apparently also connected to the activity of methanotrophic bacteria (Uemura and Ishiwatari, 1995; Blumenberg et al., 2009). There are reports of methanotrophic and methylotrophic activity in the lake (Antony et al., 2010). However, on the basis of high $\delta^{13}\text{C}$ values for these biomarkers (Prasad et al., unpublished results) a methanotrophic origin for diploptene, moretene or tetrahymanol appears unlikely.

3.4.2.2 *Spatial patterns of aquatic biomarker abundance in sediments reflect nutrient supply*

The highest concentrations of the major aquatic biomarkers (tetrahymanol and carotenoids) were found on the eastern and western shores. Currently, the area near the eastern shore is heavily influenced by human activity as a result of agriculture in the alluvial fan. Due to the presence of one of the most active temples on the western shore of the crater (Fig. 3.1), human impact is significant.

It is therefore possible that anthropogenic activity increased nutrient supply to the lake and led to a proliferation in primary productivity (cyanobacteria) and hence benthic mat organisms feeding on the cyanobacteria, along the eastern shore and western shore. Consequently, human influence may at least be partly responsible for the extraordinarily high concentration of tetrahymanol in the nearshore samples.

It has been suggested that greater precipitation in the late 1980s and subsequent reduction in lake water salinity accompanied by nutrient loading was responsible for the algal bloom in the lake (Badve et al., 1993). Based on these few years of observations, the conclusion of a role of climate in eutrophication would be biased. Currently, data about lipid biomarkers from sediments over a considerable time period are lacking. The reduction in lake water salinity after the monsoon and the increased supply of nutrients to the lake during monsoonal rains may be responsible for these blooms on a seasonal basis.

3.4.3 *General implications for paleolimnological studies*

In general, we found substantial heterogeneity in biomarker composition in the surface sediments, which was, however, averaged in the center of the lake, in particular for leaf wax *n*-alkanes. Nevertheless, the results have implications for a robust paleolimnological interpretation of biomarker distributions and abundance in lacustrine sediments. The finding that aquatic biomarkers, such as tetrahymanol and carotenoids were concentrated mainly in nearshore samples

and showed much lower concentration in the central part of the lake, where a deep sediment core would be taken, has implications for the interpretation of downcore changes in the abundance of these lipids. For example, a change in lake level and consequently shoreline proximity of the central core location could change the concentration of these biomarkers, without any change in the productivity of the source organisms. Therefore, unlike terrigenous biomarkers, lake level fluctuation may potentially affect aquatic lipid biomarker abundance in lacustrine sediments, in addition to source changes.

On the other hand, terrestrial biomarkers showed a slightly different distribution depending on location, which was likely influenced by different plant sources. As such, a change in long chain (leaf wax) *n*-alkane composition or ACL index in the sediment core could be due to a change in source/transport of these biomarkers without any change in catchment vegetation. Similar results that certain proxies better represent catchment-scale variability compared with others, have also been observed from investigation of the spatial heterogeneity of lake sediments proxies (Dong et al., 2012), but other than lipid biomarkers. We therefore suggest that, in order to reliably interpret changes in lipid biomarker distributions from a downcore record, the factors governing their distribution in the modern lake environment should be thoroughly studied.

3.5 Conclusions

We conducted a study to understand the origins of heterogeneity of lipid biomarker distributions in lake surface sediments from Lonar Lake and have shown that aquatic and terrestrial lipid biomarkers provide a detailed picture of the lake ecosystem and its catchment area.

The major plants from dry deciduous mixed forest type produced a greater amount of leaf wax *n*-alkanes and a greater fraction of *n*-C₃₁ and *n*-C₃₃ alkanes relative to *n*-C₂₇ and *n*-C₂₉. The relatively high ACL values (29.6–32.8) for these plants seem common for vegetation from an arid and warm climate.

The composition of leaf wax lipids such as long chain *n*-alkanes in sediments represents the distribution of these compounds in the catchment vegetation. The similarity in average ACL values for vegetation and sediments and the lower variability found in the sediments compared with modern plants, highlights the integrative capacity of lake sediments for these compounds.

The triterpene tetrahymanol, representative of a specific microbial community, occurred in unusually large amount in surface sediment and benthic microbial mat samples. Due to its spatial distribution in the lake surface sediments, we conclude that it was derived from benthic microbial mats growing in nearshore areas. Other biomarkers, such as diploptene and carotenoids, may be also related to this mat ecosystem in the lake. On the contrary, *n*-heptadecane originated from floating microbial mats in the lake. Additionally, we conclude that increased primary productivity may be related to human influence causing, an unusually high concentration of tetrahymanol, especially in the nearshore lake sediments.

Our results indicate that a single core from the depocentre of the lake best represents the average variability in terrigenous biomarkers in the lake basin. However, our study also shows that other factors, such as lake level fluctuation may affect the abundance of aquatic biomarkers in a core from a central location within the lake and should be taken into account for a valid paleolimnological

interpretation of sediment core data.

3.6 Acknowledgements

This research was supported by the DFG-Graduate School 1364/1 “Interactions between Tectonics, Climate and Biosphere in the African-Asian monsoonal region” of the University of Potsdam, funded by the German Science Foundation (DFG). We thank M. Strecker, acting representative of the Graduate School, for constant support. We also thank all those who provided help during field and laboratory work, especially K. Deenadayalan, P. Menzel, Md. Arif and S. Pinkerneil. Additionally cooperation from the Forest and Wildlife Department of Maharashtra State, India is gratefully acknowledged. D.S. was supported by an Emmy-Noether Grant of the DFG (SA1889/1-1).

Finally we would like to thank two anonymous reviewers for helpful and constructive comments on the paper.

4. Monsoon source shifts during the drying mid-Holocene: biomarker isotope based evidence from the core ‘monsoon zone’ (CMZ) of India

Saswati Sarkar^a, Sushma Prasad^a, Heinz Wilkes^b, Nils Riedel^c, Martina Stebich^c, Nathani Basavaiah^d, Dirk Sachse^a

^aInstitute for Earth- and Environmental Science, University of Potsdam, Karl-Liebknecht-Straße 24–25, 14476 Potsdam, Germany.

^bSection 4.3, Organic Geochemistry, Helmholtz Centre Potsdam GFZ German Research Centre for Geosciences, Telegrafenberg, D-14473 Potsdam, Germany.

^cSenckenberg Research Institute, Research Station of Quaternary Palaeontology, Am Jakobskirchhof 4, D-99423 Weimar, Germany.

^dIndian Institute of Geomagnetism, New Panvel, Navi Mumbai, India.

Submitted to Quaternary Science Reviews

Abstract

A better understanding of past variations of the Indian Summer Monsoon (ISM), that plays a vital role for the still largely agro-based economy in India, can lead to a better assessment of its potential impact under global climate change scenarios. However, our knowledge of spatiotemporal patterns of ISM strength is limited due to the lack of high-resolution, continental paleohydrological records. Here, we reconstruct centennial-scale hydrological variability during the Holocene associated to changes in the intensity of the ISM based on a record of lipid biomarker abundances and compound-specific stable isotopic composition of a 10 m long sediment core from saline-alkaline Lonar Lake, situated in the core ‘monsoon zone’ of central India.

We identified three main periods of distinct hydrology over the Holocene in central India. The period between 10.1 and 6 cal. ka BP was likely the wettest during the Holocene. Lower ACL (average chain length) index values (29.4 to 28.6) of leaf wax n-alkanes and their negative $\delta^{13}\text{C}$ values (-34.8‰ to -27.8‰) indicate the dominance of woody C_3 vegetation in the catchment, and negative δD_{wax} values (-171‰ to -147‰) argue for a wet period due to an intensified monsoon. After 6 cal. ka BP, a gradual shift to less negative $\delta^{13}\text{C}$ values for n-alkanes (particularly for the grass derived n- C_{31}) and appearance of the triterpene lipid tetrahymanol, generally considered as a marker for salinity and water column stratification, mark the onset of drier condition. At 5.1 cal. ka BP increasing flux of leaf wax n-alkanes along with the highest flux of tetrahymanol indicate a major lowering of the lake level. Rapid fluctuations in abundance of both terrestrial and aquatic biomarkers between 4.8 and 4 cal. ka BP indicate an unstable lake ecosystem, culminating in a transition to arid conditions. A pronounced shift to less negative n-alkane $\delta^{13}\text{C}$ values, in particular for n- C_{31} (-25.2‰ to -22.8‰), over this period indicates a change of dominant vegetation to C_4 grasses. Along with a 40% increase in leaf wax n-alkane δD values, which likely resulted from less rainfall and/or higher plant evapotranspiration, we interpret this period to reflect the driest conditions in the region during the last 10.1 ka. This transition led to protracted late Holocene arid conditions and the presence of a permanent saline lake, supported by the high abundance of tetrahymanol. A late Holocene peak of cyanobacterial biomarker input at 1.3 cal. ka BP might represent an event of lake

eutrophication, possibly due to human impact and the onset of cattle/livestock farming in the catchment.

A unique feature of our record is the presence of a distinct transitional period between 4.8 and 4 cal. ka BP, which was characterized by very variable δD_{wax} values and tetrahymanol flux. Variable δD_{wax} values possibly represent a shift in monsoon moisture sources or seasonality between the wet early Holocene and the dry late Holocene. We hypothesize that orbital induced weakening of the summer solar insolation and associated reorganization of the general atmospheric circulation led to an unstable hydroclimate during the mid-Holocene, with frequent change in precipitation source or seasonality.

Our findings shed light onto the sequence of changes during mean state changes of the monsoonal system, once an insolation driven threshold has been passed, and show that small changes in solar insolation can be associated with major hydroclimate changes, a scenario that may be relevant with respect to future changes in the ISM system.

Keywords: Indian Summer Monsoon; Holocene; Lonar Lake; lipid biomarkers; compound-specific stable isotopic composition

4.1 Introduction

The Indian monsoon is an important component of the Earth's climate system. More than 15% of the world's population lives in areas affected by the monsoon. Rainfall from the Indian summer monsoon (ISM) was and still is largely responsible for the development and sustenance of the largely agro-based economy on the Indian subcontinent (Gadgil et al., 2005). The ISM is predicted to change under global warming (Goswami et al., 2006a; Malik et al., 2012), but the magnitude and regional consequences of these changes are uncertain (Ghosh et al., 2011). Thus, knowledge of the magnitude and timing of past ISM variation on regional scales is crucial to better predict its response to anthropogenic climate change (Prasad et al., 2014). Marine as well as continental records, mainly from the peripheral realm of the ISM, have indicated a largely insolation-driven smooth transition from early Holocene wet to late Holocene arid conditions (Fleitmann et al., 2003; Gupta et al., 2003; Fleitmann et al., 2007; Ponton et al., 2012). However, no high-resolution Holocene records from continental archives exist, particularly from the core 'monsoon zone' (CMZ), (MZ: Gadgil, 2003), that allows to evaluate the nature of this transition on land. Here, we reconstruct centennial-scale hydrological variability associated to changes in the intensity of the ISM over the Holocene, based on aquatic and terrestrially sourced lipid biomarkers and their stable carbon and hydrogen isotopic composition ($\delta^{13}\text{C}$ and δD values), of a 10 m long sediment core from saline-alkaline Lonar Lake (Fig. 4.1). Lonar Lake lies in the CMZ in central India and is currently the only lake providing a continuous Holocene sediment record in this region (Prasad et al., 2014).

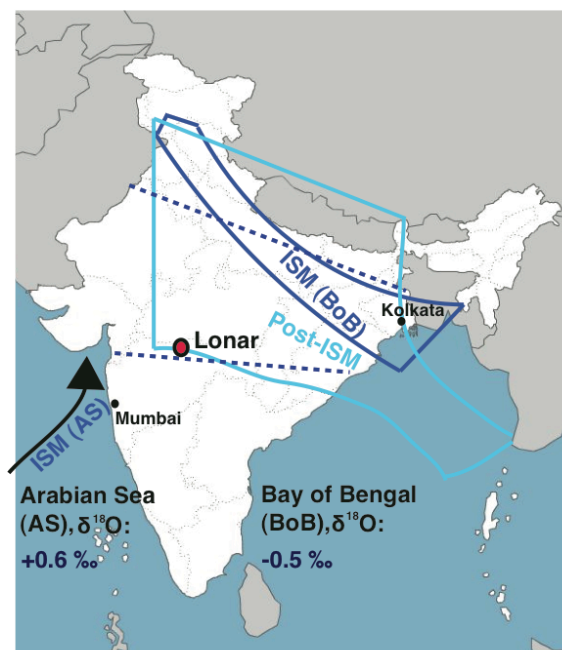


Fig. 4.1. Location of Lonar crater lake in the ‘monsoon zone’ (Gadgil, 2003) marked by the blue dashed line. Envelopes in dark and light blue represent storm-tracks from Bay of Bengal (BOB) in monsoon and post-monsoon, respectively; the smaller arrow represents the Arabian Sea (AS) branch (modified after Sengupta and Sarkar, 2006). Modern seawater $\delta^{18}\text{O}$ values are indicated for Arabian Sea and Bay of Bengal (from Kumar et al., 2010).

The general trends in the temporal development of the ISM are well known for the Indian Ocean basins based on the analysis of several marine sediment cores (Fleitmann et al., 2003; Gupta et al., 2003; Fleitmann et al., 2007), revealing a significant decrease in monsoon strength around 5–4.5 cal. ka BP and protracted arid conditions during the late Holocene. In contrast, the associated changes in continental hydrology and ecosystems are not explored. In our present study we apply organic geochemical proxies on a sediment core from the closed-basin precipitation fed Lonar Lake, to assess the consequences of the change in ISM mean state at around 5–4 ka BP, directly on the Indian subcontinent.

From previous multi-proxy investigations on the same sediment core from Lonar Lake, which we investigate here, two phases of severe aridity (between 4.6–3.9 and 1.5–0.6 cal. ka BP) have been identified following an early Holocene wet phase (Prasad et al., 2014). In addition, these available data on Holocene climate changes (Prasad et al., 2014) as well as investigations of the modern catchment and lake environment (Menzel et al., 2013; Basavaiah et al., 2014; Sarkar et al., 2014; Menzel et al., (under revision)) provide us with a well-constrained modern framework in which the biomarker and isotope data can be interpreted.

In this study we specifically focus on the transition from wet to dry conditions during mid-Holocene to obtain additional information on monsoon hydrology during the change from early Holocene wet to late Holocene dry conditions.

4.1.1 Organic geochemical proxies as indicators of paleoclimate changes

4.1.1.1 Biomarkers

The potential to separate the aquatic and terrestrial response of lake ecosystem changes using techniques such as elemental and isotope geochemistry as proxies is limited since bulk sediments represent a mixture of many components (Krishnamurthy et al., 1995). Among newer techniques, lipid biomarkers and their stable isotope ratios have recently been applied in investigating the hydrological changes. Due to higher source-specificity of individual compounds relative to bulk material/sediment, the analysis of biomarkers from lake sediments has become a useful tool for studying terrestrial ecology and environment (Castañeda and Schouten, 2011). In addition to the information about sources of the biomarkers, the analysis of their temporal distribution in lake sediments can provide insight into changes in lake and catchment ecosystem and hydrology over time (Schwark et al., 2002; Romero-Viana et al., 2012).

For example, long chain *n*-alkanes (with 27 to 35 carbon atoms) are produced as leaf wax constituents of terrestrial higher plants but also of emerged macrophytes growing in the lake (Eglinton and Hamilton, 1967; Cranwell et al., 1987; Ficken et al., 2000; Gao et al., 2011). Changes in the abundance of leaf wax compounds can be used mainly as proxies for transport of terrigenous OM to the lake (Meyers, 2003). The average distribution of long chain *n*-alkanes differs between plant types, especially among C₃ trees, grasses and C₄ grasses (Eglinton and Eglinton, 2008). Average ACL index values of C₃ trees and grasses for tropical vegetation from southern Africa varied between 29.43 ± 0.70 and 30.01 ± 0.93 respectively whereas C₄ grasses showed higher ACL values of 31.26 ± 0.98 , (Rommerskirchen et al., 2006). Therefore changes in ACL can potentially record changes in vegetation type such as trees and grasses, which would be prominent for a change between C₃ trees and C₄ grasses. For the aquatic component, compositional variations in aquatic lipids can be used to assess changes in the lake ecosystem. For example, variations in the abundance of the cyanobacterial biomarkers, such as *n*-heptadecane can be used as proxies for changes in primary productivity.

Based on previous work on modern surface sediments from the Lonar Lake we have assessed processes that control the distribution of leaf wax *n*-alkanes or aquatic biomarkers, respectively (Sarkar et al., 2014). For example, strong surficial erosion in the catchment due to sparse vegetation cover may result in higher flux of leaf wax compounds whereas lake level fluctuation may potentially affect aquatic biomarker distributions in lacustrine sediments.

Abundant biomarkers of aquatic origin in modern Lonar Lake sediments are tetrahymanol, diploptene and moretene, likely derived from a benthic bacterial mat community whereas the major source of *n*-heptadecane seemed to be floating cyanobacterial mats (Sarkar et al., 2014). Among different biological origins of tetrahymanol (Prasad et al., 2014 (suppl. mat.); Sarkar et al., 2014), predatory ciliates appear to be the most relevant in sedimentary records (Mallory et al., 1963; Harvey and McManus, 1991) and in Lonar Lake surface sediments (Sarkar et al., 2014). A similar distribution of tetrahymanol and moretene/diploptene in Lonar surface sediment samples suggested a common origin, either from the same species or from a microbial community.

4.1.1.2 Carbon and hydrogen isotopes

The analysis of the stable carbon and hydrogen isotopic composition of these biomarker compounds (expressed as $\delta^{13}\text{C}$ and δD values) has emerged as a powerful tool that can provide detailed insights into ecosystem and hydrological development (Tierney et al., 2008; Rach et al., 2014).

With the help of $\delta^{13}\text{C}$ values of long chain *n*-alkanes changes in vegetation (e.g., C_3 trees/ C_4 grasses) can be detected (Sinninghe Damsté et al., 2011), since $\delta^{13}\text{C}$ values of these leaf wax compounds clearly differ between C_3 and C_4 plants (Rommerskirchen et al., 2006; Tipple and Pagani, 2010) due to differences in the carbon assimilation pathways (Eglinton and Eglinton, 2008). From $\delta^{13}\text{C}$ values of aquatic biomarkers the carbon source of individual compounds and carbon cycling through the ecosystem can be assessed. $\delta^{13}\text{C}$ values of lipids from primary producers, such as cyanobacteria, would reflect carbon isotopic composition of DIC (dissolved inorganic carbon), which can be affected by factors such as productivity or salinity (alkalinity) in the lake. On the other hand $\delta^{13}\text{C}$ values of lipids from heterotrophic organisms would reflect carbon isotopic composition of their food sources.

δD values of biomarkers are increasingly applied as a proxy to detect changes in paleohydrology, as the ultimate hydrogen source of any photosynthetic organism is environmental water. As such, δD values of leaf wax biomarkers can be used to detect changes in the processes that affect the isotopic composition of precipitation, such as moisture source or rainfall amount. Recent research has shown that leaf wax lipid δD values can additionally be affected by evapotranspiration in soils (Smith and Freeman, 2006) and higher plants leaves (Kahmen et al., 2013a; Kahmen et al., 2013b). Differences in photosynthetic pathways (C_3 and C_4) used by plants and plant functional types (such as trees, shrubs or grasses) can lead to distinct δD values among plants growing at the same location under the same climatic condition (Sachse et al., 2012). δD values of biomarkers derived from aquatic organisms in general also record the δD values of the water source used by the organism, but can additionally be affected by processes such as salinity or growth rate (Sachs, 2014).

4.1.2 Study site, modern hydrology and vegetation

Lonar Lake in central India ($19^\circ 58'\text{N}$, $76^\circ 30'\text{E}$; Buldhana district, Maharashtra State, India) lies within a small crater (diameter: 1.8 km; depth: 150 m) and was formed by a meteorite impact on the Deccan trap basalts (Fredriksson et al., 1973). The site is extensively described in Prasad et al. (2014) and Sarkar et al. (2014). Briefly, Lonar Lake is small (diameter: 1.2 km; depth: 5 m) and alkaline–saline (pH 10.5, salinity 10.5; La Touche, 1912; Jhingran and Rao, 1958; Nandy and Deo, 1961). The lake is located in the semi-arid region of central India, with an average annual rainfall of 760 ± 50 mm. Two general climatic periods, due to seasonality in the monsoon system, are: (i) a wet season from June to the end of September (summer monsoon/southwest monsoon), with an average rainfall of 670 ± 40 mm and (ii) a dry season from early October to June.

Belts of thornshrub and dry deciduous mixed forest characterize the crater rim. The aquatic biocenosis predominantly consists of floating cyanobacterial mats and emerged macrophytes, which are abundant mainly near an alluvial fan in the NE of the crater.

4.2 Material and methods

4.2.1 Sediment core and age model

In May-June 2008 a 10 m long composite core was retrieved from Lonar Lake during a joint scientific expedition between IIG, Mumbai and GFZ, Potsdam. The core was retrieved at a water depth of 5.4 m, using a UWITEC Sediment Piston corer (Anoop et al., 2013b; Prasad et al., 2014).

The core chronology/age model is based on ^{14}C AMS dating of wood, leaf, gaylussite and bulk material from the core sediment (Anoop et al., 2013b; Prasad et al., 2014).

4.2.2 Sample preparation and lipid biomarker analysis

For extraction of lipid biomarkers, the sediment core was sub-sampled initially for every 10 cm, resulting in 44 samples. Later 26 additional subsamples were included to improve sampling resolution during the transitional period (4.8–4 cal. ka BP) and also the early Holocene period. Subsamples of 2 cm thickness represented a time span ranging from 8–20 years until 5.1 cal ka to 60–120 years in older sediments.

Ca. 2–4 g of sample, freeze-dried and homogenized, were extracted using an accelerated solvent extractor (Dionex ASE 350) with a mixture of dichloromethane (DCM)/methanol (9:1) at 100 °C and 103 bar (1500 psi) for 15 min in 2 cycles. After removal of elemental sulphur (passing through activated copper pipette columns) and addition of internal standards (5 α -androsterane, 5 α -androstan-3 β -ol and erucic acid) the total extracts were separated on SPE silica gel columns (ca. 2 g of silica gel 60, 230–400 mesh) into three fractions of different polarity, namely an aliphatic hydrocarbon (eluted with 10 ml of *n*-hexane), an alcohol (eluted with 15 ml of DCM/acetone (9:1)) and a fatty acid fraction (eluted with 10 ml of DCM/methanol (5:1)).

Major alcohols, like tetrahymanol, were present in very high concentrations and could be analyzed without derivatization on our GC-MS system. Fraction one and two (containing aliphatic hydrocarbons and alcohols, respectively) were measured on a GC-FID/MSD system for compound identification and quantification. The GC-FID/MSD system consisted of an Agilent 7890A gas chromatograph equipped with a flame ionization detector (FID) and an Agilent 5975C mass selective detector. The system used a programmable temperature vaporization (PTV) inlet with split injection (5:1), a capillary column (Agilent DB-5MS) (length 30 m, inner diameter 0.25 mm and film thickness 0.25 μm) with helium as carrier gas. 1 μl of the sample was injected into the GC. The temperature of the injector was 70 °C and after 2.5 min the temperature was increased at 720 °C/min to 300 °C; while the temperature of the GC oven was kept constant for 2 min at 70 °C initially. Subsequently the oven was heated to 280 °C at 7 °C/min and then to 320 °C at 3 °C/min (15 min isothermal). Identification of compounds was based on comparison of mass spectra with published data.

4.2.3 Compound-specific stable carbon and hydrogen isotope analysis

The stable isotope composition of long chain *n*-alkanes was measured on 32 samples (for $\delta^{13}\text{C}$) and 36 samples (for δD). Since the study focus was on the analysis of *n*-alkane δD values, not all samples could be analyzed for their $\delta^{13}\text{C}$ values as well, since sample material was exhausted. The stable isotope composition of *n*-heptadecane could be determined on 27 samples (for $\delta^{13}\text{C}$) and 24 samples (for δD). The stable isotope composition of tetrahymanol was measured on 8 samples (for $\delta^{13}\text{C}$, δD).

The stable carbon isotope composition ($\delta^{13}\text{C}$) of biomarkers was measured on a GC system (Agilent 6890N) coupled via combustion interface (GC-C III), to a Thermo Scientific MAT 253 isotope ratio mass spectrometer (GC-irm-MS). The system was equipped with a programmable temperature vaporization (PTV) inlet using split injection (1:1) and a fused silica capillary column (Agilent Ultra1) (length 50 m, inner diameter 0.2 mm and film thickness 0.33 μm). Helium was used as carrier gas. 1–3 μl of the sample were injected into the GC. The temperature (T) programs for the injection and GC oven/column were as follows: PTV injector T-program: 230 $^{\circ}\text{C}$ (Start-T), with 700 $^{\circ}\text{C}/\text{min}$ up to 300 $^{\circ}\text{C}$ (hold for the complete run); Oven T-program: 40 $^{\circ}\text{C}$ (Start-T) hold for 2 min. with 4 $^{\circ}\text{C}/\text{min}$ up to 300 $^{\circ}\text{C}$ (hold for 45 min).

For tetrahymanol, the system was equipped with a PTV inlet using split injection (1:1) and a fused silica capillary column (BPX5) (length 50 m, inner diameter 0.2 mm and film thickness 0.25 μm). Helium was used as carrier gas. 3 μl of the sample were injected into the GC. The temperature (T) program for GC oven/column was as follows: 80 $^{\circ}\text{C}$ (Start-T) hold for 1 min, with 15 $^{\circ}\text{C}/\text{min}$ up to 250 $^{\circ}\text{C}$, 1 $^{\circ}\text{C}/\text{min}$ up to 310 $^{\circ}\text{C}$ (hold for 15 min).

GC-irm-MS analyses were run in triplicate. Calibration of isotope analysis was performed by injecting several pulses of CO_2 at the beginning and at the end of each GC run. Isotopic ratios are expressed as $\delta^{13}\text{C}$ values in per mil. $\delta^{13}\text{C}$ values of compounds measured in laboratory reference scale are converted to the Vienna Pee Dee Belemnite (V-PDB) scale using a linear regression function derived from the relationship of measured values and known values in V-PDB scale, for the compounds of a certified standard between sample runs. The average standard deviation for standards over sequences was between 0.5 and 1.8 and for samples it was 0.5.

The stable hydrogen isotope composition (δD) of biomarkers was measured on a GC system (Agilent 6890N) coupled via pyrolysis interface to a Thermo Scientific Delta V Plus isotope ratio mass spectrometer (GC-irm-MS). The system was equipped with a PTV inlet using split injection (1:3) and a fused silica capillary column (Agilent Ultra1) (length 50 m, inner diameter 0.2 mm and film thickness 0.32 μm). Helium was used as carrier gas. 1–3 μl of the sample were injected into the GC. The temperature (T) programs for the injection and GC oven/column were as follows: Injector T-program: 230 $^{\circ}\text{C}$ (Start-T), with 700 $^{\circ}\text{C}/\text{min}$ up to 300 $^{\circ}\text{C}$ (hold for the complete run); Oven T-program: 40 $^{\circ}\text{C}$ (Start-T) hold for 2 min. with 4 $^{\circ}\text{C}/\text{min}$ up to 300 $^{\circ}\text{C}$ (hold for 45 min).

For tetrahymanol, the system was equipped with a PTV inlet using split injection (1:1) and a fused silica capillary column (DB-FFAP) (length 60 m, inner diameter 0.25 mm and film thickness 0.25 μm). Helium was used as carrier gas. 3 μl of the sample were injected into the GC. The temperature (T) program for GC

oven/column was as follows: 80 °C (Start-T) hold for 1 min, with 15 °C/ min up to 250 °C, 1 °C/ min up to 310 °C (hold for 15 min).

GC-irm-MS analyses were run in triplicate. Calibration of isotope analysis was performed by injecting several pulses of H₂ at the beginning and at the end of each GC run. Isotopic ratios are expressed as δD values in per mil. δD values of compounds measured in laboratory reference scale are converted to the Vienna Standard mean ocean (VSMOW) scale using a linear regression function derived from the relationship of measured values and known values in VSMOW scale, for the compounds of a certified standard between sample runs. The average standard deviations for standards and samples were 3.

4.2.4 Precipitation, isotope data and backward trajectory analysis

Currently stable isotope data for precipitation are not available from the Lonar region but from the adjacent Sagar region (23°49'N, 78°45'E, 551 m a.s.l.), Madhya Pradesh (ca. 486 km NE of Lonar). Monthly rainfall data for the Sagar station (WMO code: 42671) is archived in the database of the Global Historical Climate Network (GHCN version 2), available at Climate Explorer of the Royal Netherlands Meteorological Institute (climexp.knmi.nl). Rainfall isotope data from Sagar is provided by IAEA/WMO (Global Network of Isotopes in Precipitation GNIP database; isohis.iaea.org) and also published in Kumar et al. (2010).

In order to determine the moisture source areas and their isotope fingerprint for Sagar an ensemble of backward air mass trajectories has been calculated using the Hybrid Single-Particle Lagrangian Integrated Trajectories (HYSPLIT) ARL trajectory tool database of NOAA. Trajectories for time periods of 96 h were computed at the lower troposphere (1500 m a.s.l.) for the pre-monsoon, the monsoon (ISM), and the post-monsoon seasons, for the years with existing precipitation isotopes data (2003 to 2005).

4.2.5 Pollen analysis

Pollen analysis was undertaken on 125 samples representing a temporal resolution of 100 to 150 years from 9,130 to 5,000 BP and 40 years between 5,000 and 0 years BP. Sediment samples were prepared using KOH; HCL; HF and hot acetolysis-mixture. All samples were sieved with 200 and 5 μ m mesh gauze. At least 600 pollen grains were counted per sample. Identification of palynomorphs is based on Nayar (1990); Tissot et al. (1994); the web-based pollen atlas for the Australasian realm (APSA Members 2007); and the pollen collection for south Asia at Senckenberg Research Station of Quaternary Palaeontology, Weimar, Germany.

4.3 Results

4.3.1 Higher terrestrial plant biomarkers

4.3.1.1 Abundance and distribution of leaf wax *n*-alkanes in the core

Long chain *n*-alkanes (C₂₅ to C₃₅) were abundant throughout the core. Since sedimentation rate varied in the sediment core (Prasad et al., 2014) we express

the abundance of compounds as annual fluxes, i.e., concentrations normalized to sediment amount and deposition time [$\mu\text{g/g}$ dry sediment/year].

The total flux of leaf wax *n*-alkanes (summed flux of major (odd-numbered) long chain *n*-alkanes with 25 to 35 carbons) was stable and low at ca. 0.2 $\mu\text{g/g}$ dry sediment/yr. from 10.1 cal. ka BP to 5.2 cal. ka BP. The flux abruptly increased to values up to 1.2 $\mu\text{g/g}$ dry sediment/yr. at 5.1 cal. ka BP. A higher flux of leaf wax *n*-alkanes persisted until recent time, however, with few lower values shortly in between (at 4.3 and 0.2 cal. ka BP and between 3.5 to 2.9 cal. ka BP) (Fig. 4.2c).

The ACL index (concentration weighted average chain length for *n*-alkanes, $\sum n \times C_n / \sum C_n$, where *n* = number of carbons; here *n* = 25–35 and *C_n* = concentration of the *n*-alkane) remained relatively low and varied between 28.6 and 29.4, from 10.1 to 4.8 cal. ka BP. The ACL index showed a slight increasing trend reaching values up to 31.0 from 4 cal. ka BP onwards, with intervening periods of lower values as 28.4, 29.2 and 29.5 at 3.5, 1.3 and 0.3 cal. ka BP, respectively (Fig. 4.2d).

Between 4.6 and 4.1 cal. ka BP the ACL index varied significantly from 29.8 to 28.2.

4.3.1.2 Stable carbon isotopic composition ($\delta^{13}\text{C}$) of long chain *n*-alkanes in the core

Here we report $\delta^{13}\text{C}$ values of major *n*-alkanes with 27, 29 and 31 carbon atoms. While overall trends of changes in *n*-alkane $\delta^{13}\text{C}$ values were consistent, significant differences in the temporal variations of $\delta^{13}\text{C}$ values for the individual homologues existed. Over the core, long chain *n*-alkane $\delta^{13}\text{C}$ values showed similar covariance among each other (i.e., *n*-C₂₇ with *n*-C₂₉ and *n*-C₃₁) (correlation coefficient (*r*): *r* = 0.7, *p* < 0.05). $\delta^{13}\text{C}$ values of *n*-C₂₇, *n*-C₂₉ and *n*-C₃₁ were consistently more negative (–34.5‰ to –27.8‰) from 10.1 to 4.8 cal. ka BP. From 4.8 ka BP onwards the $\delta^{13}\text{C}$ values of the individual compounds showed markedly different responses. $\delta^{13}\text{C}_{\text{C}_{27}}$ values increased towards less negative values (up to –23.8‰) between 4.8 and 4 cal. ka BP and remained at these values until today. $\delta^{13}\text{C}_{\text{C}_{29}}$ values showed less variability over the core. While more negative (–33.3‰ to –29.1‰) from 10.1 until 5.1 cal. ka BP they increased to values of –26.5‰ at 4.5 cal. ka BP before decreasing again to values around –28.2‰ which remained relatively constant until modern times. $\delta^{13}\text{C}_{\text{C}_{31}}$ values showed a prominent shift of ~12‰ from –34.8‰ to –22.7‰ after 6 cal. ka BP until 4.5 cal. ka BP and remained less negative (between –22.8‰ and –25.2‰) until 4 cal. ka BP (Fig. 4.2e), before decreasing again to values around –27.5‰, where they remained until today.

4.3.1.3 Stable hydrogen isotopic composition (δD) of long chain *n*-alkanes in the core

Here we report δD values of major *n*-alkanes with 27, 29 and 31 carbon atoms. Over the core, $\delta\text{D}_{\text{C}_{27}}$ values showed higher covariance with $\delta\text{D}_{\text{C}_{29}}$ values (*r* = 0.9, *p* < 0.05) than $\delta\text{D}_{\text{C}_{31}}$ (*r* = 0.7, *p* < 0.05). $\delta\text{D}_{\text{C}_{31}}$ values were enriched in D (ϵ : enrichment factor; difference of δD values; $\epsilon_{\text{C}_{31}-\text{C}_{27}}$ varied from ~ 35 to 4) until 2.2 cal. ka BP (Fig. 4.2f). $\delta\text{D}_{\text{C}_{27}}$ and $\delta\text{D}_{\text{C}_{29}}$ values were relatively stable between 9.9 to 5.7 cal. ka BP and varied between –145‰ to –160‰, with few very negative values (up to –177‰) in between. These values from $\delta\text{D}_{\text{C}_{27}}$ and $\delta\text{D}_{\text{C}_{29}}$ showed a shift to more negative values around –172‰ after 5.7 cal. ka BP but again

became less negative (-136‰) at 5.1 cal. ka BP. δD_{C27} and δD_{C29} values showed a shift from -175‰ to -135‰ from 5.1 to 4.4 cal. ka BP. These values became relatively stable around -122‰ to -141‰ from 3.5 cal. ka BP onwards (Fig. 4.2f). Between 4.4 and 4 cal. ka BP these values fluctuated between -145‰ and -180‰ .

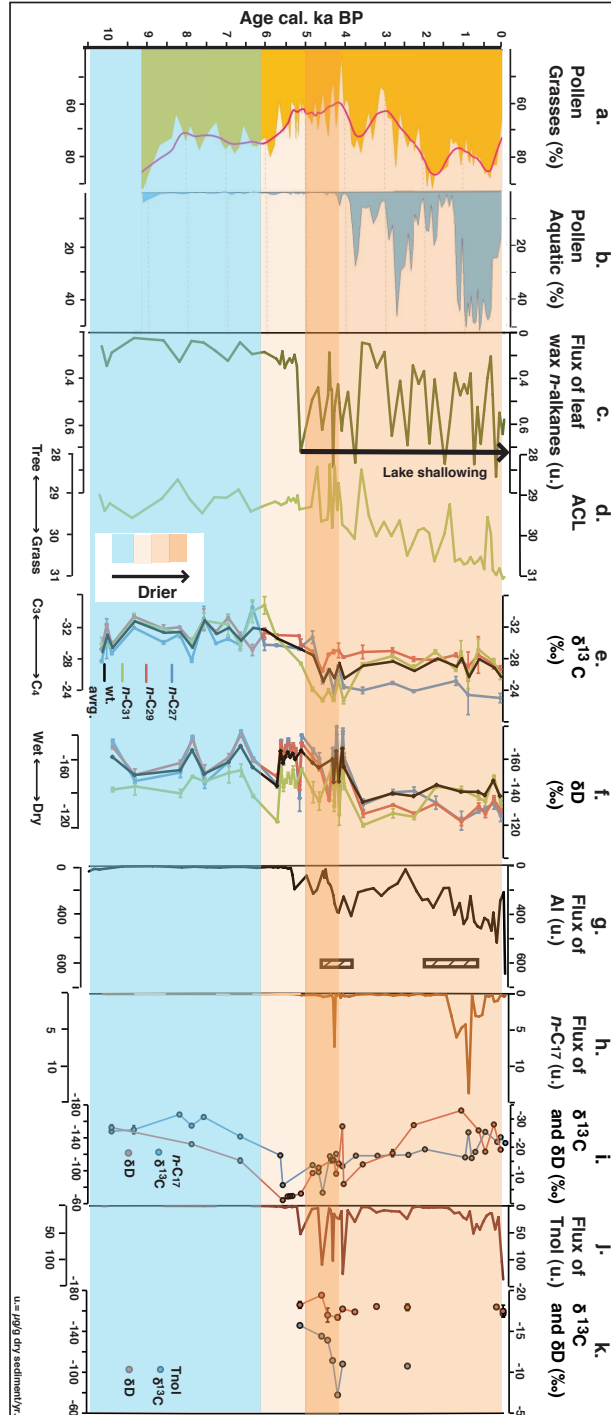


Fig. 4.2. Flux of major biomarkers and their stable isotopic composition ($\delta^{13}\text{C}$, δD) at Lonar Lake during the Holocene, along with other proxies (pollen and Al). a. abundance (%) of pollen from grasses, b. abundance (%) of pollen from aquatic plants, c. flux of leaf wax n -alkanes, d. ACL, e. $\delta^{13}\text{C}$ of long chain n -alkanes, f. δD of long chain n -alkanes and $\delta\text{D}_{\text{wax}}$, g. flux of Al (normal counts); boxes represent zones where evaporites (gaylussite crystals) were found (modified from Prasad et al., 2014), h. flux of $n\text{-C}_{17}$, i. $\delta^{13}\text{C}$ and δD of $n\text{-C}_{17}$, j. flux of total tetrahymanol (tnol), k. $\delta^{13}\text{C}$ and δD of tetrahymanol (tnol). Unit for fluxes of all biomarkers is $\mu\text{g/g}$ dry sediment/year.

4.3.2 Aquatic biomarkers

4.3.2.1 Abundance of aquatic biomarkers in the core

As for the leaf wax biomarkers, the abundance of all aquatic compounds has also been expressed as annual flux. Aquatic biomarkers were virtually absent (or present only in trace amounts) before 6 cal. ka BP.

Similar as observed in modern surface sediments from Lonar Lake (Sarkar et al., 2014) the most abundant biomarkers found in the upper core section were tetrahymanol and the corresponding ketone gammaceranone. Tetrahymanol was absent before 10.1 cal. ka BP and its concentration (and flux) started to increase only after ca. 6 cal. ka BP onwards. Tetrahymanol reached its first maximum abundance at 5.1 cal. ka BP with total (summed for tetrahymanol and gammaceranone) concentration and flux of 1060 $\mu\text{g/g}$ dry sediment and 52.3 $\mu\text{g/g}$ dry sediment/yr., respectively, which persisted until 3.7 cal. ka BP (Fig. 4.2j). Between 4.6 and 3.9 cal. ka BP total tetrahymanol concentrations and fluxes varied significantly and reached maximum values of up to ca. 1600 $\mu\text{g/g}$ dry sediment and 126 $\mu\text{g/g}$ dry sediment/yr., respectively. After continuing with lower values, tetrahymanol concentration (or flux) started to increase from 1.4 cal. ka BP onwards and reached values of 482 $\mu\text{g/g}$ dry sediment (137 $\mu\text{g/g}$ dry sediment/yr.) in recent times.

As in surface sediments (Sarkar et al., 2014), other major biomarkers of aquatic origin in the core included *n*-heptadecane, diploptene, moretene, fernene and carotenoids (Tab. B.1). Additionally, some compounds were observed in smaller amounts such as phytene, hopene, phytol and hopanol.

The flux of *n*-heptadecane (*n*-C₁₇) began to increase later compared to that of tetrahymanol, i.e., after ca. 5.1 cal. ka BP. *n*-Heptadecane showed peaks of very high concentration or flux of up to ca. 113 $\mu\text{g/g}$ dry sediment or 13.7 $\mu\text{g/g}$ dry sediment/yr., once at 4.2 cal. ka BP and between 1.3 to 0.5 cal. ka BP (Fig. 4.2h). During both periods, other short chain *n*-alkanes such as *n*-C₁₅, *n*-C₁₆ and *n*-C₁₈ were also identified in higher concentrations (up to 5.2, 2.8 and 1.1 $\mu\text{g/g}$ dry sediment respectively).

The flux of tetrahymanol was up to two orders of magnitude higher compared to that of moretene, diploptene, fernene, *n*-heptadecane and carotenoids, respectively (Tab. B.1).

Over the period from 6 cal. ka BP until today, the flux of tetrahymanol showed the highest covariance with that of moretene and diploptene (correlation coefficient (*r*): *r* = 0.8 and 0.9, *p* < 0.05), moderate covariance with that of fernene and phytene (*r* = 0.6 and 0.7, *p* < 0.05), and no significant covariance with *n*-heptadecane and carotenoids). While *n*-heptadecane and carotenoids showed a different pattern, diploptene, moretene, phytene and to some extent fernene showed a similar pattern of concentration/flux as of tetrahymanol over the core. *n*-Heptadecane showed a covariance with phytene (*r* = 0.4, *p* < 0.05) and no significant covariance with carotenoids and fernene.

4.3.2.2 Stable carbon isotope composition ($\delta^{13}\text{C}$) of aquatic biomarkers in the core

Although only measured on selected samples, with a focus to cover the transition between early and late Holocene, $\delta^{13}\text{C}$ of all the aquatic biomarkers in

the core showed less negative values ($> -30\text{‰}$). Further $\delta^{13}\text{C}$ of all the aquatic biomarkers in the core did not show any significant covariance with their respective concentrations/fluxes.

$\delta^{13}\text{C}$ values of tetrahymanol varied between -17.2‰ and -7.2‰ . We observed enrichment in ^{13}C (from -15.7‰ to -7.2‰) for tetrahymanol during the period between ca. 5.1 to 4 cal. ka BP (Fig. 4.2k).

$\delta^{13}\text{C}$ values of *n*-heptadecane varied between -31.6‰ and -3.9‰ . Enrichment in ^{13}C (from -17.1‰ to -6.6‰ and -13.7‰ to -3.9‰) of *n*-heptadecane was evident after 6 and 5.1 cal. ka BP, with a maximum value of -3.9‰ at 4.8 cal. ka BP (Fig. 4.2i). $\delta^{13}\text{C}$ values of *n*-heptadecane did not vary significantly between 4.5 and 0.8 ka BP with an average value of -17.5‰ .

4.3.2.3 Stable hydrogen isotope composition (δD) of aquatic biomarkers in the core

δD values of *n*-heptadecane varied substantially between -173‰ and -64‰ . As for $\delta^{13}\text{C}$ a trend of enrichment in D of *n*-heptadecane was also evident starting from 9.9 cal. ka BP. $\delta^{13}\text{C}$ and δD values for *n*-heptadecane showed covariance ($r = 0.8$, $p < 0.05$), with less negative $\delta^{13}\text{C}$ values corresponding to less negative δD values. The maximum enrichment in D revealed by less negative δD values (-64‰ to -72‰) was observed for *n*-heptadecane during the period between ca. 5.6 to 5.1 cal. ka BP (Fig. 4.2i). The period after until 4 cal. ka BP was characterized by more negative δD values of *n*-heptadecane, with the most negative value at 4.0 cal. ka BP (-154‰). Afterwards another trend in depletion in D continued until 1.0 cal. ka BP.

δD values of tetrahymanol from 5.1 cal. ka BP onwards, varied between -175‰ and -154‰ . A trend of enrichment in D of tetrahymanol was evident from 4.5 to 4.0 cal. ka BP (Fig. 4.2k).

4.4 Discussion

4.4.1 Environmental sensitivities of stable isotope based proxies

4.4.1.1 $\delta^{13}\text{C}$ values of leaf wax *n*-alkanes as an indicator of vegetation type and aridity

The stable carbon isotopic composition ($\delta^{13}\text{C}$) of leaf wax compounds (long chain *n*-alkanes) is determined by plant's specific photosynthetic pathway (such as C_3 and C_4) and the isotopic composition of atmospheric CO_2 (Farquhar et al., 1989) among other factors. Accordingly $\delta^{13}\text{C}$ values of leaf wax compounds have been used to reconstruct past changes in the abundance of C_3 vs. C_4 vegetation (Feakins et al., 2005; Eglinton and Eglinton, 2008). C_4 vegetation has an ecological advantage under aridity, high temperature, and low atmospheric CO_2 conditions over C_3 plants (Eglinton and Eglinton, 2008). Therefore, sedimentary leaf wax $\delta^{13}\text{C}$ records are often used as a proxy for aridity (Ponton et al., 2012). $\delta^{13}\text{C}$ values of leaf wax *n*-alkanes from Lonar Lake sediments might represent prevailing hydro-climate in the catchment, as reflected in dominant photosynthetic pathways used (such as C_3 vs. C_4).

4.4.1.2 δD values of leaf wax *n*-alkanes as indicator of *P-E* balance

The stable hydrogen isotopic composition (δD) of leaf wax compounds (long

chain *n*-alkanes) is determined by the δD values of plant (leaf) water, which in turn is controlled by δD values of environmental water (Sachse et al., 2012; Kahmen et al., 2013a; Kahmen et al., 2013b), which to a large extent is influenced by the moisture source and precipitation amount (especially in the tropics) (Dansgaard, 1964). Drier conditions therefore should result in D-enriched *n*-alkanes, because of less rainfall and stronger plant transpiration and vice versa. Therefore δD values of long chain *n*-alkanes from Lonar Lake sediments are expected to reflect the isotopic composition of precipitation, modified by evaporation. We interpret the variability of δD_{wax} values (concentration weighted average δD values of long chain *n*-alkanes) rather than individual δD values of long chain *n*-alkanes, as representing largely hydrological changes.

4.4.1.3 Variations in $\delta^{13}\text{C}$ values of aquatic biomarkers as a consequence of changes in lake water salinity

Cyanobacteria, which are the major source of *n*-heptadecane in Lonar lake sediments (Sarkar et al., 2014), are photosynthetic organisms. Therefore the carbon isotopic composition ($\delta^{13}\text{C}$) of *n*-heptadecane should reflect the carbon isotopic composition of dissolved inorganic carbon (DIC). Less negative $\delta^{13}\text{C}$ values of *n*-heptadecane would suggest a ^{13}C enrichment of lake water DIC. Lake water DIC can become enriched in ^{13}C as a result of increased primary productivity in an aquatic system, as this would preferentially remove ^{12}C into biomass and thus enrich ^{13}C in the lake water DIC (Meyers, 2003). However, in Lonar Lake sediments no covariance of flux and $\delta^{13}\text{C}$ values for *n*-heptadecane was observed, which would be expected under the above described scenario.

Another possible origin of the ^{13}C enriched carbon source for organisms producing *n*-heptadecane could be HCO_3^- ions in alkaline lakes that are characterized by less negative $\delta^{13}\text{C}$ values (Meyers, 2003). The unusual enrichment in ^{13}C observed for *n*-heptadecane can then be explained fully by the utilization of a ^{13}C -enriched carbon source by cyanobacteria indicating increasing lake water alkalinity and likely also salinity. Therefore changes in $\delta^{13}\text{C}$ values of *n*-heptadecane in Lonar Lake likely reflect lake water salinity and pH related changes in the lake water.

Since we interpret tetrahymanol as originating from predatory ciliates occurring in the biocenosis, it can be assumed that the carbon isotopic composition of this lipid would reflect the carbon isotopic composition of the utilized prey (i.e., bacteria and hence their carbon source). The similarity of $\delta^{13}\text{C}$ values of tetrahymanol and *n*-heptadecane, more so than with moretene-diploptene, suggests that tetrahymanol-producing ciliates depend, at least partly, on cyanobacteria synthesizing *n*-heptadecane.

4.4.1.4 Variations in δD values of aquatic biomarkers as consequence of change in lake water hydrology

The hydrogen isotopic composition of photosynthesizing organisms depends on the hydrogen isotopic composition of the lake water (fed by precipitation) (Sachse et al., 2012), where less negative δD values would reflect drier conditions through stronger lake water evaporation. However, salinity of the lake water exerts additional control on the hydrogen isotopic composition of cyanobacterial biomarkers via decrease of isotopic fractionation (between lipid and source water), resulting in even more deuterium enriched lipids (Sachse and Sachs,

2008), therefore amplifying the proxy response to dry conditions. Less negative δD values for *n*-heptadecane would indicate an influence of increased salinity. Higher growth rate of organisms can also exert an influence on the hydrogen isotopic composition of certain lipids via increase of isotopic fractionation (between lipid and source water), resulting in strongly deuterium-depleted lipids (Sachs, 2014). Since we observed unusually high concentrations for *n*-heptadecane over the period between 1.3 to 0.5 cal. ka BP, we consider growth rate changes of cyanobacteria could be relevant with respect to the abundance of their biomass deposited in a sediment sample integrating up to 20 years. Therefore more negative δD values for *n*-heptadecane, at times when *n*-C₁₇ concentrations in the sediment were high, might indicate an increase of isotopic fractionation (between lipid and source water), which could result from higher growth rate of their producers.

4.4.2 *Holocene climate (lake level) changes from biomarkers and their stable isotopes*

Based on stable isotope based proxies from biomarkers, we identified three periods of distinct hydrology over the Holocene.

4.4.2.1 *The early Holocene period between 10.1 and 6 cal. ka BP*

The early Holocene period between 10.1 and 6 cal. ka BP was characterized by most negative $\delta^{13}C$ values of leaf wax *n*-alkanes (-34.8% to -27.8%) in the studied sedimentary record, relatively low ACL values (29.4 to 28.6) and lower flux of long chain *n*-alkanes. These proxies indicate predominance of woody C₃ vegetation in the catchment. Reduced supply of terrigenous OM to the lake might imply less erosion in the catchment due to thicker vegetation cover and less transport of terrigenous OM into the lake due to higher water levels (Sarkar et al., 2014). δD_{wax} values of long chain *n*-alkanes were relatively constant with values of around -158% during this period. No biomarker evidence for halophilic microbial communities was found in this core section, which is prominent in the biomarker record of the modern lake (Sarkar et al., 2014). $\delta^{13}C$ values of *n*-C₁₇ were mostly low, with up to -31.6% , during the study period.

Together with previously published data from the Lonar Lake sedimentary record such as pollen and geochemical proxies (Prasad et al., 2014), these data indicate a positive precipitation-evaporation (P-E) balance in the catchment and a higher lake level, as a consequence of an intensified summer monsoon, in agreement with previous studies/ published data from the Indian Ocean basins (Fleitmann et al., 2003; Ponton et al., 2012).

4.4.2.2 *The mid-Holocene period between 6 and 4 cal. ka BP*

After ca. 6 cal. ka BP, a gradual shift to less negative $\delta^{13}C$ values (up to $\sim 12\%$), particularly for *n*-C₃₁, indicates a replacement of C₃ vegetation, development of open C₄ grassland and therefore onset of drier conditions. In addition an increasing flux of biomarkers like tetrahymanol at the same time likely marked the onset of saline conditions in the lake. An increase in lake water salinity/pH was also evident in proxies measured on bulk sediments (less negative $\delta^{13}C_{bulk}$ and $\delta^{15}N$ values) at ca. 6.2 cal. ka BP (Prasad et al., 2014).

After the onset of more arid conditions at ca. 6 cal. ka BP, we observed an

abrupt increase in the fluxes of leaf wax *n*-alkanes and tetrahymanol at 5.1 cal. ka BP (Fig. 4.2c and j). At 5.2 cal. ka BP an increase in detrital influx of aluminum (Al) (Fig. 4.2g) and an almost 8-fold increase in sedimentation rate was observed (Prasad et al., 2014). These proxies point to a drastic decrease in the lake level and as such in shoreline proximity of the coring location. The flux of tetrahymanol showed a significant correlation ($r = 0.5$, $p < 0.05$) with flux of Al. Therefore we hypothesize that higher transport of lipids from the shore in a smaller lake might be contributing to the large fluxes of these lipids.

The highest $\delta^{13}\text{C}$ and δD value of *n*-heptadecane (-3.9‰ and -64‰ respectively) observed at 5.5 cal. ka BP indicate likely the most alkaline and saline lake conditions and therefore suggest onset of the driest period. The time span between 4.8 and 4 cal. ka was characterized by the least negative $\delta^{13}\text{C}$ values for long chain *n*-alkanes (-22.7‰ to -25.2‰) and some less negative $\delta\text{D}_{\text{wax}}$ values ($\sim -140\text{‰}$) compared to the early Holocene, suggesting widespread occurrence of C_4 grasses and a negative (P-E) balance in the catchment. As such, this likely was the driest period in central India during the last 10.1 ka. The presence of a distinct zone of evaporitic carbonate (gaylussite) crystals between 4.6 to 3.9 cal. ka BP provides additional support for this interpretation (Anoop et al., 2013b, Prasad et al., 2014). Peak concentration and flux of the cyanobacterial biomarker *n*-heptadecane coincided with this drier period (at 4.3 cal. ka BP) and therefore possibly represented events of lake eutrophication, driven by more saline conditions: persistent saline conditions in the lake provided an opportunity for blooming of halophilic cyanobacteria in the ecological niche, reflected by unusually high fluxes of *n*-heptadecane. Carbon isotope values of tetrahymanol showed a steep trend of enrichment in ^{13}C during this period. While tetrahymanol δD values may reflect several hydrogen sources, since it is derived from non-photosynthetic organisms, it is interesting to note that the maximum enrichment in D and ^{13}C of tetrahymanol occurs at the same period (5–4 cal. ka BP), likely also reflecting the effect of lake water salinity on δD of tetrahymanol.

This period was also characterized by large swings in terrigenous as well as aquatic biomarker fluxes. To explain the fluctuations of biomarker proxy data two scenarios can be envisioned. First, proximity of the shoreline to the lake center reached its threshold limit and then a smaller decrease in lake level resulted in excessive supply of tetrahymanol from the lakeshore. Alternatively, this period was characterized by episodic but strong rainfall events, resulting in higher fluxes of tetrahymanol due to higher surficial erosion and nutrient supply from the catchment to the lake. Strong rainfall events causing stronger erosion could also result in higher fluxes of leaf wax *n*-alkanes. However due to the relatively low number of samples for this period, we cannot examine the covariance of fluxes of tetrahymanol with leaf wax *n*-alkanes.

An intriguing feature of the period 4.8–4 cal. ka BP is the high amplitude and rapid fluctuations in $\delta\text{D}_{\text{wax}}$ values between 20‰ and 40‰, sometimes over a period of only ca. 40 years. While short-term fluctuations may be an artifact of the higher sampling resolution during this period, counter intuitively we observed some of the most negative $\delta\text{D}_{\text{wax}}$ values during the Holocene (up to -180‰) during the driest period between 5 and 4 cal. ka BP. Since all other organic and inorganic proxy data from that period characterize it as the driest period during the Holocene it is unlikely that these changes in $\delta\text{D}_{\text{wax}}$ were a consequence of changes in evapotranspiration. In addition, to achieve a 40‰

difference in plant source water δD (i.e., leaf water) under similar temperatures would require a 50% change in relative humidity (Kahmen et al., 2013b), which would have resulted in contrasting humid and arid phases, which is not supported by any other proxy data during this period. Therefore, the only explanation for the high amplitude fluctuations in δD_{wax} during this period supported by multi-proxy data is a change in the isotopic composition of moisture and/or precipitation tracks, due to a different origin.

4.4.2.2.1 Monsoon source shifts during the drying mid-Holocene

Here we explore the possible mechanisms for changing moisture sources during the mid-Holocene. For example changing ENSO variability can result in changes in isotopic composition of moisture over India, with up to 2‰ increase in $\delta^{18}O$ values (i.e. $\sim 16‰$ in δD) during El Niño events (Ishizaki et al., 2012). ENSO activity was relatively weak before 4 ka BP (Moy et al., 2002; Rein et al., 2005; Conroy et al., 2008) but started to increase in frequency and intensity after 4 ka. However, more frequent El Niño events would have resulted in increasing precipitation δD values (Ishizaki et al., 2012) during that time, which is contrary to our observations.

Air masses for modern-day rainfall events in Lonar during different seasons show that in addition to ISM summer monsoonal rainfall sourced mainly from the Arabian Sea (AS), generally drier air is also delivered from the NW region of India, the Bay of Bengal (BoB), or the NE region of India during the rest of the year (Sarkar et al., unpublished). An enhanced influence of any of these three potential moisture sources (NW, BoB and NE) versus the regular ISM rainfall sourced from the AS would result in a change in precipitation δD values. In order to characterize the seasonality of moisture sources and associated precipitation isotopic values in the CMZ, we analyzed modern day IAEA-GNIP data available from the nearest location Sagar and carried out a back trajectory analysis. Back trajectories of air masses during monsoon months show that more negative precipitation δD values are often associated with a moisture source from the BoB (Fig. 4.3), in addition to the major summer monsoonal rainfall sourced mainly from the AS.

Due to the large influx of monsoonal runoff from Himalayan rivers to the BoB the average seawater isotopic composition of the BoB is $\sim 1‰$ depleted in $\delta^{18}O$ (or $\sim 8‰$ depleted in δD) with respect to the AS (Kumar et al., 2010). An enhanced transport of moisture from the BoB, which occurs mostly today in post-monsoon (Sept. and Oct.) (Sengupta and Sarkar, 2006) would also result in more negative precipitation δD values in the CMZ, due to a longer transport pathway. We therefore presume that during the mid-Holocene transition AS sourced ISM summer rainfall was often strongly reduced and precipitation in the CMZ had different sources. This scenario would result in arid condition and more negative δD_{precip} values in the CMZ, coherent with our observations.

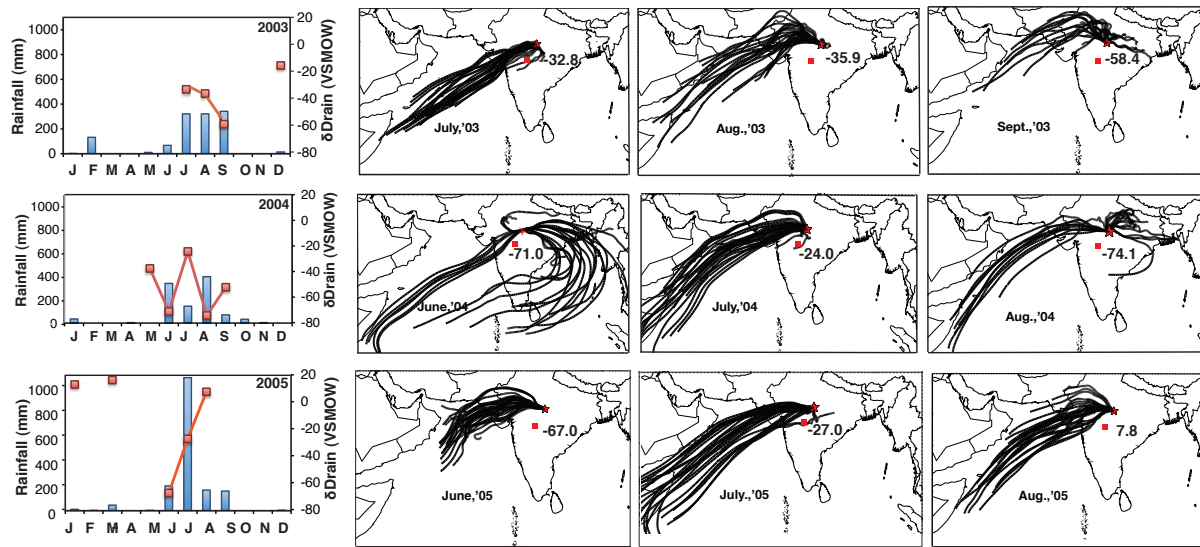


Fig. 4.3. Monthly rainfall and δD_{rain} variability at Sagar from 2003 to 2005 (left panel) and four day backwards trajectories for air parcels during selected rainfall events affecting Sagar (asterisk) during Monsoon (3 right panels), calculated using an ensemble (24 members) of the Air Resources Lab Hysplit Program, to represent moisture source for the region.

In order to test our hypothesis of a possible effect of changing moisture sources during the mid-Holocene transition, we compare two Holocene monsoon records, one from Oman cave speleothem and the other from Mawmluh cave speleothem, NE India (Fig. 4.4).

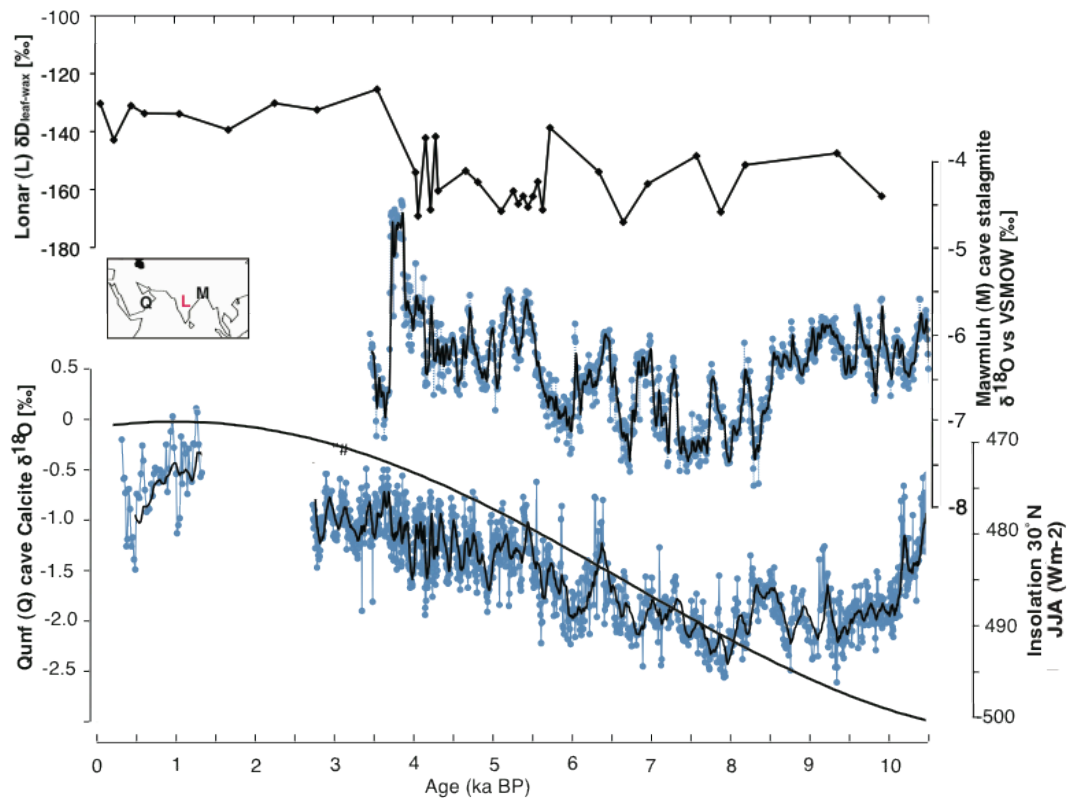


Fig. 4.4. Holocene ISM variability from ISM domain. Locations of the records (inset), records: Current study, Fleitmann et al., 2003, Berkelhammer et al., 2012.

Due to their locations the Oman cave speleothem receives moisture exclusively from the AS whereas the Mawmluh cave lies within the reach of BoB sourced moisture, but also receives AS sourced ISM moisture during the summer months (mean $\delta^{18}\text{O}$ of -7.2‰) (Breitenbach et al., 2010).

During the post-monsoon months, when less precipitation falls, the moisture source area is exclusively the BoB, characterized by more negative $\delta^{18}\text{O}$ values. Interestingly the Mawmluh cave record showed large fluctuations in $\delta^{18}\text{O}$ values (Berkelhammer et al., 2012) not observed in the $\delta^{18}\text{O}$ record from Oman during the period between 5.5 and 4 ka, possibly reflecting alternating BoB and AS moisture sources in addition to drier conditions at Mawmluh cave.

We therefore argue, that the high variability of $\delta\text{D}_{\text{wax}}$ along with the most negative $\delta\text{D}_{\text{wax}}$ during the mid-Holocene was a result of changing moisture sources, due to strongly reduced or even completely absent ISM rainfall. As such, the transition from early Holocene wet to late Holocene dry conditions in central India was not gradual, but characterized by high-amplitude hydroclimate fluctuations, with at times probably a complete failure of summer monsoonal rainfalls, especially between 5 and 4 ka BP.

Such a mid-Holocene transition has been recognized throughout the Asian monsoon domain, but its nature is debated. Morrill et al. (2003) discussed an abrupt (century scale) change in ISM while Fleitmann et al. (2007) argued for gradual weakening of the ISM during the Holocene. The weakening of the ISM in the CMZ at Lonar started between 6 cal. ka BP, as such at the same time (~ 6.3 ka BP) that has been postulated for the orbital induced reduction in solar insolation (Fleitmann et al., 2003; Ponton et al., 2012) and as observed in records throughout the Indian Ocean. However, contrary to other records in the CMZ around the Arabian Sea we observed a distinct period characterized by hydrological variability.

Since the high amplitude fluctuations of $\delta\text{D}_{\text{wax}}$ were observed over a short period only we hypothesize that such instability may only occur under certain threshold conditions of radiative forcing, which pushed the monsoonal circulation system to changes from a relatively stable wet to stable dry mode. Thus we suggest that orbital induced weakening of the summer solar insolation and associated reorganization of the general atmospheric circulation led to the unstable hydroclimate in the mid-Holocene. Abrupt climatic changes during the mid-Holocene (~ 4.5 to 5.0 cal. ka) have also been observed in many records from the Tropical areas supporting the notion of instability of tropical atmospheric circulation patterns. A pronounced shift in ecological conditions during the mid-Holocene (ca. 4 ka BP) was reported from tropical Africa and South America (Marchant and Hooghiemstra, 2004), and African lakes experienced major lake level drops at ~ 4.5 cal. ka and did not re-expand to the previous levels (Gasse, 2000). A decrease in vegetation and an increase in aeolian dust transport in North Africa were suggested as earlier at ~ 5.5 cal. ka (deMenocal et al., 2000). Though slightly earlier in Lonar, the mid-Holocene unstable transition condition appeared as wide-spread in the tropics.

4.4.2.3 The late Holocene period from 4 cal. ka BP onwards

From 4 cal. ka BP onwards less negative $\delta^{13}\text{C}$ values for long chain n -alkanes, particularly for $n\text{-C}_{27}$ (-25.1‰ minimum) indicate that the catchment vegetation became mixed C_3 and C_4 type, such as a forest with grassy ground). An almost

40‰ increase in δD_{wax} values relative to the early Holocene, indicates substantially drier conditions in the catchment. All these proxy data along with sustained higher flux of tetrahymanol indicate protracted late Holocene arid climate, in agreement with previous paleoclimate reconstructions throughout the ISM realm.

Over this period, the flux of leaf wax *n*-alkanes did not show a significant correlation with flux of Al. It is reasonable to assume that the flux of leaf wax *n*-alkanes might have been influenced by other factors, in addition to surficial erosion and lake level changes. In addition to terrigenous input, long chain *n*-alkanes can also be sourced from emerged macrophytes, which are common near the alluvial fan in the modern lake (Sarkar et al., 2014). Pollen spectra reveal that abundance (%) of pollen from telmatic plants started to increase after 4 cal. ka BP (Fig. 4.2b). Therefore the flux of leaf wax *n*-alkanes might have been influenced by surficial erosion and lake level changes initially, but later got influenced by combination of surficial erosion and within the lake by leaf wax input from macrophytes. A comparison of the ACL index with pollen spectra reveals a striking resemblance between variability of ACL and abundance (%) of pollen from macrophytes, from 3.7 cal. ka BP onwards (Fig. 4.2b and d). Higher ACL values during periods with higher macrophyte abundance probably indicate that longer chain *n*-alkanes such as *n*-C₂₉ and *n*-C₃₁ were also sourced from emerged macrophytes. Further, the prominent emerged macrophyte (*C. laevigatus*) abundant near the alluvial fan was analyzed and showed a higher ACL value of 31.0 (Sarkar et al., 2014). Increasing input from emerged macrophytes, from 4 cal. ka BP onwards, is also supported by the observation of different $\delta^{13}\text{C}$ values for the different long chain *n*-alkane homologues. $\delta^{13}\text{C}$ values for *n*-C₂₇ were influenced by the catchment vegetation (as % of C₄ plants) compared to $\delta^{13}\text{C}$ values for *n*-C₂₉ and *n*-C₃₁, which do not reflect the C₄ signal in the catchment. Therefore less negative $\delta^{13}\text{C}$ values for *n*-C₂₇ (~ -24‰), which is terrigenous, reflects C₄ occurrence in the catchment vegetation, as opposed to $\delta^{13}\text{C}$ values for *n*-C₂₉ and *n*-C₃₁ (~ -27.9‰ and -27.5‰ respectively) of aquatic origin.

Persistent higher fluxes of *n*-heptadecane along with more negative δD value (up to -173‰) represent another episode of lake eutrophication from 1.4 to 0.8 cal. ka BP, probably from human influence in the catchment. An increase in human impact was also evident from increase of herb pollen in the sediment and therefore spread of herbaceous taxa in the catchment (Prasad et al., 2014).

4.5 Conclusions

With our high-resolution Holocene record from continental India we successfully reconstructed the timing and magnitude of past ISM variation and related changes in the hydrology. Early Holocene wet conditions due to an intensified monsoon shifted to arid conditions during the late Holocene with a mid-Holocene unstable transition period in between.

In particular, we show that:

- The early Holocene (until 6 cal. ka BP) was wet, characterized by woody vegetation in the catchment, as evident from more negative $\delta^{13}\text{C}$ values of long chain *n*-alkanes. The near absence of bacterial biomarkers typical for saline lakes, pointed towards a fresh water lake. All these proxies indicate a positive P-

E balance, coherent with the intensified ISM.

- From 6 cal. ka BP, an increase in C₄ grass abundance inferred from a gradual shift of $\delta^{13}\text{C}$ values in leaf wax biomarkers, in particular of *n*-C₃₁ coupled with an increase in the abundance of tetrahymanol, a biomarker for salinity marked the onset of drier conditions and the establishment of a saline/alkaline lake.
- The onset of lake shallowing at 5.1 cal. ka BP increased the flux of leaf wax *n*-alkanes, along with the first highest flux of tetrahymanol triggered by increased nutrient supply and shoreline proximity.
- $\delta^{13}\text{C}$ leaf wax *n*-alkanes reached the least negative $\delta^{13}\text{C}$ values between 4.8 to 4 cal. ka BP indicating maximum C₄ abundance and the driest period. The mid-Holocene dry period was characterized by variation in the flux of major biomarkers including tetrahymanol, indicating either a threshold condition in lake level decrease or periods of variable nutrient supply and surficial erosion due to episodic rainfall events.
- A reduction in aridity from ca. 4 cal. ka BP onwards resulted in mixed (C₃ and C₄) catchment vegetation with less negative $\delta^{13}\text{C}$ values. An almost 40‰ increase in $\delta\text{D}_{\text{wax}}$ values relative to the early Holocene indicates a substantially lower P-E balance in the catchment. All these proxy data along with sustained higher flux of tetrahymanol indicate a protracted late Holocene arid climate and a saline lake.

The most intriguing feature of the mid-Holocene driest period was the high amplitude and rapid fluctuations in $\delta\text{D}_{\text{wax}}$ values, probably due to a change in the isotopic composition of source and/or precipitation tracks. We suggest that the mid-Holocene weakening of the ISM was not gradual, but highly variable. As such transitions from one hydrological state into another due to small changes in solar insolation can be associated with major environmental changes/ large fluctuations in moisture source, a scenario that may be relevant with respect to future changes in the ISM system.

4.6 Acknowledgements

This research was supported by the DFG-Graduate School 1364/1 “Interactions between Tectonics, Climate and Biosphere in the African–Asian monsoonal region” of the University of Potsdam, funded by the German Science Foundation (DFG). We thank M. Strecker, acting representative of the Graduate School, for constant support. We also thank all those who provided help during field and laboratory work, especially S. Pinkerneil. We thank S. Polanski for helpful advices in running the HYSPLIT model. Additionally cooperation from the Forest and Wildlife Department of Maharashtra State, India is gratefully acknowledged. D.S. was supported by an Emmy-Noether Grant of the DFG (SA1889/1-1).

5. Prolonged monsoon droughts and links to Indo-Pacific warm pool: A Holocene record from Lonar Lake, central India

Sushma Prasad^{a, c}, A. Anoop^a, N. Riedel^b, S. Sarkar^c, P. Menzel^d, N. Basavaiah^e, R. Krishnan^f, D. Fullers^g, B. Plessen^a, B. Gaye^d, U. Röhl^h, H. Wilkes^a, D. Sachse^c, R. Sawantⁱ, M.G. Wiesner^d, M. Stebich^b

^aHelmholtz Centre Potsdam, GFZ German Research Centre for Geosciences, D-14473 Potsdam, Germany

^bSenckenberg Research Institute, Research Station of Quaternary Palaeontology, Am Jakobskirchhof 4, D-99423 Weimar, Germany

^cInstitute for Earth and Environmental Science, University of Potsdam, Karl-Liebknecht Straße 24–25, 14476 Potsdam, Germany

^dUniversität Hamburg, Institute of Biogeochemistry and Marine Chemistry, Hamburg, Germany

^eIndian Institute of Geomagnetism, New Panvel, Navi Mumbai, India

^fIndian Institute of Tropical Meteorology, Pune, India

^gInstitute of Archaeology, University College London, London, UK

^hMARUM – Center for Marine Environmental Sciences, University of Bremen, 28359 Bremen, Germany

ⁱDeccan College, Post-Graduate and Research Institute, Pune-411006, India

Published in Earth and Planetary Science Letters 391 (2014) 171–182

Abstract

Concerns about the regional impact of global climate change in a warming scenario have highlighted the gaps in our understanding of the Indian Summer Monsoon (ISM, also referred to as the Indian Ocean summer monsoon) and the absence of long-term palaeoclimate data from the central Indian core monsoon zone (CMZ). Here we present the first high resolution, well-dated, multiproxy reconstruction of Holocene palaeoclimate from a 10 m long sediment core raised from the Lonar Lake in central India. We show that while the early Holocene onset of intensified monsoon in the CMZ is similar to that reported from other ISM records, the Lonar data shows two prolonged droughts (PD, multidecadal to centennial periods of weaker monsoon) between 4.6–3.9 and 2–0.6 cal ka. A comparison of our record with available data from other ISM influenced sites shows that the impact of these PD was observed in varying degrees throughout the ISM realm and coincides with intervals of higher solar irradiance. We demonstrate that (i) the regional warming in the Indo-Pacific Warm Pool (IPWP) plays an important role in causing ISM PD through changes in meridional overturning circulation and position of the anomalous Walker cell; (ii) the long term influence of conditions like El Nino-Southern Oscillation (ENSO) on the ISM began only ca. 2 cal ka BP and is coincident with the warming of the southern IPWP; (iii) the first settlements in central India coincided with the onset of the first PD and agricultural populations flourished between the two PD, highlighting the significance of natural climate variability and PD as major environmental factors affecting human settlements.

Keywords: Indian summer monsoon, ENSO, prolonged droughts, Holocene, Lonar Lake

5.1 Introduction

The ISM is a major component of the Asian monsoon system (Wang et al., 2005). While considerable data is available on Holocene East Asian monsoon variability (e.g., Yancheva et al., 2007; Dong et al., 2010; Wohlfarth et al., 2012; Chawchai et al., 2013), not much is known about the ISM that affects climate throughout south Asia, and as such the livelihood of more than a billion people in largely agriculture dependent societies (Krishna Kumar et al., 2011) over a variety of timescales. The devastating socio-economic impacts of droughts (a deficit of 10% below the long term mean rainfall) in the ISM realm are well documented (Mooley and Parthasarathy, 1982; Sinha et al., 2011), yet little is known about the dynamical processes underlying these natural catastrophes. ENSO is commonly linked to droughts in the ISM realm – the weakening of this relationship in recent decades has implications on the predictability of the ISM (e.g., Krishna Kumar et al., 1999). While indirect indicators of “ENSO-like” (ENSO-l) activity during the Holocene over multidecadal to centennial scales are available (Moy et al., 2002; Rein et al., 2005), testing the long term stability of the link between ENSO-l conditions with the ISM has not been possible as long term palaeoclimate reconstructions exist mostly from the peripheral ISM regions (Enzel et al., 1999; Staubwasser et al., 2003; Berkelhammer et al., 2012). There are no continuous well-dated Holocene palaeoclimate records from central India, the core of the monsoon zone (CMZ) (Gadgil, 2003).

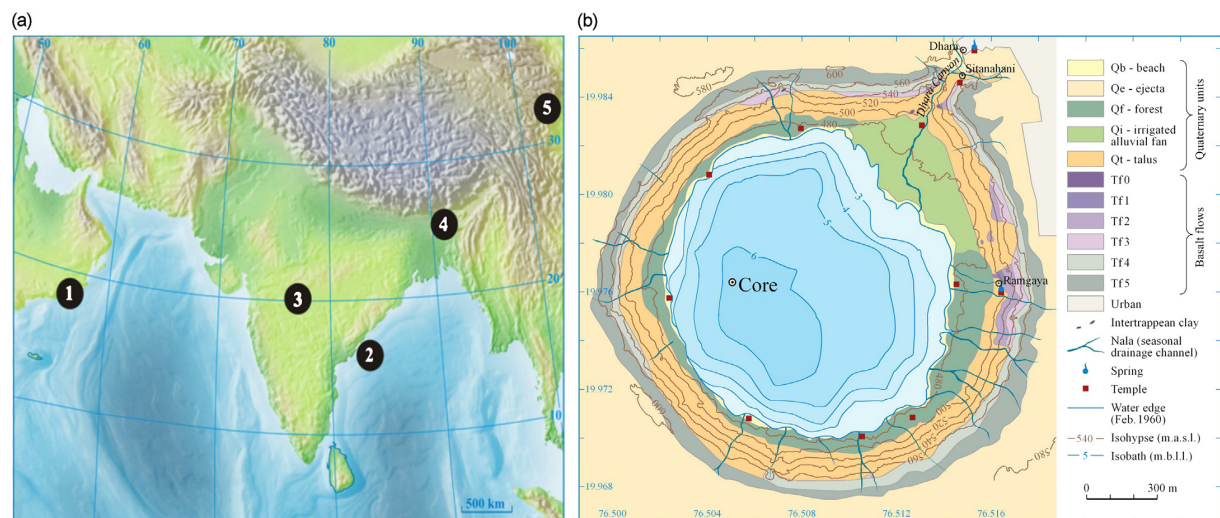


Fig. 5.1. (a) Location of sites discussed in the text-1: $\delta^{18}\text{O}$ from Oman Stalagmite (Fleitmann et al., 2003); 2: Marine core with catchment in Godavari delta (Ponton et al., 2012); 3: Lonar Lake (our study); 4: $\delta^{18}\text{O}$ from Mawmluh cave stalagmite (Berkelhammer et al., 2012); 5: Hyongong peat (Hong et al., 2003). (b) Geology of the Lonar Lake (after Maloof et al., 2009) and position of the core.

Here we present the first well-dated Holocene palaeoclimate reconstruction from the CMZ of central India. Our archive, Lonar Lake, is the only long term “rain gauge” for central India (Fig. 5.1a) and its sedimentary record is used here to reconstruct the long term regional palaeomonsoon variability in high-resolution. This lake is the only natural lake in central India as most of this region is covered by the Deccan basalts and lacks natural lakes, with the exception of Lonar crater that was formed by a meteorite impact ca. 570 ka

(Jourdan et al., 2011) on the ~65 Ma old (Fredriksson et al., 1973; Milton et al., 1975) basalt flows of the Deccan Traps. Currently, this crater contains a shallow (6 m deep, 1.2 km diameter) saline lake. We also compare the Lonar record with the reconstructed ENSO-1, and sea surface temperature (SST) changes in the IPWP to examine the forcing mechanisms behind extended droughts in the ISM realm.

5.1.1 Study area

5.1.1.1 Geology

Lonar crater is a near-circular depression (Fig. 5.1b) with a rim to-rim diameter of 1.8 km and an average depth of around 135 m from the rim crest to the lake level. The lake is fed by surface runoff from ISM precipitation and three perennial streams (Dhara, Sitanahani and Ramgaya). Since the lake has no outlet, the water level is presently controlled by the balance between evapotranspiration and precipitation, plus discharge from the groundwater fed springs. Tritium dating (Anoop et al., 2013b) indicated a modern to sub-modern age for the groundwater. This is consistent with the local observations that a succession of below average rainfall results in partial or, as in AD 1982 (single year), a complete drying of the lake.

5.1.1.2 Modern climate, hydrology, and hydrochemistry

The modern-day rainfall in the Lonar region is mostly provided by the Arabian Sea branch of the southwest monsoon (Sengupta and Sarkar, 2006). Temperatures during the pre-monsoon period are around 31 °C, but may increase up to 45 °C; southwest monsoon and post-monsoon temperatures average 27 °C and 23 °C respectively. The average summer monsoon rainfall is ca. 680 mm.

The Lonar Lake is a closed (endorrheic), hyposaline, and alkaline lake (Jhingran and Rao, 1958; Joshi et al., 2008). The lake is stratified with an anoxic bottom layer below 4 m water (AD 2011) depth with pH values between 9.5 and 10.4. The water level in Lonar Lake fluctuates in response to ISM precipitation with higher lake level during stronger monsoon years with input from both the surface runoff and groundwater (Komatsu et al., in press). During the dry season, the evaporation from the lake exceeds the input resulting in the significant drop of the lake level (Komatsu et al., in press). The $\delta^{18}\text{O}$ and δD of the inflowing streams range from -2.1 to -3.1‰ and -15.4 to -21.4‰ respectively. However, the lake waters showed relatively enriched values for $\delta^{18}\text{O}$ and δD fluctuating between +4.2 to +5.5‰ and +14.7 to +21‰ respectively. Similarly, $\delta^{13}\text{C}_{\text{DIC}}$ was enriched (+11 to +14.8‰) in lake waters and relatively depleted (between -9.9 and -12.6‰) in the inflowing streams indicative of biological productivity and evaporative enrichment in lake waters (Anoop et al., 2013b).

5.1.1.3 Modern vegetation

Lonar crater is located within the Southern Tropical Dry Deciduous Forest biome sensu Champion and Seth (1968). Our investigations indicate that the landscape outside the crater is heavily influenced through grazing, fuel cutting and agriculture, thus only shrubby thorn-vegetation occurs with *Acacia* spp., *Annona squamosa*, *Senna auriculata*, and *Ziziphus mauritiana*. Forest vegetation inside Lonar crater is roughly divided into three zones, which form

concentric belts. The crater slope between ca. 500 and 560 m asl is vegetated with tropical dry deciduous forest vegetation comprising teak (*Tectona grandis*), *Azadirachta indica*, *Cassia fistula*, *Wrightia tinctoria*, and *Butea monosperma*. Vegetation on the crater ground is dominated by *Prosopis juliflora*, with an admixture of *Alangium salviifolium*, *Ficus benghalensis*, *Trewia nudiflora*, *Ailanthus excelsa*, etc. The lakeshore is solely vegetated with *Prosopis juliflora*. The north-eastern part of the crater ground is used for agricultural purposes. Except in the dense and shady forest vegetation on the crater ground, the open character of vegetation on the crater slopes and outside Lonar crater promotes a rich understory dominated by Poaceae and various herbs of the Fabaceae, Asteraceae, and Acanthaceae families. The mouth of the Dhara rivulet features extensive stands of swamp vegetation comprising Cyperaceae and *Typha* sp.

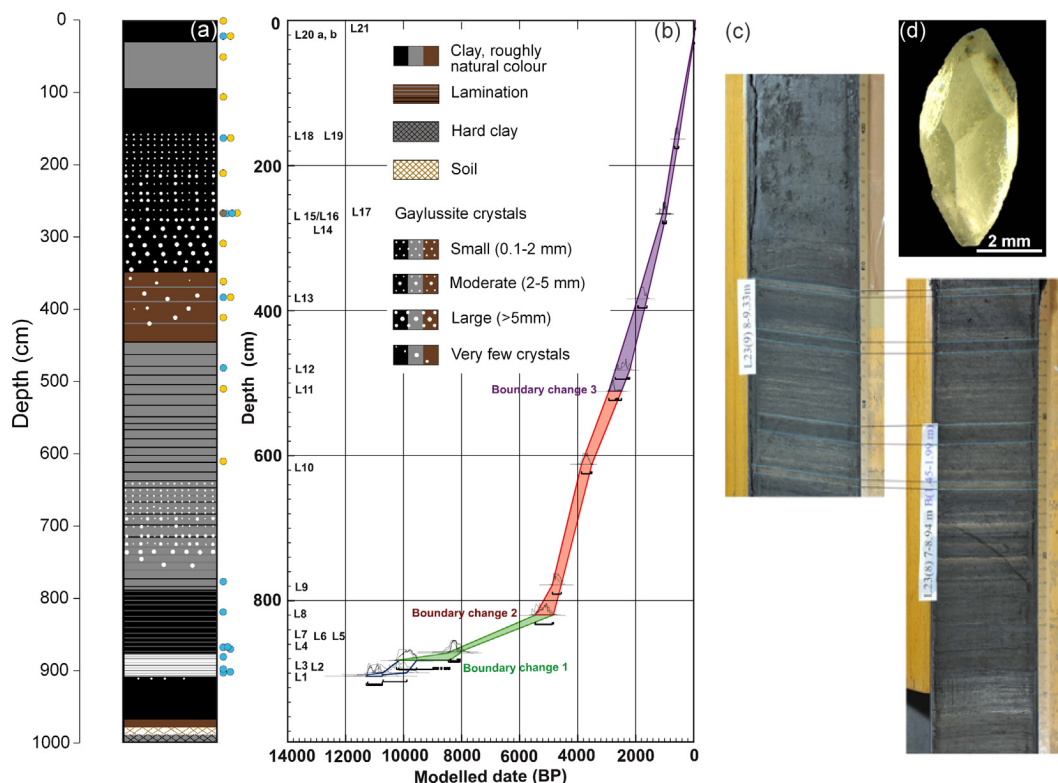


Fig. 5.2. (a) Lonar litholog. Two prominent evaporite gaylussite horizons indicate drier conditions. Symbols adjacent to the lithology indicate the position of dated samples: blue circles: terrestrial fragments, yellow circles: bulk organic matter, and brown circles: dated gaylussite. (b) Age model of composite Lonar profile, derived from the P_Sequence depositional model implemented in OxCal 4.1 (Bronk Ramsey, 1999, 2008). The coloured shading represents the 2σ probability range. Individual AMS ^{14}C dates obtained from bulk organic matter, terrestrial fragments, and gaylussite crystal are displayed as calibrated 2σ probability functions. (c) Correlation using marker layers. (d) Evaporitic gaylussite crystal.

5.2 Sample collection and methodology

5.2.1 Coring, documentation and correlation

Two long cores, with an offset of 50 cm were raised from the Lonar Lake in May-June AD 2008 using a floating platform and a UWITEC piston corer. Samples were collected in 1–2 m long plastic liners with an inner diameter of 9

cm. The cores were opened and the lithology documented in detail in the laboratory. The correlation between cores was achieved using a combination of at least two of the three parameters: marker layers, magnetic susceptibility, and XRF scanner data. The overlap between cores ranged from a few centimeters to tens of centimeters. A continuous composite core of 10.04 m is now available from the Lonar Lake (Fig. 5.2a) and has been subdivided into 14 lithostratigraphic units (Table 5.1 in Supplementary Online Material (SOM)-1).

5.2.2 *Thin section preparation*

A continuous set of overlapping petrographic thin sections (10 cm long) from selected core sections was prepared for microfacies analyses from the composite part following the method described by Brauer and Casanova (2001). Thin-section images were obtained with a digital camera (Carl Zeiss AxioCam) and the software Carl Zeiss Axiovision 2.0.

5.2.3 *Chronology*

We have collected terrestrial wood samples throughout the core to obtain a radiocarbon chronology (Fig. 5.2b, Table 5.2 in SOM-1). We have also selectively dated the carbonate crystals, bulk organic matter, and leaf fragments along with the wood fragments to ascertain the possibility of errors arising from reworked samples and/or any “hard water effect”.

For age modelling, we have used the P_Sequence method from OxCal (e.g., Bronk Ramsey 1999, 2008; Blockley et al., 2008). This method recognises that many processes are in fact a series of events and can be modelled by using representative information on the relationships between individual events. This model requires the estimation of the factor (k) which is the relationship between the events and the overall stratigraphical process – a high value for k would rigidly constrain the data and would be suitable for very simple sedimentary processes with little change in the sedimentation rate, whereas a low k value would be the opposite.

5.2.4 *Isotope analyses*

The stable isotope compositions of bulk (gaylussite was removed by handpicking under the microscope) carbonates ($\delta^{13}\text{C}_{\text{carb}}$ and $\delta^{18}\text{O}_{\text{carb}}$) were determined using a Finnigan GasBenchII with carbonate option coupled to a DELTAplusXL mass spectrometer, following the analytical procedure described in Spötl and Vennemann (2003). The TC, TN, and TOC contents and the $\delta^{15}\text{N}$ and $\delta^{13}\text{C}_{\text{org}}$ isotopic compositions were determined using an elemental analyser (NC2500 Carlo Erba) coupled with a ConFlowIII interface on a DELTAplusXL mass spectrometer (Thermo Fischer Scientific). Subsamples (0.5 cm thickness) were collected for isotope (organic and carbonate) analyses representing a time resolution ranging from <10 years between 0 and 5.5 cal ka to multidecadal (ca. 10–80 years) in older sediments.

5.2.5 XRF core scanning

Continuous down-core X-ray fluorescence (XRF) scanning of the sediment core surface was performed using the Avaatech XRF Core Scanner III. The tube voltage was operated at 10 kV, with 5 mm resolution, and the X-PIPS SXP5C-200-1500 detector from Canberra to allow obtaining the elemental abundances of major elements (Al, Si, Ca, K, Fe, Ti and Mn). The data was normalised using the calculated sedimentation rate.

5.2.6 Lipid biomarker and stable isotope ($\delta^{13}\text{C}$) analysis

The sediment core was sub-sampled (70 samples) for extraction of lipid biomarkers. Subsamples (2 cm thickness) represented a time resolution ranging from 8–20 years until 5.1 cal ka to 60–120 years in older sediments. Ca. 2–4 g of samples, freeze-dried and homogenized, were extracted using an accelerated solvent extractor (Dionex ASE 350) with a 9:1 mixture of dichloromethane and methanol. After removal of elemental sulphur (passing through activated copper pipette columns) and addition of internal standards the total lipid extracts (TLEs) were separated on SPE silica gel columns into fractions of different polarity. Fractions (containing alcohols) were measured on an Agilent GC-FID/MSD system for compound identification (comparison of mass spectra with published data) and quantification.

The stable isotope ($\delta^{13}\text{C}$) composition of tetrahymanol was measured on a GC system (Agilent 6890N) coupled via combustion interface (GC-C III), to a Thermo Fischer Scientific (model 253) isotope ratio mass spectrometer (GC-IRM-MS). Calibration of isotope values was performed by injecting several pulses of CO_2 at the beginning and at the end of each GC run and by measurement of certified standards between sample runs. GC-IRM-MS analyses were run in triplicate with standard deviations better than 0.5‰. Isotopic ratios are expressed as $\delta^{13}\text{C}$ values in per mil relative to the Vienna Pee Dee Belemnite (V-PDB) standard.

5.2.7 Pollen analysis

Pollen assemblages were studied at a resolution of 1 cm between 878 and 870 cm composite core depth, 2 cm between 870 and 794 cm and 10 cm between 790 cm and the composite core top. In total, 120 sediment samples were analysed, representing a time resolution between 150 and 40 years. Samples were treated with HF and hot acetolysis mixture and sieved on 200 μm and 5 μm following the standard guidelines of Faegri and Iversen (1989). All samples were spiked with *Lycopodium* marker grains (Stockmarr, 1971). At least 600 pollen grains were counted per sample. For identification of the pollen types, the reference collection of the Senckenberg Research Station Weimar, the pollen atlas for Maharashtra (Nayar, 1990), and a web-based pollen atlas for the Australasian realm (APSA Members, 2007) were consulted.

5.3 Results

5.3.1 Chronology

The core chronology is based on AMS dating (Fig. 5.2b and Table 2 in SOM-1) of wood, leaf, gaylussite, and bulk material from the sediments. The radiocarbon dates on terrestrial fragments (wood, twigs and leaf) and a gaylussite crystal (see Section 3.2) are in stratigraphic order. Paired radiocarbon dates obtained on bulk sediments and terrestrial fragments at the same depth show similar ages (within errors) except for the single paired sample at 383.5 cm where the date on bulk material is significantly older (Table 2 in SOM-1). Only two bulk organic matter dates between 511–612 cm lie on the trend formed by the dates on terrestrial fragments. The magnitude of the “ageing” of bulk organics is not constant throughout the profile and ranges from ca. 450 to 1500 years. The apparent “older” ages for the bulk sediments could be caused by several factors, potentially the most important being hard water effect (Fontes et al., 1996; Björck and Wohlfarth, 2001). However, the absence of carbonate outcrops in the region eliminates the overestimation of bulk ^{14}C due to hard water effect. Because the Lonar Lake shows high salinity, stratification, and high pH, the apparent “ageing” could be most likely caused by lack of equilibration with the atmosphere. The coincidences of some of the older ages with zones of gaylussite crystals (high pH, stratification, and salinity) also support such a scenario.

We have excluded the dates that are obvious outliers (see Table 2 in SOM-1). For the remaining dates the calibration was done using the OxCal programme (Bronk Ramsey, 2008) using the INTCAL04 and NH3 curves. In the P_sequence method, we have used three boundaries based on lithological changes and used a k value of 0.1. The agreement index (AI) for single ages, a measure of the fit between the data and the model should be above the threshold of 60 (Bronk Ramsey, 2008). The overall AI of 115.8 testifies to the suitability of this approach. The clay in the lower section (904–980 cm) is similar in appearance and texture to the clay found in the upper core, hence age extrapolation for this part was done using the sedimentation rate for the uppermost section (0–446 cm).

5.3.2 Lithology and evaporitic mineralogy

The lithology of the Lonar core is shown in Fig. 5.2a. Thin section investigations reveal that the laminated calcareous clay (11.15–9 cal ka; Fig. 5.2c) comprises of seasonality controlled sub-laminations: clay (monsoon rainfall erosion) with intercalations of organic (productivity) and calcareous (summer evaporation) layers, indicating these laminae to be varves. Several terrestrial wood fragments and one leaf were also found in this horizon indicating strong surficial inflow into the lake. Calcareous silty clay with evaporitic gaylussite crystals (Fig. 5.2), indicate highly saline conditions in two zones: mid (4.6–3.9 cal ka) and upper (2–0.6 cal ka) parts of the core (Anoop et al., 2013b). Although no modern analogues are available, we note that between 2002 and 2011 AD the average summer rainfall was ca. 20% below the long term mean (Indian Meteorological Department). However, there was no gaylussite formation clearly indicating that a substantially longer interval of reduced summer monsoon is needed for the formation of these evaporites. Most of the crystals in the core

appear parallel to the original sediment laminations and range in length from sub-mm to 8 mm. With a few exceptions, the crystals are devoid of any sediment inclusions (Fig. 5.2d). Their evaporative origin is also confirmed by isotope analyses (Anoop et al., 2013b).

5.3.3 Geochemistry, isotope, and biomarker studies

XRF data (see SOM-2 for data) show that the elements K, Ti, Fe and Si are significantly correlated with Al ($r = 0.89, 0.81, 0.63, 0.93$) for the whole core. Hence, Al was chosen as a representative for these elements. Our investigations of modern catchment and lake surface sediments (Basavaiah et al., in press) show that Al is contributed by catchment erosion and its distribution parallels the lithogenic content in surface sediments with higher values near the shoreline. Hence, Al can be used as an indicator of detrital input into the lake and proximity to the shoreline. The detrital input is highest between 11.4–11.15 cal ka and remains consistently low until 5.2 cal ka when higher detrital inflow is seen (Fig. 5.3).

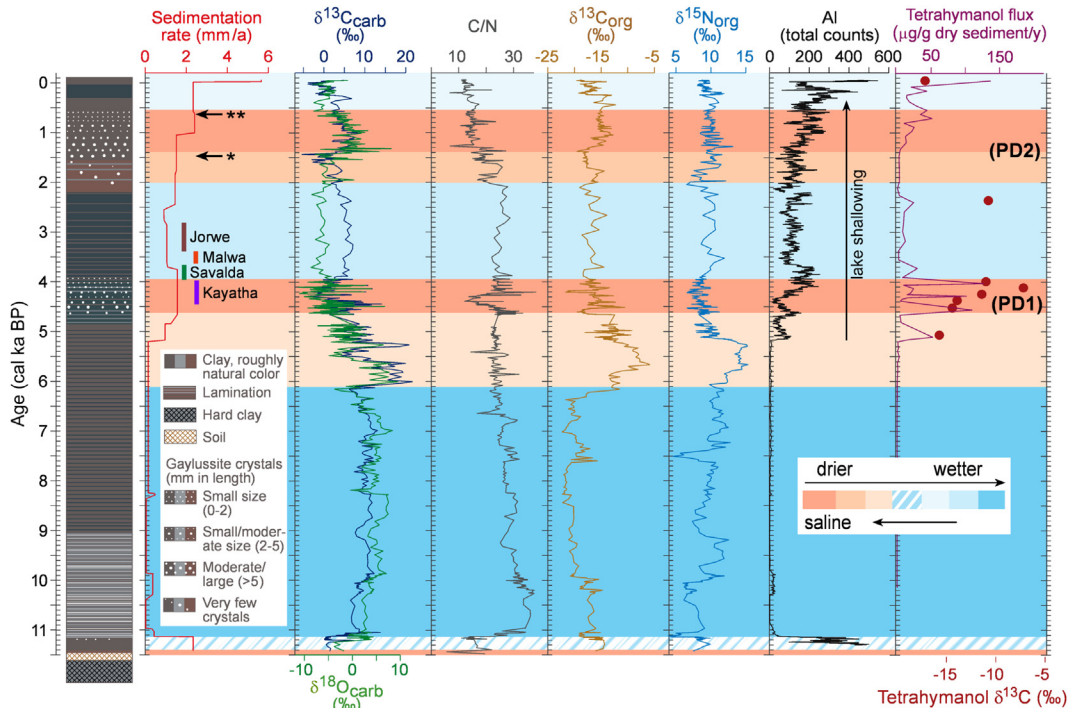


Fig. 5.3. Results of multiproxy investigations on the 10 m long Lonar core. In the first column (dotted grey box) are shown the prominent chalcolithic cultural periods (Kayatha, Savalda, Malwa and Jorwe) (Misra, 2001) detected in this region. Arrow with (*) indicates adoption of low rainfall crop patterns, and arrow with (**) indicates decadal scale drought induced famines. The Al (total counts) have been normalised with respect to sedimentation rate.

The C_{org}/N values of bulk organic matter remain consistently high (>25) except for short intervals (11.4–11.2; 4.4–4.2, and from 1.4 cal ka to present) when they fall to <15 (Fig. 5.3).

The $\delta^{13}C_{org}$ and $\delta^{15}N$ values vary between -22‰ and -6‰ and between $+4\text{‰}$ and $+15\text{‰}$ respectively. The variability is low between ca. 11 and 6.2 cal ka when a shift towards enriched values, most prominently between 6.2 and 5.3 cal ka is

seen. Subsequently, a depletion is observed but the values remain higher than during the early Holocene. The $\delta^{13}\text{C}_{\text{carb}}$ and $\delta^{18}\text{O}_{\text{carb}}$ values (after removal of gaylussite) are high ($\delta^{13}\text{C}_{\text{carb}} = 6\text{--}20\text{‰}$ and $\delta^{18}\text{O}_{\text{carb}} = \text{ca. } 3\text{--}9\text{‰}$) during the 11.2–5.8 cal ka. $\delta^{13}\text{C}_{\text{carb}}$ and $\delta^{18}\text{O}_{\text{carb}}$ co-vary ($r = 0.78$) for the whole core indicating their evaporative origin (Fig. 5.3).

The bacterial/ciliate community biomarker tetrahymanol makes its first appearance at ca. 5.2 cal ka in exceptional concentrations and persists until 3.9 cal ka and in lower abundance subsequently. An unusual enrichment in $\delta^{13}\text{C}$ (ca. 5.1–4 cal ka) is observed for tetrahymanol (-17.2‰ to -7.2‰) (Fig. 5.3).

5.3.4 Pollen

Poaceae contribute between 63.5 and 96.5% to the terrestrial pollen assemblage, while other herbs (e.g., Amaranthaceae and Asteraceae) account for 0.6 to 14.2% of the terrestrial pollen spectrum. Arboreal pollen contribute between 1.2 and 32.6% to the total terrestrial pollen assemblage. Pollen of woody plants representing moist forest communities appear with up to 7.7% between 8.9 and 5 cal ka (Fig. 5.4). Pollen of dry deciduous forest trees prevail steadily throughout the core, highest values of up to 30% are found between 8.6 and 7.1 cal ka, 5.6 and 4.1 cal ka and again at 3.0 cal ka. Pollen percentages of xeric thorn shrub elements occur from 5 cal ka BP onwards, with maxima of 6.3% between 3.8 and 2.8 cal ka. Pollen of *Ailanthus excelsa*, a tree species considered as disturbance indicator, appear between 4.6 and 3.0 cal ka, and around 1.5 cal ka, with up to 10%.

5.4 Discussion

In our palaeoclimate reconstruction from a 10 m long sediment core, we have used clastic influx, isotopic data from bulk organic matter, pollen, biomarker flux and compound-specific isotope data, together with published data (Anoop et al., 2013b) on evaporite mineral assemblages and their respective isotopic composition, to reconstruct past hydrological changes in the CMZ.

5.4.1 Environmental sensitivity of Lonar core proxies

The $\text{C}_{\text{org}}/\text{N}$ ratio of sediments is used as an organic matter source indicator. Based on the analysis of modern Lonar Lake sediments, it was inferred that a $\text{C}_{\text{org}}/\text{N}$ ratio ≥ 25 represents a major terrestrial contribution and a $\text{C}_{\text{org}}/\text{N}$ ratio below 25 a mixed plankton and terrestrial signal (Menzel et al., 2013). Changes in phytoplankton biological productivity are reconstructed here from variations in carbon and nitrogen isotopes of bulk organic matter. $\delta^{13}\text{C}$ values of terrestrial organic material are mainly determined by the contribution of plants using the C_3 (wetter conditions; $\delta^{13}\text{C} = -25$ to -30‰) or the C_4 (drier; $\delta^{13}\text{C} = -10$ to -15‰) pathway for CO_2 uptake (Meyers, 1994). The $\delta^{13}\text{C}$ record of the phytoplankton component is governed by changes in organic productivity, salinity, and pH of the water (Stuiver, 1975). Photosynthetic organic productivity preferentially uses ^{12}C and ^{14}N , leaving the DIC and DIN pools enriched in ^{13}C and ^{15}N , respectively (Swart, 1983; Talbot and Laerdal, 2000). Under CO_2 deficient conditions (<0.01 mol/l), which are promoted in highly alkaline water (Schelske and Hodell, 1991;

Xu et al., 2006), phytoplankton may be forced to change from CO_2 to HCO_3^- based metabolism, which produces relatively ^{13}C enriched organic matter (Talbot, 1990; Leng and Marshall, 2004). Additionally, high evaporation during drier (saline) conditions can cause supersaturation of carbonate in the lake water, and consequently $^{12}\text{CO}_2$ degassing (Lei et al., 2012).

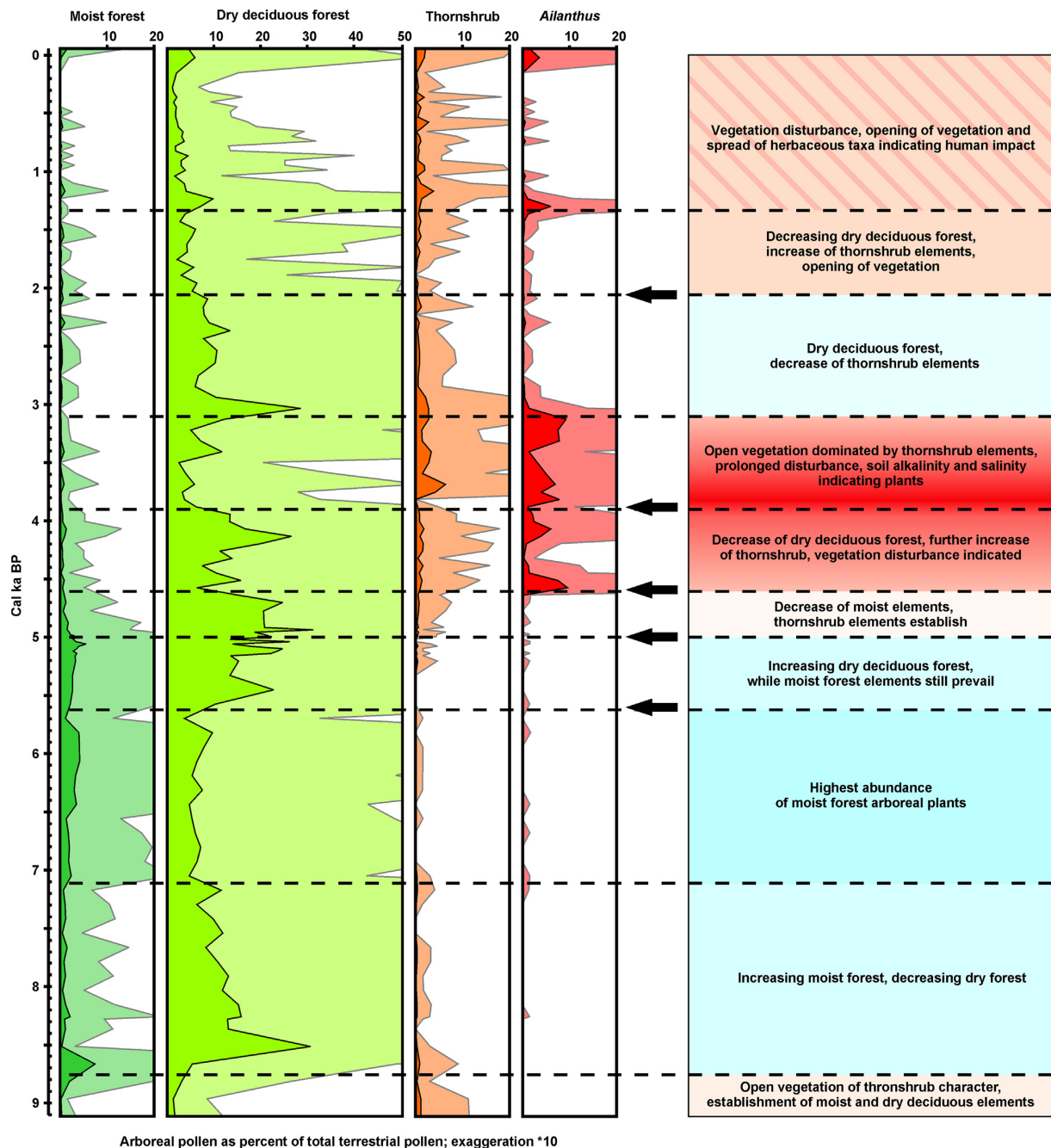


Fig. 5.4. Simplified pollen diagram for the Lonar Lake sediment sequence. The colours in the far right column have the same implications for climate as in Fig. 5.3. Arrows indicate the major transition points in the catchment vegetation.

Increased or decreased productivity in a stratified lake therefore should be reflected in increasing or decreasing $\delta^{13}\text{C}$ and $\delta^{15}\text{N}$ values of organic matter that was produced in surface waters (Hodell and Schelske, 1998).

Within the core, the oxygen and carbon isotope values of calcium carbonate

($\delta^{13}\text{C}_{\text{carb}}$ and $\delta^{18}\text{O}_{\text{carb}}$) correlate ($r = 0.78$) indicating their evaporative origin (Li and Ku, 1997). The carbonates in surface sediments show less enriched values near the stream inflow (shore proximity) as compared with deep water due to the dilution by the isotopically depleted inflowing streams (Anoop et al., 2013b). We note that due to the damping of the drying signal by the stream inflow (≤ 5 years of age) and the high solubility of the evaporites (Anoop et al., 2013b), the Lonar isotopic record is sensitive to, and preserves, only the evidence of weaker than normal decadal ISM fluctuations.

The normalised aluminium (Al) (XRF, total counts) content indicates clastic influx – in the closed Lonar Lake, an increased detrital influx could be indicative of increased catchment erosion and/or shoreline proximity (lake level changes). However, since the stream inflow is linked to recharge by monsoon, a combination of both the proxies ($\delta^{13}\text{C}_{\text{carb}}$ and $\delta^{18}\text{O}_{\text{carb}}$, and Al) can give a clear picture of the lake level changes and monsoon inflow.

Pollen analysis is used for vegetation reconstruction in the Lonar Lake catchment and the discrimination between different vegetation types. Pollen of woody plants were assigned to three forest types, with wet to moist forest today occurring under annual rainfall values of 5000 to 1800 mm and a 7–8 month-long dry season, represented by *Olea*, *Ligustrum*, *Eleaodendron*, *Trema* and *Trewia*, semi-arid dry deciduous forest (1500–800 mm/a rainfall, 7 month-long dry season), with *Combretaceae*, *Phyllanthus*, *Tectona*, *Lagerstroemia* and *Grewia*, and arid thorn shrub vegetation (800–400 mm/a, 7–8 month dry season), comprising *Acacia*, *Prosopis*, *Rhamnaceae* and *Azadirachta*. The classification follows Gaussen et al. (1964, 1966, 1970) and Champion and Seth (1968). Following these data, available moisture which controls the distribution of the different trees and forest types on regional scale is primarily determined by the strong gradient in annual rainfall amounts. Grasses of the Poaceae family dominate the lower stratum of most vegetation formations in tropical India, including moist forest types (Dabadghao and Shankarnarayan, 1973). An identification of Poaceae pollen grains on higher taxonomic levels is usually not possible using light microscopy (Beug, 2004) and thus grass pollen are not indicative for changes in rainfall amounts at Lonar crater.

The identification of pollen grains of cultivated plants is commonly used to detect agricultural activity in the past (Bottema, 1992). However, based on the pollen morphology an identification of common cultivated cereals in S-India is not feasible (Vishnu-Mittre, 1975). Moreover, pollen of cultivated pulses were not identified in the Lonar pollen record, because of the large number of native Fabaceae herbs occurring in the vegetation. However, we interpret increasing herb pollen values after ca. 1.3 cal ka as indirect indicators for artificial changes in the understory vegetation, since herbs might be promoted over grasses through prolonged grazing pressure. Additionally, many woody thorn shrub taxa may also reflect anthropogenic degradation of dry deciduous vegetation (Asouti and Fuller, 2008).

The lipid biomarker tetrahymanol is a pentacyclic triterpenoid lipid that frequently occurs in lake sediments (e.g., Thiel et al., 1997; Castañeda et al., 2011). It may have different biological origins among which predatory ciliates appear to be the most relevant in sedimentary records (Harvey and McManus, 1991). Other documented sources of tetrahymanol are the phototrophic purple non-sulphur bacterium *Rhodospseudomonas palustris* (Kleemann et al., 1990), the

fern *Oleandra wallichii* (Zander et al., 1969) and the rumen fungus *Piromonas communi* (Kemp et al., 1984). In Lonar, tetrahymanol occurs in high amounts in surface sediments and bacterial mats retrieved from various locations in Lonar Lake (Sarkar et al., 2014) suggesting that bacteria/ciliate communities are the most likely source of tetrahymanol in this ecosystem.

Sinninghe Damsté et al. (1995) proposed that tetrahymanol may be synthesised by anaerobic ciliates living at or below the chemocline, and thus may be indicative of water column stratification. Periods of increased abundance of tetrahymanol during the Holocene in the saline and alkaline Lake Van (Turkey) have been related to pronounced stagnation accompanied by the establishment of an anoxic water body (Thiel et al., 1997). In Lonar Lake sediments we interpret tetrahymanol as originating from bacteria/ ciliate communities and consider it as a marker for watercolumn stratification (Sinninghe Damsté et al., 1995) and its $\delta^{13}\text{C}$ is used here to assess alkalinity of the lake water.

5.4.2 Holocene proxy variability and climate reconstruction

In contrast to the lakes in NW India that dried out or became seasonal after 4 cal ka (Prasad and Enzel, 2006), the Lonar Lake has retained water level until today and provides the best preserved, high resolution record of Holocene climate variability from the core monsoon region. The driest period (>11.4 cal ka) (Fig. 5.2a), was marked by soil developing on the dry lake bed and followed by a short period (~300 years) of intensive erosion, fluctuating salinity as indicated by the presence of evaporative gaylussite, and high aquatic productivity (low $\text{C}_{\text{org}}/\text{N}$, high $\delta^{13}\text{C}_{\text{org}}$ and $\delta^{15}\text{N}$) that resulted from a sudden increase in precipitation (Fig. 5.3). During ~11–6.2 cal ka, wet conditions are indicated by the lowest $\delta^{13}\text{C}_{\text{org}}$ values (indicating C_3 plants) and low clastic influx. We infer stratified, deep-water conditions between 11–9 cal ka when seasonally laminated (varved) sediments were deposited. Counterintuitively, the early Holocene evaporative carbonates show less negative $\delta^{18}\text{O}$ values that could be related to reduce dilution by the isotopically depleted stream inflow during periods of higher lake levels. However, the amplitude of spatial isotopic variability (8.5‰ for $\delta^{13}\text{C}$ and 4‰ for $\delta^{18}\text{O}$) in surface bulk carbonates (Anoop et al., 2013b) cannot alone explain the range of variability seen in the core bulk carbonate isotopic composition. We exclude any contribution from the winter westerlies as this region was under the influence of the ISM during the Holocene (Prasad and Negendank, 2004) – the only possible explanation for the apparently reverse trend in carbonate isotope values is a change in source water composition or paths of precipitation tracks related to shifts in the mean position of the ITCZ (Haug et al., 2001).

Moist forests occurred from 8.8 cal ka onwards throughout the early and lower middle Holocene, as evident from the pollen data. Gradually decreasing pollen of dry deciduous forest elements after ca. 8.5 cal ka, indicates further increasing rainfall amounts. A significant rise in moist forest pollen types around 7.1 cal ka attests to the wettest phase.

From 6.2 cal ka a stepwise shift to a weaker summer monsoon is evident from salinity and pH related enrichments of $\delta^{13}\text{C}_{\text{org}}$ and $\delta^{15}\text{N}$ (Fig. 5.3) that precede the expansion (5.6–3.9 cal ka) of semi-arid dry deciduous forest (Fig. 5.4). Lake shoaling, accompanied by an increase in clastic influx, sedimentation rate (Fig. 5.3, >1.5 mm/yr. compared to 0.18 mm/yr. in lower sediments), and less enriched

evaporitic isotope values indicating increased proximity to inflowing streams, indicate onset of drier conditions ca. 5.2 cal ka. The bacterial/ciliate community biomarker tetrahymanol makes its first appearance at this time in exceptional concentrations and persists until 3.9 cal ka and in lower abundance subsequently. The unusual enrichment in $\delta^{13}\text{C}$ (ca. 5.1–4 cal ka) observed for tetrahymanol (-17.2‰ to -7.2‰) can only be explained fully by the utilisation of a ^{13}C -enriched carbon source by the tetrahymanol-producing organism indicating increasing lake water alkalinity. This shift to drier climate conditions is accompanied by a marked shift in the composition of the pollen assemblage at ca. 5 cal ka (Fig. 5.4), pointing to a significant reduction of moist arboreal vegetation while dry thorn shrub elements become established. The drying trend beginning ca. 5.2 cal ka culminates in the formation of evaporative gaylussite (Anoop et al., 2013b) between 4.6 and 3.9 cal ka when lake salinity increased. We refer to the highly saline, drier periods as prolonged droughts (PD, centennial long intervals with weak summer monsoon) as $\geq 20\%$ below the long-term mean is needed for the formation of gaylussite. Within this interval (PD1: 4.6–3.9 cal ka), tetrahymanol showed the least negative $\delta^{13}\text{C}$ values, pollen of dry deciduous forest elements declined, and pollen of light demanding species (*Ailanthus excelsa*) increased indicating a noticeable opening of the vegetation. Within PD1, between ca. 4.4 and 4.2 cal ka, the $\text{C}_{\text{org}}/\text{N}$ ratios drop to values ≤ 10 . Although these values are typical of planktonic organic matter (Meyers and Lallier-Vergès, 1999), and thus might indicate enhanced aquatic productivity, we attribute them to reduced supply of terrestrial organic matter due to drier conditions, as no corresponding $\delta^{13}\text{C}_{\text{org}}$ enrichment is seen, and the drop in $\text{C}_{\text{org}}/\text{N}$ occurs during the cycle of continuous evaporation and reduced Al supply (Anoop et al., 2013b) – this short arid event led to a rapid reduction of the forest vegetation, followed by a considerable expansion of thorn shrub and savanna vegetation. Within dating errors, this short dry period coincides with the 4.2 ka event (Staubwasser et al., 2003; Anoop et al., 2013b), but our data demonstrate that the pronounced drying began at least ca. 200 years earlier in the CMZ.

The disappearance of evaporitic gaylussite between 3.9 and 2 cal ka (Fig. 3) indicates reduced salinity. Nearly in parallel, a gradual humidification is seen in the change from arid thorn shrub vegetation to semi-arid deciduous forest between 3.8 and 3 cal ka with the denser forest vegetation persisting until ca. 2 cal ka (Fig. 5.4). The onset (ca. 2 cal ka) of PD2 is marked by the re-appearance of gaylussite crystals that become abundant 1.4–0.6 cal ka when enrichment in $\delta^{13}\text{C}_{\text{carb}}$ and $\delta^{18}\text{O}_{\text{carb}}$, lowered $\text{C}_{\text{org}}/\text{N}$ and higher $\delta^{13}\text{C}_{\text{org}}$ indicate increasing eutrophication of the lake. During PD2 the pollen (Fig. 5.4) of dry deciduous forest plants decline while thorn shrub vegetation expanded after 1.2 cal ka. A marked increase in herb pollen values furthermore points to intensified anthropogenic impacts on the vegetation from ca. 1.2 cal ka onwards. The occurrence of severe droughts (PD2) is also seen in the Dandak cave record (Sinha et al., 2007) but the drier periods in the latter occur after (0.7–0.3 ka) those found in the Lonar Lake. This may be due to either differing proxy sensitivities or spatial heterogeneity in ISM precipitation during the late Holocene.

5.4.3 Possible climate-culture link?

An examination of archaeological data from the region reveals that it is only around 4.5 cal ka that sedentary agricultural villages first occur in the northern and central Deccan, in response to the ISM weakening in the CMZ (Fuller, 2011). The cultural development (Kayatha, see Misra, 2001) is significantly later than the establishment of the early Indus Valley Civilisation (5.2–3.9 cal ka), with Indus urbanism from 4.6 cal ka (Possehl, 1999). The majority of the northern Deccan sites dated to this period are close to the rivers (Misra, 2001; Fuller, 2011) suggesting a need for a reliable source of water. After 4 cal ka there is a major increase in the known archaeological sites (Savalda, Malwa, Jorwe), focused on 3.8–3.4 cal ka (Misra, 2001; supplementary text in Ponton et al., 2012) and migration to locations distant from the rivers probably in response to wetter climate. This expansion would have extended and maintained thorn shrub vegetation (Asouti and Fuller, 2008). The cultivation systems of this period incorporated winter crops, like wheat and barley that had been adopted from the northwest, as well as indigenous monsoon-grown millets (Fuller, 2011). Wheat and barley cultivation was facilitated by the relatively wetter conditions of this period as they would have needed to be grown on water retained by clay-rich soils for the northern peninsula or artificial irrigation. This is indicated in the higher presence of wheat and barley during this era and on the northern peninsula, with the representation of millets increasing after 3.5 cal ka and even further after 3 cal ka (Fuller, 2011). In central India, archaeological evidence indicates adoption of low rainfall crop patterns beginning ca. 1.5 cal ka (Deotare, 2006), while decadal scale drought induced famines are documented in historical records from the 13th and 14th centuries AD (Dhavalikar, 1992; Maharatna, 1996; Sinha et al., 2007).

5.4.4 Regional correlation

Modern meteorological studies show differing climatic pattern between regions in India (Hoyos and Webster, 2007). However, the palaeoclimate data clearly show synchronicity of several events throughout the ISM realm. The onset of ISM at ca. 11.4 cal ka, following the drier period in the Lonar Lake, is coincident with the Arabian Sea (Sirocko et al., 1993), the Indus catchment (Limmer et al., 2012), and the Bay of Bengal (Govil and Naidu, 2011) records. The generally wetter phase recorded in Lonar between 11 and 6.2 cal ka is not seen in NW India (Prasad and Enzel, 2006) but this could be related to the low precipitation/evaporation rates in NW India. A change in Lonar hydrology beginning at ca. 6.2 cal ka coincides with the final reduction in the monsoon rainfall contribution to the water balance in NW Indian lakes (Prasad and Enzel, 2006), Oman (Fleitmann et al., 2003), and NE India (Berkelhammer et al., 2012), as well as eastern Tibet (Hong et al., 2003). A pivotal change in Lonar hydrology is seen ca. 4.6 cal ka with the occurrence of two PD separated by a less saline phase (Fig. 5.3). The impact of both these PD is seen to varying degrees at several sites in the ISM realm (Fleitmann et al., 2003; Ponton et al., 2012; Berkelhammer et al., 2012; Hong et al., 2003) (Fig. 5.5).

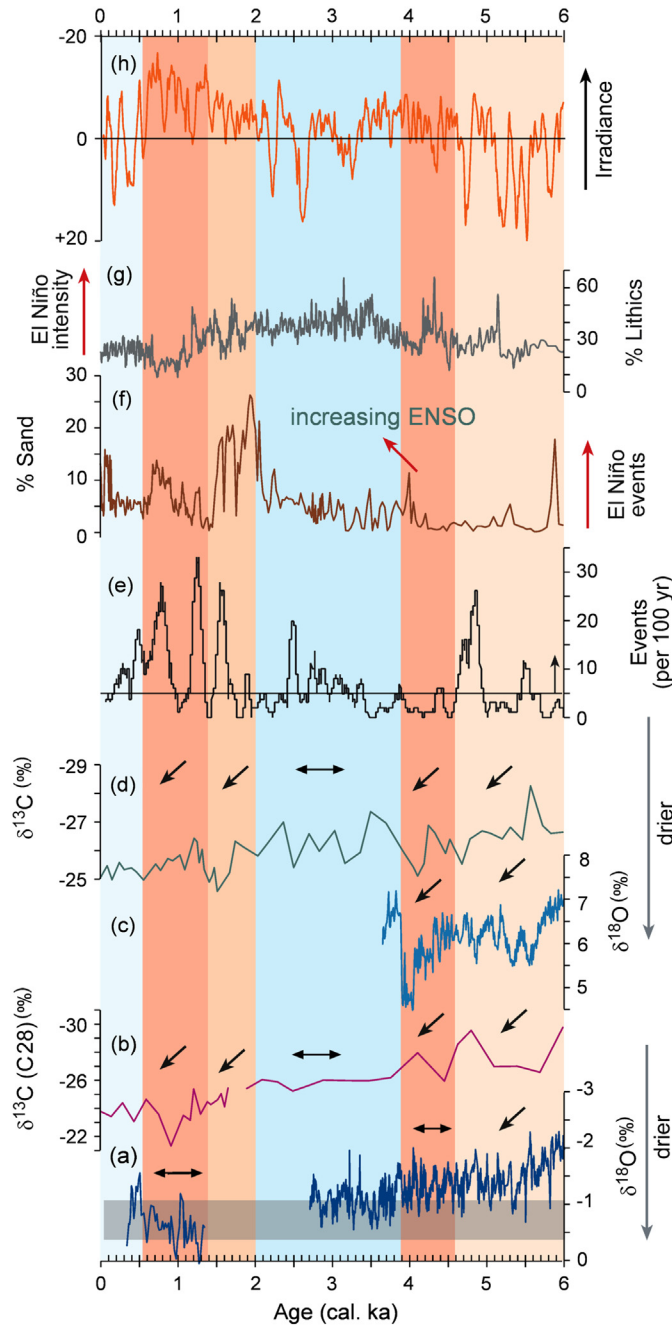


Fig. 5.5. Comparison of Holocene reconstructions of the ISM. Location of sites is shown in Fig. 5.1a. The colour bars have the same interpretation as in Fig. 5.3. (a) Oxygen isotope record from Oman (Fleitmann et al., 2003). The light grey bar shows the range of modern stalagmite. (b) Carbon isotope data from biomarkers (C_{28}) derived from the Godavari catchment (Ponton et al., 2012). (c) Oxygen isotope record from NE India (Berkelhammer et al., 2012). (d) Carbon isotopic composition from Hyongyang peat, eastern Tibet (Hong et al., 2003). (e) ENSO reconstruction from Laguna Pallacocha, Ecuador (Moy et al., 2002). (f) Percentage of sand in a core from El Junco Lake, San Cristobal, Galápagos (Conroy et al., 2008). (g) A 10-year running mean of the relative percentage of lithic sediments in a deep-sea core off the coast of Peru (Rein et al., 2005). (h) The $\Delta^{14}C$ record from tree rings which largely reflects changes in solar activity (Stuiver et al., 1998). Single point arrows indicate direction of increase/decrease while double pointed arrow indicates no major change.

5.4.5 What could have caused the prolonged droughts?

The onset of weakening of the ISM at 6.2 cal ka recorded in the Lonar data is

coincident with the orbitally forced weakening of solar insolation. However, a comparison of available ISM records (Fig. 5.5) with solar variability (Stuiver et al., 1998) show that, contrary to the previously known studies (Neff et al., 2001; Fleitmann et al., 2003; Gupta et al., 2005), the mid to late Holocene prolonged droughts occurred during periods of stronger solar irradiance. Clearly, a simple model linking solar insolation, southward shift of the mean position of the ITCZ (Haug et al., 2001) and reduced ISM strength in observed regions cannot explain the late Holocene PD observed in the ISM realm (Fig. 5.5) and alternative internal forcing mechanisms need to be explored. Variations in ISM precipitation can also be driven by ENSO, which modulates the regional monsoonal circulation through anomalous changes in the planetary scale Walker circulation (e.g., Krishna Kumar et al., 2006). We note that ENSO is an interannual phenomenon and long, high resolution records that can provide information on palaeo-ENSO activity currently are not available. We have therefore used reconstructions of ENSO-1 on centennial and millennial scales (Moy et al., 2002; Rein et al., 2005) that resulted in precipitation changes. However, during PD1, ENSO-1 is moderately intense (Rein et al., 2005) but less frequent as compared to the subsequent interval (Moy et al., 2002; Conroy et al., 2008) indicating some other forcing mechanism for the ISM weakening. A late Holocene interval with highly variable, intense ENSO-1 activity occurred 3.5–2.5 cal ka (Moy et al., 2002; Rein et al., 2005) and had a widespread impact elsewhere (Moy et al., 2002; Rein et al., 2005; Langton et al., 2008; Toth et al., 2012), but does not appear to have had any significant impact in the CMZ where Lonar shows reduced salinity after the PD1. Other ISM sites show little or no change (Fig. 5.5). The ISM and ENSO-1 link is established between 2 and 0.6 cal ka when PD2, coincident with increased solar activity, is recorded in the CMZ.

Climate model simulations indicate a likely intensification of the Walker circulation with stronger easterly trade winds and enhanced cooling over the eastern Pacific during periods of increased solar irradiance (Meehl et al., 2009). Therefore, it is rather intriguing to note the coincidence of PD associated with increased solar irradiance (Fig. 5.5). We argue that during such periods, the impact of the direct or indirect warming of the equatorial Indian Ocean (IO) and the IPWP can actually weaken the ISM. The basis for this argument comes from understanding of the link between the Indian summer monsoon rainfall (ISMR) variability and the Indian Ocean SST warming. It is important to mention that the period of PD1 coincided with positive temperature anomalies in the western Pacific Warm Pool (WPWP) (Stott et al., 2004; Linsley et al., 2010) and eastern IO (Govil and Naidu, 2011) (Fig. 5.6a). Terrestrial archives indicate anomalous cooling in the western IO (Thompson et al., 2002), fall in lake levels in eastern Africa (Garcin et al., 2012), and stronger monsoon in southern Indonesia (Griffiths et al., 2009) – these temperature and precipitation anomalies strongly resemble those during the negative phase of the Indian Ocean Dipole (IOD, Saji et al., 1999) (warming in the eastern equatorial Indian Ocean). The primary role of the eastern IO in causing spatial climate heterogeneity is also supported by the larger amplitude change in NE India (Berkelhammer et al., 2012) as compared to Oman (Fleitmann et al., 2003). While the enhanced SST warming in the eastern IO favours increased precipitation over the equatorial IO, the regional equatorial anomalies actually tend to weaken the boreal summer monsoon circulation by inducing subsidence and rainfall suppression over the Indian subcontinent (see

Krishnan et al., 2006). In turn the weakened summer monsoon winds can amplify the SST warming in the eastern IO through wind-thermocline feedback (Krishnan et al., 2006; Swapna et al., in press).

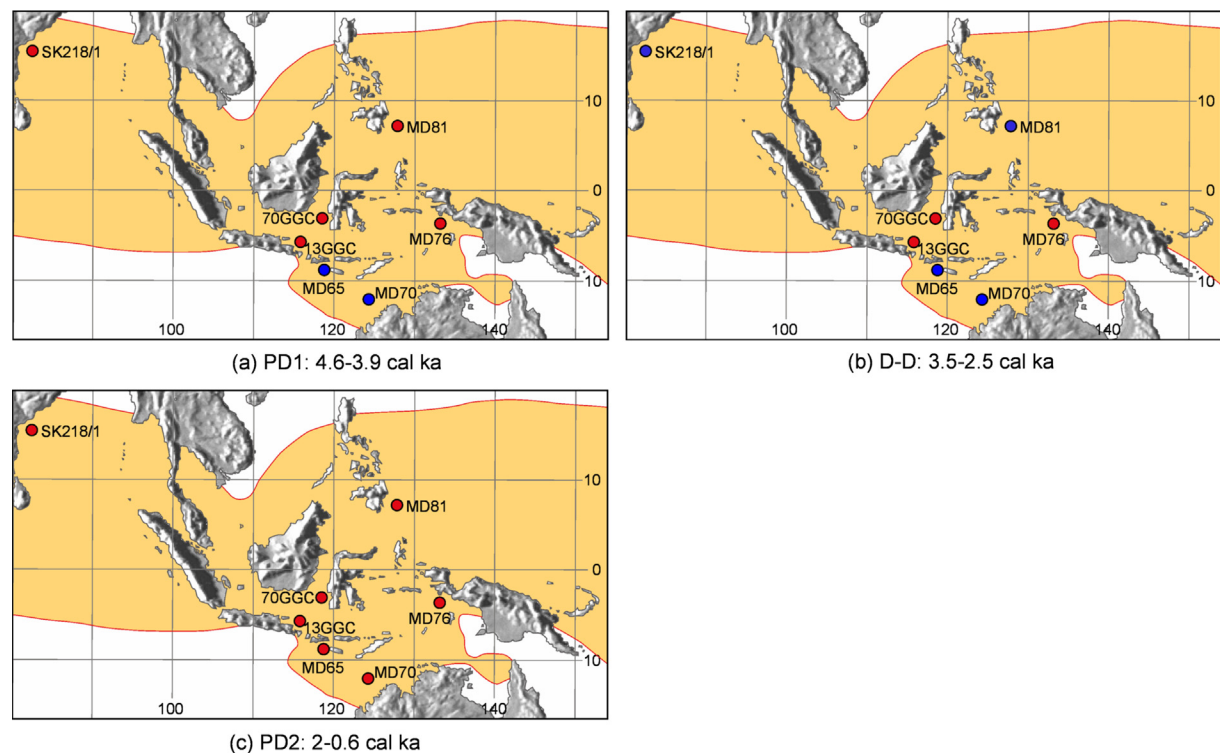


Fig. 5.6. SST anomalies in the IPWP calculated with respect to averaged SST over last 2 cal ka during PD1 (a), in the less saline interval (D-D) sandwiched between the two PD (b), and PD2 (c). See text for references. Only records covering all the three time slices are shown. Red circles and blue circles indicate warmer and cooler SST anomalies respectively. (For interpretation of the references to colour in this figure legend, the reader is referred to the web version of this article.)

The interval 3.5–2.5 cal ka, coincident with reduced solar irradiance is characterised by highly variable and intense ENSO-1 activity (Moy et al., 2002; Rein et al., 2005) with little impact over CMZ where Lonar showed reduced salinity after the preceding PD1 (Fig. 5.3, 5.4). At this time, the eastern IO is cooler (Govil and Naidu, 2011). Between 2 and 0.6 cal ka (PD2) the stronger solar irradiance during PD2 is consistent with the enhanced SST warming of the equatorial eastern IO and the southward expansion of positive temperature anomalies in the WPWP, with stronger impacts over CMZ (Fig. 5.6c). A comparison of the SSTs in the IPWP during the three time slices (Fig. 5.6), suggests that the ISM and ENSO-1 link on millennial scales is dependent on the SST anomalies in the equatorial eastern IO and the southern part of the WPWP. Notwithstanding the mechanisms that control the position and magnitude of temperature anomalies in the equatorial IO and WPWP (Newton et al., 2011; Abram et al., 2009), it appears that the occurrence of persistent droughts over India involve not only changes in the Pacific east-west Walker circulation (Krishna Kumar et al., 2006), but also regional changes in the meridional overturning circulation over the Indian Ocean (Krishnan et al., 2006; Swapna et al., in press).

5.5 Conclusions

The high resolution Holocene palaeoclimate reconstruction from the Lonar Lake in central India provides evidence of an extended dry period prior to 11.4 cal ka. This was followed by the establishment of a shallow lake (for ca. 300 years) marked by high aquatic productivity and increased detrital input. The Holocene wetter period lasted from 11 to 6.2 cal ka BP. Subsequently, two prolonged intervals of drier conditions (PD) are indicated by the presence of evaporative gaylussite (PD1: 4.6–3.90 cal ka) and (PD2: 2.03–0.56 cal ka) that are separated by calcareous clay sediments indicative of lower salinity. Archaeological evidence indicates that the first settlements in this region coincided with the onset of the first PD and agricultural populations flourished between these two prolonged droughts. A comparison of the Lonar record with ENSO-1 activity indicates that PD1 occurred during lower ENSO-1 activity. Our data show that the ISM and ENSO-1 link, proposed for the modern time, was established only ca. 2 cal ka. The Holocene PD occur largely during periods of higher solar irradiance suggesting that the solar signal could have amplified and/or modified the IPWP teleconnections through changes in sea surface temperatures. While in recent decades the warming in the western Pacific may be faster and result in more frequent ENSO (Hansen et al., 2006), it is the warming of the eastern IO and southern part of the WPWP that will crucially determine the long term monsoon rainfall activity over the subcontinent.

5.6 Acknowledgements

We thank all the people that have provided help during field work including K. Deenadayalan and Md. Arif. Cooperation by the Forest and Wildlife Department of Maharashtra State, India is gratefully acknowledged. This work was funded by the German Research Foundation (FOR 1380) within the framework of the HIMPAC project. This research used data acquired in the XRF Core Scanner Lab at the MARUM – Center for Marine Environmental Sciences, University of Bremen, Germany, and was supported by the DFG-Leibniz Center for Surface Process and Climate Studies at the University of Potsdam. Additional support was provided through the DFG Graduate School (GRK 1364). The hard work invested by Richard Niederreiter for raising the core in 40 °C summer temperatures is gratefully acknowledged.

6. Future perspectives

The outcomes from this thesis allow us to conceive the issues needed to be addressed for future investigations. Accordingly, the following hierarchy of studies may be relevant where real and proxy data will be combined with climate model simulations:

1. *Understanding the modern monsoonal climate with real data:*

As the current study shows, the monsoon moisture pathways are sensitive to natural forcings that are not yet fully understood. For example, an insolation driven threshold in radiative forcing might directly or indirectly (via ENSO) change the atmospheric circulation and therefore switch the moisture source for example from Arabian Sea (AS) to Bay of Bengal (BoB), as happened in the mid-Holocene transition. Change in moisture pathways along with rainfall amount has significant implications for agro-based societies such as in India.

The stable isotopic composition of oxygen and hydrogen in water ($\delta^{18}\text{O}$ and δD values) within the hydrological cycle and its spatial distribution are powerful tracers for identifying fluxes within the hydrological cycle. In particular water isotopic values in precipitation can be used to detect changes in the processes that affect the isotopic composition of precipitation such as the different sources and transport pathways of moisture (Bowen, 2010; Sachse et al., 2012). Therefore to understand the forcing mechanisms, modern monsoon precipitation sources, its seasonality and moisture pathways need to be better characterized with data from isotope stations, with high spatiotemporal resolution and by using state-of-the-art water isotope based methods. In order to determine the seasonality in moisture sources at Lonar I could use rainfall isotope data available for Sagar station (ca. 486 km NE of Lonar). Clearly a network of isotope stations would be beneficial. A network could be established along certain transects in monsoonal affected regions (e.g., CMZ). This is particularly important to study the sensitivity of the forcings (e.g., solar radiation) on the influence of large-scale teleconnection patterns such as ENSO.

2. *Understanding the proxies:*

There are still scopes for better characterization of the hydrological proxies (e.g., biomarkers, isotopes, pollen) in the regional context, for meaningful interpretations. For example, before interpretation of $\delta^{13}\text{C}$ values of sedimentary leaf wax biomarkers it is important to determine the contribution of any aquatic plants to the sediments, along with the terrestrial sources. In this regard, studying modern sediments and core-top sediments can be useful. Additionally monitoring with sediment-traps in longer terms, can be helpful to understand seasonal variability of deposition of certain proxy.

Further, characterization of vegetation (for example C_3 and C_4), especially on the Indian subcontinent, can be useful for the interpretation of some hydrological proxies (e.g., biomarkers, isotopes, pollen) and to understand the role of vegetation for the above mentioned proxies.

Lastly, human activities (and land use patterns) should be better identified with the help of paired biomarkers, isotopes and pollen based proxies. As an

example from biomarker based proxies, relevant cereals (wheat, rice, millets) can be characterized for their biomarker signatures and can be used to study the agricultural activities in the past.

A multi-proxy approach (e.g., pollen data with $\delta^{13}\text{C}$ values of leaf wax biomarkers) can also be helpful for a comprehensive understanding of hydrological changes. Again, a detailed evaluation of the sensitivity of an individual proxy, from the study of modern environments, can be useful to solve the complications which may arise due to different sensitivity of various proxies to climate changes and their response time.

3. Intercomparison between reconstructions and climate model simulations:

Further research in a broader interdisciplinary context can be worthwhile for improved understanding of past monsoon changes. Proxy based reconstructions lack a high spatiotemporal resolution. Therefore, reconstructions can be compared and evaluated with climate model simulations with higher spatiotemporal resolution. Furthermore, climate models are powerful tools to analyze the physical drivers behind monsoon variability and the interactions within the system, e.g., to test the threshold of radiative forcing and its feedbacks to internal modes of the ocean such as ENSO, the atmospheric circulation and moisture pathways. In this regard, a global General Circulation Model of the atmosphere (AGCM) can be used to test the sensitivity of complex non-linear feedbacks between variations in solar forcing, ENSO and changes in large-scale atmospheric circulation patterns (e.g., Hadley and Walker circulation). In addition, the human impact (e.g., changes in vegetation and land use) can be better detected by coupling a AGCM with a land surface model or scheme. However, due to their coarse spatial grid resolution (ca. 180×180 km) these AGMs are not able to capture regional-scale atmospheric circulation and moisture patterns, which are strongly affected by the realistic representation of the local topography (Polanski et al., in press). In order to better study sub-grid scale patterns such as precipitation, Regional Climate Models (RCMs) are nested within a AGCM using dynamical downscaling approach. RCMs have a higher spatial resolution which further leads to a better agreement between simulated and reconstructed moisture patterns especially in mountainous regions such as the Himalaya compared to coarse resolved AGCMs (Polanski et al., in press).

Appendices

Appendix A (referring to chapter 3)

Tab. A.1

Species	Description	Vegetation belt	<i>n</i> - C23	<i>n</i> - C25	<i>n</i> - C27	<i>n</i> - C29	<i>n</i> - C31	<i>n</i> - C33	<i>n</i> - C35	Total	ACL
Poaceae indet.		Streamside vegetation		0.96	2.60	3.96	10.5	16.5	9.39		32.1
Poaceae indet.		Agricultural field	1.23	3.84	9.45	15.5	21.5	28.7	5.01	43.9	30.7
<i>Cyperus laevigatus</i>	Sedge common in alkaline-saline water	Meadow and telmatic vegetation	3.19	2.86	3.44	12.7	24.2	32.5	4.31	85.3	31.0
<i>Prosopis juliflora</i>	Shrub, non-native, invasive	Shrub belt, moist mixed forest					8.57	82.1		83.2	32.8
<i>Setaria italica</i>	Millet grass, annual	Moist mixed forest	3.05	4.78	10.5	19.2	34.1	27.4	5.58	90.7	30.5
<i>Annona squamosa</i>	Shrub/small trees, semi-deciduous	Moist mixed forest, thornshrub	2.14	2.74	3.11	6.64	4.64	14.6		105	30.1
<i>Tectona grandis</i>	Deciduous	Dry deciduous mixed forest		10.01						33.9	32.8
<i>Azadirachta indica</i>	Evergreen, in drought sheds leaves	Dry deciduous mixed forest, moist mixed forest		3.27	15.5	20.0	71.4	364	124	604	30.4
<i>Wrightia tinctoria</i>		Dry deciduous mixed forest		1.23	42.6	344	349	114	31.3	885	30.4
<i>Butea monosperma</i>	Dry season deciduous	Dry deciduous mixed forest			2.75	8.80	17.2	7.14		37.2	29.6
Poaceae indet.		Dry deciduous mixed forest			21.9	116.5	61.7	13.6		214	32.0
Poaceae indet.		Dry deciduous mixed forest	3.94	2.37	2.12	6.80	16.2	28.8	23.1	83.3	32.0
Poaceae indet.		Thorn-shrub vegetation	10.9	7.04			61.5	55.4	16.5		30.4
					30.9	28.1				210	

Tab. A.1. Species (if available, indent., not identified), concentration of *n*-alkanes ($\mu\text{g/g}$ dry leaf) and ACL (C₂₃ to C₃₅) of Lonar crater modern vegetation.

Tab. A.2

Sample	Type	<i>n</i> - C15	<i>n</i> - C16	<i>n</i> - C18	<i>n</i> - C25	<i>n</i> - C27	<i>n</i> - C29	<i>n</i> - C31	<i>n</i> - C33	<i>n</i> - C35	*Phyt.	*Carotds.	Diploptene	Moretene	Ferrene	Hopene	*Unsaturated HC.	Squalene	*Gammone	*Thnol	Phytols	Hopanol
C17																						
A10	Floating mat	54.1	1.15	1.54	0.18	0.52	1.66	2.02	1.74	0.85	2.69	43.7	3.75	1.12	0.43				48.9	556	13.5	33.8
F11	Floating mat	219	3.12	6.35	1.02	2.75	3.62	1.67	0.81		3.88						2.78			66.5	322	
M11	Floating mat	725	18.4	19.4	1.32	3.91	9.73	6.06	2.58		8.40	68.8	2.34							214	107	
O11	Floating mat	1646	83.5	53.5		4.27	14.6	4.50	2.39		252	6.04	2.21					163		305	608	
A10(1)	Benthic mat	0.18						0.08									0.10		23.2	244	3.54	12.0
A10(2)	Benthic mat	1.27							0.68								0.42		183	1892	14.1	
O11	Benthic mat	122				42.2	17.6	58.3				929	271	62.0	38.8	203				2519	79.3	
LoF5	POM (above redox)	46.4																				65.5
LoF6	POM (above redox)	54.2																				71.4
* Phyt.= Phytanes and Phetenes Carotds.= Total Carotenoid Unsaturated hydrocarbons Gammone= Gammaceranone Thnol=Tetrahymanol																						

Tab. A.2. Mat and water samples with concentration of compounds ($\mu\text{g/g}$ dry mat and $\mu\text{g/l}$ water respectively) from Ionar crater lake.

Tab. A.3

Sample	*Lat.	*Long.	<i>n</i> - C17	<i>n</i> - C25	<i>n</i> - C27	<i>n</i> - C29	<i>n</i> - C31	<i>n</i> - C33	<i>n</i> - C35	Moretene	Fernene	Diploptene	*Carotds.	*Gmnone	*Thnol	*Total Thnol
1	19.978	76.513	5.31	0.49	1.60	4.89	4.24	4.47	2.26	3.58	1.64	16.0	41.9	99.7	993	1093
2	19.975	76.513	0.70	0.26	0.83	3.22	1.92	1.30	0.46	0.86	0.70	1.90	1.46	24.9	275	300
3	19.973	76.513	0.31	0.05	0.32	1.32	0.91	0.48	0.02	1.20	0.16	1.76	0.03	2.39	34.2	36.5
4	19.972	76.512										1.43	6.83	12.1	125	1367
5	19.971	76.511	4.50	0.35	1.74	7.30	4.91	2.50	0.67	7.36	1.62	13.2	3.62		360	360
6	19.972	76.506	0.41		0.39	0.82	1.04	1.38	0.47		0.30			14.0	77.6	91.6
7	19.978	76.503	1.72	0.17	0.61	1.84	1.13	0.86	0.37	1.85	0.88	9.41	40.8	40.8	623	664
8	19.982	76.505	2.71	0.47	3.00	8.20	6.56	3.86	1.16	0.31	1.93	0.43		16.8	250	266
9	19.982	76.509	3.12	0.45	1.20	2.75	2.87	1.97	0.90	1.81	0.92	7.12	22.7	41.6	480	522
10	19.980	76.510	0.74	0.20	0.48	1.15	1.56	2.28	1.34	0.00	0.00	0.00		6.44	43.5	50.0
11	19.979	76.511	0.60	0.33	1.18	4.17	3.29	2.63	0.75	4.27	0.94	4.81		11.8	268	280
12	19.978	76.510	0.12	0.13	0.42	1.04	1.47	1.60	0.58	1.04	0.22	0.56		10.8	108	118
13	19.980	76.508	0.06	0.12	0.53	1.36	1.93	2.32	0.81	0.91	0.76	0.68		10.1	128	138
14	19.979	76.506	0.35		0.38	0.70	1.04	1.33	0.49	0.90	0.87	2.09	7.97	9.82	92.8	103
15	19.976	76.507	0.59	0.23	0.67	1.29	1.85	1.95	0.75	0.49	0.49	0.73	0.44	9.66	69.3	78.9
16	19.975	76.511		0.33	0.80	1.59	1.78	1.48	0.55	1.40	0.67	1.86	2.47	33.1	285	318
17	19.974	76.509	0.22	0.13	0.43	0.86	1.10	1.33	0.54	0.55	0.69	0.81		18.3	136	154

* Lat.= Latitude, Long.= Longitude

Carotds. =Total Carotenoid, Gmnone= Gammaceranone, Thnol= Tetrahymanol, Total Thnol= Gammaceranone+Tetrahymanol, Total Terrestrial= *n*-C₂₅ to *n*-C₃₅, Gmnone%= Gammaceranone %.Tab. A.3. Surface sediment samples with location, concentration of compounds ($\mu\text{g/g}$ dry sediment) and ACL (C₂₅ to C₃₅) from Lonar crater lake.

Appendix B (referring to chapter 4)

Age (cal. ka BP)	Fluxes ($\mu\text{g/g}$ dry sediment/year)					
	Carotenoids	Moretene	Fernene	Diploptene	*Tnol	n-C ₁₇
-56.2	1.04	0.61	0.30	0.69	137	0.21
-19.9	0.14	0.44	0.27	0.60	104	0.40
65.3	0.58	0.10	0.05	0.12	20.8	0.16
150.5	0.06	0.19	0.10	0.25	43.5	0.97
235.7	0.00	0.05	0.02	0.05	14.2	1.06
282.5	0.11	0.00	0.00	0.00	14.1	0.18
367.7	0.09	0.00	0.00	0.00	18.1	0.36
452.8	1.73	0.15	0.06	0.19	29.3	0.32
538.0	0.00	0.19	0.06	0.26	43.9	2.91
622.1	2.75	0.16	0.05	0.21	34.1	3.14
704.9	5.86	0.17	0.06	0.26	51.2	3.06
795.9	1.32	0.05	0.00	0.06	10.4	0.19
878.6	0.00	0.10	0.03	0.15	25.0	13.7
961.3	0.79	0.08	0.03	0.12	21.6	4.23
1060.4	0.00	0.09	0.02	0.11	12.4	4.68
1190.7	0.00	0.06	0.02	0.07	13.6	5.99
1321.0	0.00	0.06	0.00	0.08	4.70	3.01
1451.4	0.05	0.19	0.28	0.26	2.95	0.15
1708.8	1.40	0.05	0.02	0.08	3.09	0.08
1842.0	0.00	0.13	0.25	0.12	3.16	0.19
1978.0	6.79	0.06	0.00	0.00	3.22	0.21
2114.1	1.37	0.05	0.03	0.06	0.72	0.01
2260.3	2.08	0.03	0.01	0.01	3.49	0.08
2396.4	0.81	0.41	0.10	0.32	24.2	0.22
2584.3	0.50	0.09	0.02	0.06	10.6	0.11
2794.7	0.37	0.14	0.03	0.07	9.78	0.25
2981.1	0.13	0.04	0.01	0.02	8.05	0.06
3176.9	0.05	0.07	0.02	0.03	12.1	0.16
3363.4	0.04	0.02	0.00	0.01	2.55	0.03
3549.8	0.09	0.00	0.00	0.00	2.18	0.00
3724.3	0.61	0.28	0.05	0.14	29.8	0.12
3907.4	0.05	0.27	0.02	0.16	8.2	0.37
4033.6	0.33	1.20	0.15	0.59	126	0.31
4065.2	0.18	0.09	0.00	0.00	9.80	0.10
4128.3	0.00	0.34	0.05	0.17	24.10	0.56
4159.9	0.07	0.47	0.05	0.30	22.88	0.05
4223.0	0.04	0.42	0.06	0.12	19.91	0.23
4254.6	0.00	0.13	0.00	0.08	14.87	0.14
4286.2	0.07	0.72	0.12	0.26	101	7.29
4317.7	0.00	0.13	0.00	0.00	16.0	0.70
4349.3	0.00	0.03	0.00	0.00	7.39	0.20
4380.9	0.00	0.00	0.00	0.00	5.05	0.10
4412.4	0.00	0.17	0.02	0.05	20.5	0.28
4564.5	0.00	0.76	0.12	0.28	109	0.44
4665.0	0.00	0.09	0.00	0.00	4.35	0.21
4818.2	0.00	0.38	0.04	0.18	5.78	0.15
5112.3	0.00	0.72	0.25	0.30	52.3	0.18
5203.9	0.00	0.09	0.11	0.04	1.39	0.00

5265.4	0.00	0.05	0.08	0.02	1.30	0.00
5326.9	0.00	0.06	0.12	0.03	2.26	0.00
5388.3	0.00	0.06	0.10	0.02	0.82	0.01
5449.8	0.00	0.04	0.08	0.02	2.17	0.00
5511.2	0.00	0.06	0.11	0.01	3.08	0.00
5572.7	0.00	0.03	0.05	0.01	1.97	0.00
5634.2	0.00	0.04	0.06	0.02	0.56	0.00
5726.3	0.00	0.03	0.05	0.03	1.17	0.01
6033.6	0.00	0.04	0.01	0.01	0.23	0.01
6340.9	0.00	0.05	0.02	0.04	0.24	0.01
6955.5	0.00	0.03	0.02	0.02	0.00	0.01
7262.8	0.00	0.02	0.01	0.01	0.12	0.01
7570.1	0.00	0.01	0.01	0.00	0.21	0.02
8184.7	0.00	0.00	0.00	0.00	0.05	0.01
8588.0	0.00	0.00	0.00	0.00	0.03	0.00
9338.0	0.00	0.00	0.00	0.00	0.00	0.00
10029.6	0.00	0.00	0.02	0.00	0.11	0.02
10158.1	0.00	0.00	0.01	0.00	0.23	0.01

Tab. B.1. Fluxes for aquatic biomarkers in $\mu\text{g/g}$ dry sediment/year.

*Tnol = total tetrahymanol (tetrahymanol and gammaceranone)

Appendix C (referring to chapter 5)

Supplementary material related to the article (Prasad et al., 2014) can be found online at <http://dx.doi.org/10.1016/j.epsl.2014.01.043>.

References

- Abram, N.J., McGregor, H.V., Gagan, M.K., Hantoro, W.S., Suwargadi, B.W., 2009. Oscillations in the southern extent of the Indo-Pacific Warm Pool during the mid-Holocene. *Quaternary Science Reviews* 28, 2794–2803.
- Agnihotri, R., Dutta, K., Bhushan, R., Somayajulu, B., 2002. Evidence for solar forcing on the Indian monsoon during the last millennium. *Earth and Planetary Science Letters* 198, 521–527.
- An, Z., Kutzbach, J.E., Prell, W.L., Porter, S.C., 2001. Evolution of Asian monsoons and phased uplift of the Himalaya-Tibetan plateau since Late Miocene times. *Nature* 411, 62–66.
- Anoop, A., Prasad, S., Krishnan, R., Naumann, R., Dulski, P., 2013a. Intensified monsoon and spatiotemporal changes in precipitation patterns in the NW Himalaya during the early-mid Holocene. *Quaternary International* 313–314, 74–84.
- Anoop, A., Prasad, S., Plessen, B., Naumann, R., Menzel, P., Basavaiah, N., Weise, S., Gaye, B., Brauer, A., 2013b. Palaeoenvironmental implications of evaporative Gaylussite crystals from Lonar lake, Central India. *Journal of Quaternary Science* 28, 349–359.
- Antony, C.P., Kumaresan, D., Ferrando, L., Boden, R., Moussard, H., Scavino, A.F., Shouche, Y.S., Murrell, J.C., 2010. Active methylophs in the sediments of Lonar Lake, a saline and alkaline ecosystem formed by meteor impact. *The ISME journal* 4, 1470–1480.
- Antony, C.P., Kumaresan, D., Hunger, S., Drake, H.L., Murrell, J.C., Shouche, Y.S., 2013. Microbiology of Lonar Lake and other soda lakes. *The ISME journal* 7, 468–476.
- APSA Members, 2007. *The Australasian Pollen and Spore Atlas V1.0*. Australian National University, Canberra. <http://apsa.anu.edu.au/>.
- Ashok, K., Guan, Z.Y., Saji, N.H., Yamagata, T., 2004. Individual and combined influences of ENSO and the Indian Ocean Dipole on the Indian summer monsoon. *Journal of Climate* 17, 3141–3155.
- Asouti, E., Fuller, D.Q., 2008. *Trees and woodlands in South India: Archaeological Perspectives*. Left Coast Press, Walnut Creek, CA, 341 pp.
- Badve, R.M., Kumaran, K.P.N., Rajshekhar, C., 1993. Eutrophication of Lonar Lake, Maharashtra. *Current Science* 65, 347–351.

- Basavaiah, N., Wiesner, M.G., Anoop, A., Menzel, P., Nowaczyk, N.R., Deenadayalan, K., Brauer, A., Gaye, B., Naumann, R., Riedel, N., Stebich, M., Prasad, S., 2014. Physicochemical analyses of surface sediments from the Lonar Lake, central India – implications for palaeoenvironmental reconstruction. *Fundamental Applied Limnology* 184/1, 51–68.
- Becker, A., Finger, P., Meyer-Christoffer, A., Rudolf, B., Schamm, K., Schneider, U., Ziese, M., 2013. A description of the global land-surface precipitation data products of the Global Precipitation Climatology Centre with sample applications including centennial (trend) analysis from 1901-present. *Earth System Science Data* 5, 71–99.
- Berkelhammer, M., Sinha, A., Mudelsee, M., Cheng, H., Edwards, R.L., Cannariato K., 2010. Persistent multidecadal power of the Indian Summer Monsoon. *Earth and Planetary Science Letters* 290, 166–172.
- Berkelhammer, M., Sinha, A., Stott, L., Cheng, H., Pausata, F.S.R., Yoshimura, K., 2012. An abrupt shift in the Indian monsoon 4000 years ago. *Geophysical Monograph* 198, 75–87.
- Beug, H.-J., 2004. Leitfaden der Pollenbestimmung für Mitteleuropa und angrenzende Gebiete. Verlag Dr. Friedrich Pfeil, München. 542 pp.
- Bhattacharya, S.K., Froehlich, K., Aggarwal, P.K., Kulkarni, K.M., 2003. Isotopic variation in Indian Monsoon precipitation: records from Bombay and New Delhi. *Geophysical Research Letters* 30, 2285, pp. 11.
- Björck, S., Wohlfarth, B., 2001. ¹⁴C chronostratigraphic techniques in paleolimnology. In: Last, W.M., Smol, J.P. (Eds.), *Basin Analysis, Coring, and Chronological Techniques*. In: *Tracking Environmental Change using Lake Sediments*, vol. 1. Kluwer, Dordrecht, pp. 205–245.
- Blockley, S., Bronk Ramsey, C., Lane, C.S., Lotter, A.F., 2008. Improved age modeling approaches as exemplified by the revised chronology for the Central European varved lake Soppensee. *Quaternary Science Reviews* 27, 61–71.
- Blumenberg, M., Seifert, R., Kasten, S., Bahlmann, E., Michaelis, W., 2009. Euphotic zone bacterioplankton sources major sedimentary bacterioplanepolyols in the Holocene Black Sea. *Geochimica et Cosmochimica Acta* 73, 750–766.
- Bookhagen, B., Thiede, R.C., Strecker, M.R., 2005. Late Quaternary intensified monsoon phases control landscape evolution in the northwest Himalaya. *Geology* 33, 149–152.
- Bookhagen, B., Fleitmann, D., Nishiizumi, K., Strecker, M.R., Thiede, R.C., 2006. Holocene monsoonal dynamics and fluvial terrace formation in the northwest Himalaya, India. *Geology* 34, 601–604.

- Bottema, S., 1992. Prehistoric cereal gathering and farming in the Near East: The pollen evidence. *Review of Palaeobotany and Palynology* 73, 21–33.
- Bowen, G.J., 2010. Isoscapes: spatial pattern in isotopic biogeochemistry. *Annual Review of Earth and Planetary Science* 38, 161–187.
- Brauer, A., Casanova, J., 2001. Chronology and depositional processes of the laminated sediment record from Lac d'Annecy, French Alps. *Journal of Paleolimnology* 25, 163–177.
- Breitenbach, S.F.M., Adkins, J.F., Meyer, H., Marwan, N., Krishna Kumar, K., Haug, G.H., 2010. Strong influence of water vapor source dynamics on stable isotopes in precipitation observed in southern Meghalaya, NE India. *Earth and Planetary Science Letters* 292, 212–220.
- Bronk Ramsey, C., 1999. The role of statistical methods in the interpretation of radiocarbon dates. In: Evin, J., Oberlin, C., Daugas, J.P., Salles, J.F. (Eds.), *C14 and Archaeology. 3rd International Symposium. Lyon 6–10, April 1998. Société Préhistorique Française, Lyon*, pp. 83–86.
- Bronk Ramsey, C., 2008. Deposition models for chronological records. *Quaternary Science Reviews* 27, 42–60.
- Bryson, R., Swain, A., 1981. Holocene variations of monsoon rainfall in Rajasthan. *Quaternary Research* 16, 135–145.
- Bullerjahn, G.S., Sherman, L.A., 1986. Identification of a carotenoid-binding protein in the cytoplasmic membrane from the heterotrophic cyanobacterium *Synechocystis* sp. Strain PCC6714. *Journal of Bacteriology* 167, 396–399.
- Burns, S.J., Fleitmann, D., Mudelsee, M., Neff, U., Matter, A., Mangini, A., 2002. A 780-year annually resolved record of Indian Ocean monsoon precipitation from a speleothem from south Oman. *Journal of Geophysical Research* 107, 4434, pp. 9.
- Castañeda, I.S., Schouten, S., 2011. A review of molecular organic proxies for examining modern and ancient lacustrine environments. *Quaternary Science Reviews* 30, 2851–2891.
- Castañeda, I.S., Werne, J.P., Johnson, T.C., Powers, L.A., 2011. Organic geochemical records from Lake Malawi (East Africa) of the last 700 years, part II: Biomarker evidence for recent changes in primary productivity. *Palaeogeography, Palaeoclimatology, Palaeoecology* 303, 140–154.
- Champion, H.G., Seth, S.K., 1968. A revised survey of the forest types of India. Government of India, Delhi.

- Chawchai, S., Chabangborn, A., Kylander, M., Löwemark, L., Mörth, C.-M., Blaauw, M., Klubseang, W., Reimer, P.J., Fritz, S.C., Wohlfarth, B., 2013. Lake Kumphawapi – an archive of Holocene palaeoenvironmental and palaeoclimatic changes in northeast Thailand. *Quaternary Science Reviews* 68, 59–75.
- Clemens, S.C., Prell, W., Murray, D., Shimmield, G., Weedon, G., 1991. Forcing mechanisms of the Indian Ocean monsoon. *Nature* 353, 720–725.
- Clift, P.D., Plumb, R.A., 2008. *The Asian Monsoon: Causes, History and Effects*. Cambridge University Press, Cambridge, UK.
- Conroy, J.L., Overpeck, J.T., Cole, J.E., Shanahan, T.M., Steinitz-Kannan, M., 2008. Holocene changes in Eastern Tropical Pacific climate inferred from a Galapagos lake sediment record. *Quaternary Science Reviews* 27, 1166–1180.
- Craig, H., 1961. Isotopic variations in meteoric waters. *Science* 133, 1702–1703.
- Cranwell, P.A., Eglinton, G., Robinson, N., 1987. Lipids of aquatic organisms as potential contributors to lacustrine sediments. 2. *Organic Geochemistry* 11, 513–527.
- Dabadghao, P.M., Shankarnarayan, K.A., 1973. *The Grass Cover of India*. Indian Council of Agricultural Research, New Delhi. 714 pp.
- Dansgaard, W., 1964. Stable isotopes in precipitation. *Tellus* 16, 436–468.
- Dash, S.K., Singh, G.P., Shekhar, M.S., Vernekar, A.D., 2005. Response of the Indian summer monsoon circulation and rainfall to seasonal snow depth anomaly over Eurasia. *Climate Dynamics* 24, 1–10.
- Dayem, K.E., Molnar, P., Battisti, D.S., Roe, G.H., 2010. Lessons learned from oxygen isotopes in modern precipitation applied to interpretation of speleothem records of paleoclimate from eastern Asia. *Earth and Planetary Science Letters* 295, 219–230.
- Dee, D.P., Uppala, S.M., Simmons, A.J., Berrisford, P., Poli, P., Kobayashi, S., Andrae, U., Balmaseda, M.A., Balsamo, G., Bauer, P., Bechtold, P., Beljaars, A.C.M., van de Berg, L., Bidlot, J., Bormann, N., Delsol, C., Dragani, R., Fuentes, M., Geer, A.J., Haimberger, L., Healy, S.B., Hersbach, H., Hólm, E.V., Isaksen, I., Kållberg, P., Köhler, M., Matricardi, M., McNally, A.P., Monge-Sanz, B.M., Morcrette, J.-J., Park, B.-K., Peubey, C., de Rosnay, P., Tavolato, C., Thépaut, J.-N., Vitart, F., 2011. The ERA-Interim reanalysis: configuration and performance of the data assimilation system. *Quarterly Journal of the Royal Meteorological Society* 137, 553–597.

- deMenocal, P., Ortiz, J., Guilderson, T., Adkins, J., Sarnthein, M., Baker, L., Yarusinsky, M., 2000. Abrupt onset and termination of the African Humid Period: rapid climate responses to gradual insolation forcing. *Quaternary Science Reviews* 19, 347–361.
- Demske, D., Tarasov, P.E., Wünnemann, B., Riedel, F., 2009. Late glacial and Holocene vegetation, Indian monsoon and westerly circulation in the Trans-Himalaya recorded in the lacustrine pollen sequence from Tso Kar, Ladakh, NW India. *Palaeogeography, Palaeoclimatology, Palaeoecology* 279, 172–185.
- Deotare, B.C., 2006. Late Holocene climatic change: archaeological evidence from the Purna Basin, Maharashtra. *Journal Geological Society of India* 68, 517–526.
- Dhavalikar, M.K., 1992. Culture-environment interface: A historical perspective. Presidential Address. *Archaeology, Numismatics and Epigraphy Section*. In: *Indian History Congress, 52nd Session*. New Delhi, Feb. 21–23.
- Diwakar, P.G., Sharma, B.D., 2000. Flora of Buldhana District. *Flora of India Series 3*. Botanical Survey of India, Calcutta.
- Dixit, S., Bera, S.K., 2012. Holocene climatic fluctuations from Lower Brahmaputra flood plain of Assam, northeast India. *Journal of Earth System Science* 121, 135–147.
- Dixit, Y., Hodell, D.A., Sinha, R., Petrie, C.A., 2014. Abrupt weakening of the Indian summer monsoon at 8.2 kyr B.P. *Earth and Planetary Science Letters* 391, 16–23.
- Dong, J., Wang, Y., Cheng, H., Hardt, B., Edwards, R.L., Kong, X., 2010. A high resolution stalagmite record of the Holocene East Asian monsoon from Mt Shennongjia, central China Jinguo. *Holocene* 20, 257–264.
- Dong, J., Wang, Y., Zhang, S., Chi, Z., Yao, P., Zhao, Z., 2012. Environmental magnetic comparisons between distal and proximal sediments of Huangqihai Lake, Inner Mongolia, China. *Science China Earth Sciences* 55, 1494–1503.
- Douglas, P.M.J., Pagani, M., Brenner, M., Hodell, D.A., Curtis, J.H., 2012. Aridity and vegetation composition are important determinants of leaf-wax δD values in southeastern Mexico and Central America. *Geochimica et Cosmochimica Acta* 97, 24–45.
- Draxler, R.R., Rolph, G.D., 2014. HYSPLIT (Hybrid Single-Particle Lagrangian Integrated Trajectory) Model access via NOAA ARL READY Website (<http://ready.arl.noaa.gov/HYSPLIT.php>). NOAA Air Resources Laboratory, Silver Spring, MD, USA.

- Eglinton, G., Hamilton, R.J., 1967. Leaf epicuticular waxes. *Science* 156, 1322–1334.
- Eglinton, T.I., Eglinton, G., 2008. Molecular proxies of paleoclimatology. *Earth and Planetary Science Letters* 275, 1–16.
- Enzel, Y., Ely, L.L., Mishra, S., Ramesh, R., Amit, R., Lazar, B., Rajaguru, S.N., Baker, V.R., Sandler, A., 1999. High-resolution Holocene environmental changes in the Thar Desert, northwestern India. *Science* 284, 125–128.
- Faegri, K., Iversen, J., 1989. *Textbook of Pollen Analysis*, fourth ed. Wiley, Chichester. 328 pp.
- Farquhar, G.D., Ehleringer, J.R., Hubick, K.T., 1989. Carbon isotope discrimination and photosynthesis. *Annual Review of Plant Physiology and Plant Molecular Biology* 40, 503–537.
- Feakins, S.J., deMenocal, P.B., Eglinton, T.I., 2005. Biomarker records of late Neogene changes in northeast African vegetation. *Geology* 33, 977–980.
- Ficken, K.J., Li, B., Swain, D.L., Eglinton, G., 2000. An *n*-alkane proxy for the sedimentary input of submerged/floating freshwater aquatic macrophytes. *Organic Geochemistry* 31, 745–749.
- Fleitmann, D., Burns, S.J., Mudelsee, M., Neff, U., Kramers, J., Mangini, A., Matter, A., 2003. Holocene forcing of the Indian monsoon recorded in a stalagmite from southern Oman. *Science* 300, 1737–1739.
- Fleitmann, D., Burns, S.J., Mangini, A., Mudelsee, M., Kramers, J., Villa, I., Neff, U., Al-Subbary, A.A., Buettner, A., Hippler, D., Matter, A., 2007. Holocene ITCZ and Indian monsoon dynamics recorded in stalagmites from Oman and Yemen (Socotra). *Quaternary Science Reviews* 26, 170–188.
- Floyd, D.A., Anderson, J.E., 1987. A comparison of three methods for estimating plant cover. *Journal of Ecology* 75, 221–228.
- Fontes, J.C., Gasse, F., Gibert, E., 1996. Holocene environmental changes in Bangong Co Basin (Western Tibet): Part 1. Chronology and stable isotopes of carbonates of a Holocene lacustrine core. *Palaeogeography, Palaeoclimatology, Palaeoecology* 120, 25–47.
- Fredriksson, K., Dube, A., Milton, D.J., Balasund, M., 1973. Lonar Lake, India: An impact crater in basalt. *Science* 180, 862–864.
- Fudali, R.F., Milton, D.J., Fredriksson, K., Dube, A., 1980. Morphology of Lonar Crater, India: Comparisons and implications. *The Moon and the Planets* 23, 493–515.

- Fuller, D.Q., 2011. Finding plant domestication in the Indian subcontinent. *Current Anthropology* 52, S347–S362.
- Gadgil, S., 2003. The Indian monsoon and its variability. *Annual Review of Earth and Planetary Sciences* 31, 429–467.
- Gadgil, S., Rajeevan, M., Nanjundiah, R., 2005. Monsoon prediction — why yet another failure? *Current Science* 88, 1389–1400.
- Gao, L., Hou, J., Toney, J., MacDonald, D., Huang, Y., 2011. Mathematical modeling of the aquatic macrophyte inputs of mid-chain *n*-alkyl lipids to lake sediments: Implications for interpreting compound specific hydrogen isotopic records. *Geochimica et Cosmochimica Acta* 75, 3781–3791.
- Garcin, Y., Melnick, D., Strecker, M.R., Olago, D., Tiercelin, J.J., 2012. East African mid-Holocene wet-dry transition recorded in palaeo-shorelines of Lake Turkana, Northern Kenya Rift. *Earth and Planetary Science Letters* 331, 322–334.
- Gasse, F., 2000. Hydrological changes in the African tropics since the Last Glacial Maximum. *Quaternary Science Reviews* 19, 189–211.
- Gat, J.R., 1996. Oxygen and hydrogen isotopes in the hydrologic cycle. *Annual Review of Earth and Planetary Sciences* 24, 225–262.
- Gaussen, H., Legris, P., Viart, M., 1964. International map of the vegetation and environmental conditions at 1/1,000,000. Sheet Godavari. Explanatory booklet. French Institute of Pondicherry (in French).
- Gaussen, H., Legris, P., Labroue, L., Meher-Homji, V.N., Viart, M., 1966. International map of the vegetation and environmental conditions at 1/1,000,000. Sheet Bombay. Explanatory booklet. French Institute of Pondicherry (in French).
- Gaussen, H., Legris, P., Blasco, F., Meher-Homji, V.N., Troy, V.P., Viart, M., 1970. International map of the vegetation and environmental conditions at 1/1,000,000. Sheet Satpura Mountains. Explanatory booklet. French Institute of Pondicherry (in French).
- Ghosh, S., Das, D., Kao, S.C., Ganguly, A.R., 2011. Lack of uniform trends but increasing spatial variability in observed Indian rainfall extremes. *Nature Climate Change* 2, 86–91.
- Goswami, B.N., 2005. South Asian Summer Monsoon: An overview. In: Chang, C.-P., Wang, B., Lau, N.-C. G. (Eds.), *The Global Monsoon System: Research and Forecast*, Chapter 5, pp. 47.

- Goswami, B.N., Venugopal, V., Dengupta, D., Madhusoodanan, M.S., Xavier, P.K., 2006. Increasing trend of extreme rain events over India in a warming environment. *Science* 314, 1442-1445.
- Goswami, B.N., Madhusoodanan, M.S., Neema, C.P., Sengupta, D., 2006. A physical mechanism for North Atlantic SST influence on the Indian summer monsoon. *Geophysical Research Letters* 33, L02706, pp. 4.
- Govil, P., Naidu, P.D., 2010. Evaporation-precipitation changes in the eastern Arabian Sea for the last 68 ka: Implications on monsoon variability. *Paleoceanography* 25, PA1210, pp. 11.
- Govil, P., Naidu, P.D., 2011. Variations of Indian monsoon precipitation during the last 32 kyr reflected in the surface hydrography of the Western Bay of Bengal. *Quaternary Science Reviews* 30, 3871–3879.
- Griffiths, M.L., Drsydale, R.N., Gagan, M.K., Zhao, J.-x., Ayliffe, L.K., Hellstrom, J.C., Hantoro, W.S., Frisia, S., Feng, Y.-x., Cartwright, I., St. Pierre, E., Fischer, M.J., Suwargadi, B.W., 2009. Increasing Australian-Indonesian monsoon rainfall linked to early Holocene sea-level rise. *Nature Geoscience* 2, 636–639.
- Gupta, A., Anderson, D., Overpeck, J., 2003. Abrupt changes in the Asian southwest monsoon during the Holocene and their links to the North Atlantic Ocean. *Nature* 421, 354–357.
- Gupta, A.K., Das, M., Anderson, D.M., 2005. Solar influence on the Indian summer monsoon during the Holocene. *Geophysical Research Letters* 32, L17703, pp. 4.
- Haigh, J., 1996. The impact of solar variability on climate. *Science* 272, 616–636.
- Hanisch, S., Ariztegui, D., Puttmann, W., 2003. The biomarker record of Lake Albano, central Italy - implications for Holocene aquatic system response to environmental change. *Organic Geochemistry* 34, 1223–1235.
- Hansen, J., Sato, M., Ruedy, R., Lo, K., Lea, D.W., Medina-Elizade, M., 2006. Global temperature change. *Proceedings of the National Academy of Sciences USA* 103, 14288–14293.
- Harvey, H.R., McManus, G.B., 1991. Marine ciliates as a widespread source of tetrahymanol and hopan-3 β -ol in sediments. *Geochimica et Cosmochimica Acta* 55, 3387–3390.
- Haug, G.H., Hughen, K.A., Sigman, D.M., Peterson, L.C., Rohl, U., 2001. Southward migration of the intertropical convergence zone through the Holocene. *Science* 293, 1304–1308.

- Hilton, J., Lishman, J.P., Allen, P.V., 1986. The dominant processes of sediment distribution and focusing in a small, eutrophic, monomictic lake. *Limnology and Oceanography* 31, 125–133.
- Hodell, D.A., Schelske, C.L., 1998. Production, sedimentation, and isotopic composition of organic matter in Lake Ontario. *Limnology and Oceanography* 43, 200–214.
- Hoffmann, B., Kahmen, A., Cernusak, L.A., Arndt, S.K., Sachse, D., 2013. Abundance and distribution of leaf wax *n*-alkanes in leaves of Acacia and Eucalyptus trees along a strong humidity gradient in northern Australia. *Organic Geochemistry* 62, 62–67.
- Holtvoeth, J., Vogel, H., Wagner, B., Wolff, G.A., 2010. Lipid biomarkers in Holocene and glacial sediments from ancient Lake Ohrid (Macedonia, Albania). *Biogeosciences* 7, 3473–3489.
- Hong, Y.T., Hong, B., Lin, Q.H., Zhu, Y.X., Shibata, Y., Hirota, M., Uchida, M., Leng, X.T., Jiang, H.B., Xu, H., Wang, H., Yi, L., 2003. Correlation between Indian Ocean summer monsoon and North Atlantic climate during the Holocene. *Earth and Planetary Science Letters* 211, 371–380.
- Hou, J.Z., D'Andrea, W.J., MacDonald, D., Huang, Y., 2007. Hydrogen isotopic variability in leaf waxes among terrestrial and aquatic plants around Blood Pond, Massachusetts, USA. *Organic Geochemistry* 38, 977–984.
- Hoyos, C.D., Webster, P.J., 2007. The role of intraseasonal variability in the nature of Asian Monsoon precipitation. *Journal of Climate* 20, 4402–4424.
- Hughen, K.A., Eglinton, T.I., Xu, L., Makou, M., 2004. Abrupt tropical vegetation response to rapid climate changes. *Science* 304, 1955–1959.
- Ishizaki, Y., Yoshimura, K., Kanae, S., Kimoto, M., Kurita, N., Oki, T., 2012. Interannual variability of H₂¹⁸O in precipitation over the Asian monsoon region. *Journal of Geophysical Research* 117, D16308, pp. 16.
- Ivanochko, T.S., Ganeshram, R.S., Brummer, G.-J., Brummer, A., Ganssen, G., Jung, S.J.A., Moreton, S.G., Kroon, D., 2005. Variations in tropical convection as an amplifier of global climate change at the millennial scale. *Earth and Planetary Science Letters* 235, 302–314.
- Jahren, A.H., Sternberg, L.S.L., 2003. Humidity estimate for the middle Eocene Arctic rain forest. *Geology* 31, 463–466.
- Jhingran, A.G., Rao, K.V., 1958. Lonar Lake and its salinity. *Records of the Geological Survey of India* 85, 313–334.
- Joshi, A.A., Kanekar, P.P., Kelkar, A.S., Shouche, Y.S., Vani, A.A., Borgave, S.B., Sarnaik, S., 2008. Cultivable bacterial diversity of alkaline Lonar lake,

- India. *Microbial Ecology* 55, 163–172.
- Jourdan, F., Moynier, F., Koeberl, C., Eroglu, S., 2011. $^{40}\text{Ar}/^{39}\text{Ar}$ age of the Lonar crater and consequence for the geochronology of planetary impacts. *Geology* 39, 671–674.
- Jung, S.J.A., Davies, G.R., Ganssen, G., Kroon, D., 2002. Decadal-centennial scale monsoon variations in the Arabian Sea during the Early Holocene. *Geochemistry, Geophysics, Geosystems* 3, 1060, pp. 10.
- Jung, S.J.A., Davies, G.R., Ganssen, G.M., Kroon, D., 2004. Stepwise Holocene aridification in NE Africa deduced from dust-borne radiogenic isotope records. *Earth and Planetary Science Letters* 221, 27–37.
- Kahmen, A., Hoffmann, B., Schefuß, E., Arndt, S.K., Cernusak, L.A., West, J.B., Sachse, D., 2013a. Leaf water deuterium enrichment shapes leaf wax *n*-alkane δD values of angiosperm plants II: Observational evidence and global implications. *Geochimica et Cosmochimica Acta* 111, 50–63.
- Kahmen, A., Schefuß, E., Sachse, D., 2013b. Leaf water deuterium enrichment shapes leaf wax *n*-alkane δD values of angiosperm plants I: Experimental evidence and mechanistic insights. *Geochimica et Cosmochimica Acta* 111, 39–49.
- Kannenberg, E.L., Poralla, K., 1999. Hopanoid biosynthesis and function in bacteria. *Naturwissenschaften* 86, 168–176.
- Kemp, P., Lander, D.J., Orpin, C.G., 1984. The lipids of the rumen fungus *Piromonas communis*. *Journal of General Microbiology* 130, 27–37.
- Kleemann, G., Poralla, K., Englert, G., Kjösen, H., Liaaen-Jensen, S., Neunlist, S., Rohmer, M., 1990. Tetrahymanol from the phototrophic bacterium *Rhodopseudomonas palustris*: first report of a gammacerane triterpene from a prokaryote. *Journal of General Microbiology* 136, 2551–2553.
- Krishna Kumar, K., Rajagopalan, B., Cane, M.A., 1999. On the weakening relationship between the Indian monsoon and ENSO. *Science* 287, 2156–2159.
- Krishna Kumar, K., Rajagopalan, B., Hoerling, M., Bates, G., Cane, M., 2006. Unraveling the mystery of Indian monsoon failure during El Nino. *Science* 314, 115–119.
- Krishna Kumar, K., Kamala, K., Rajagopalan, B., Hoerling, M.P., Eischeid, J.K., Patwardhan, S.K., Srinivasan, G., Goswami, B.N., Nemani, R., 2011. The once and future pulse of Indian monsoonal climate. *Climate Dynamics* 36, 2159–2170.

- Krishnamurthy, R.V., Syrup, K.A., Baskaran, M., Long, A., 1995. Late glacial climate record of midwestern United States from the hydrogen isotope ratio of lake organic matter. *Science* 269, 1565–1567.
- Krishnan, R., Sugi, M., 2001. Baiu rainfall variability and associated monsoon teleconnections. *Journal of Meteorological Society of Japan* 79, 851–860.
- Krishnan, R., Ramesh, K.V., Samala, B.K., Meyers, G., Slingo, J.M., Fennessy, M.J., 2006. Indian Ocean-monsoon coupled interactions and impending monsoon droughts. *Geophysical Research Letters* 33, L08711, pp. 4.
- Krishnan, R., Sundaram, S., Swapna, P., Kumar, V., Ayantika, D.C., Mujumdar, M., 2011. The crucial role of ocean-atmosphere coupling on the Indian monsoon anomalous response during dipole events. *Climate Dynamics* 37, 1–17.
- Kristen, I., Wilkes, H., Vieth, A., Zink, K.G., Plessen, B., Thorpe, J., Partridge, T.C., Oberhaensli, H., 2010. Biomarker and stable carbon isotope analyses of sedimentary organic matter from Lake Tswaing: evidence for deglacial wetness and early Holocene drought from South Africa. *Journal of Paleolimnology* 44, 143–160.
- Kodera, K., 2004. Solar influence on the Indian Ocean Monsoon through dynamical processes. *Geophysical Research Letters* 31, L24209, pp. 4.
- Komatsu, G., Senthil Kumar, P., Goto, K., Sekine, Y., Giri, C., Matsui, T., in press. Drainage systems of Lonar Crater, India: Contributions to Lonar Lake hydrology and crater degradation. *Planetary and Space Science* 95, 45–55.
- Kudrass, H.R., Hofmann, A., Doose, H., Emeis, K., Erlenkeuser, H., 2001. Modulation and amplification of climatic changes in the Northern Hemisphere by the Indian summer monsoon during the past 80 k.y. *Geology* 29, 63–66.
- Kumar, B., Rai, S.P., Kumar, U.S., Verma, S.K., Garg, P., Vijaya Kumar, S.V., Jaiswal, R., Purendra, B.K., Kumar, S.R., Pande, N.G., 2010. Isotopic characteristics of Indian precipitation. *Water Resources Research* 46, W12548, pp. 15.
- Kurita, N., Ichiyanagi, K., Matsumoto, J., Yamanaka, M.D., Ohata, T., 2009. The relationship between the isotopic content of precipitation and the precipitation amount in tropical regions. *Journal of Geochemical Exploration* 102, 113–122.
- Lamoureux, S., 1999. Spatial and interannual variations in sedimentation patterns recorded in nonglacial varved sediments from the Canadian High Arctic. *Journal of Paleolimnology* 21, 73–84.

- Langton, S.J., Linsley, B.K., Robinson, R., Rosenthal, Y., Oppo, D.W., Eglinton, T.I., Howe, S.S., Djajadihardja, Y.S., Syamsudin, F., 2008. 3500 year record of centennial-scale climate variability from the Western Pacific Warm Pool. *Geology* 36, 795–798.
- La Touche, T., 1912. The geology of Lonar Lake. *Records of the Geological Survey of India* 41, 266–275.
- Lei, Y.B., Yao, T.D., Sheng, Y.W., Zhang, E.L., Wang, W.C., Li, J.L., 2012. Characteristics of $\delta^{13}\text{C}_{\text{DIC}}$ in lakes on the Tibetan Plateau and its implications for the carbon cycle. *Hydrological Processes* 26, 535–543.
- Leng, M.J., Marshall, J.D., 2004. Palaeoclimate interpretation of stable isotope data from lake sediment archives. *Quaternary Science Reviews* 23, 811–831.
- Li, H.C., Ku, T.L., 1997. $\delta^{13}\text{C}$ - $\delta^{18}\text{O}$ covariance as a paleohydrological indicator for closed basin lakes. *Palaeogeography, Palaeoclimatology, Palaeoecology* 133, 69–80.
- Li, S.L., Perlwitz, J., Quan, X.W., Hoerling, M.P., 2008. Modelling the influence of North Atlantic multidecadal warmth on the Indian summer rainfall. *Geophysical Research Letters* 35, L05804, pp. 6.
- Limmer, D.R., Böning, P., Giosan, L., Ponton, C., Köhler, C.M., Cooper, M.J., Tabrez, A.R., Clift, P.D., 2012. Geochemical record of Holocene to recent sedimentation on the Western Indus continental shelf, Arabian Sea. *Geochemistry Geophysics Geosystems* 13, Q01008, pp. 26.
- Linsley, B.K., Rosenthal, Y., Oppo, D.W., 2010. Holocene evolution of the Indonesian throughflow and the western Pacific warm pool. *Nature Geoscience* 3, 578–583.
- Maharatna, A., 1996. *The Demography of Famines: An Indian Historical Perspective*. Oxford Univ. Press, Delhi, India, 317 pp.
- Malik, N., Bookhagen, B., Marwan, N., Kurths, J., 2012. Analysis of spatial and temporal extreme monsoonal rainfall over South Asia using complex networks. *Climate Dynamics* 39, 971–987.
- Mallory, F.B., Conner, R.L., Gordon, J.T., 1963. Isolation of a pentacyclic triterpenoid alcohol from a protozoan. *Journal of the American Chemical Society* 85, 1362–1363.
- Maloof, A.C., Stewart, S.T., Weiss, B.P., Soule, S.A., Swanson-Hysell, N.L., Louzada, K.L., Garrick-Bethell, I., Poussart, P.M., 2010. Geology of Lonar Crater, India. *Geological Society of America Bulletin* 122, 109–126.

- Mamgain, A., Dash S.K., Parth Sarthi, P., 2010. Characteristics of Eurasian snow depth with respect to Indian summer monsoon rainfall. *Meteorology and Atmospheric Physics* 110, 71–83.
- Marchant, R., Hooghiemstra, H., 2004. Rapid environmental change in African and South American tropics around 4000 years before present: a review. *Earth-Science Reviews* 66, 217–260.
- Martin-Puertas, C., Matthes, K., Brauer, A., Muscheler, R., Hansen, F., Petrick, C., Aldahan A., Possnert G., van Geel, B., 2012. Regional atmospheric circulation shifts induced by a grand solar minimum. *Nature Geoscience* 5, 397–401.
- Masamoto, K., Riethman, H.C., Sherman, L.A., 1987. Isolation and characterization of a carotenoid-associated Thylakoid protein from the cyanobacterium *Anacystis nidulans* R2. *Plant Physiology* 84, 633–639.
- Meehl, G., Arblaster, J., Matthes, K., Sassi, F., van Loon, H., 2009. Amplifying the Pacific climate system response to a small 11-year solar cycle forcing. *Science* 325, 1114–1118.
- Melles, M., Brigham-Grette, J., Minyuk, P.S., Nowaczyk, N.R., Wenrich, V., DeConto, R.M., Anderson, P.M., Andreev, A.A., Coletti, A., Cook, T.L., Haltia-Hovi, E., Kukkonen, M., Lozhkin, A.V., Rosén, P., Tarasov, P., Vogel, H., Wagner, B., 2012. 2.8 Million years of Arctic climate change from Lake El'gygytgyn, NE Russia. *Science* 337, 315–320.
- Menzel, P., Gaye, B., Basavaiah, N., Prasad, S., Stebich, M., Das, B.K., Nagel, B., Anoop, A., Riedel, N., Wiesner, M., 2013. Impact of bottom water anoxia on nitrogen isotopic ratios and amino acid contributions of recent sediments from small eutrophic Lonar Lake, Central India. *Limnology and Oceanography* 58, 1061–1074.
- Meyers, P.A., 1994. Preservation of elemental and isotopic source identification of sedimentary organic matter. *Chemical Geology* 114, 289–302.
- Meyers, P.A., Lallier-Vergès, E., 1999. Lacustrine sedimentary organic matter records of late quaternary paleoclimates. *Journal of Paleolimnology* 21, 345–372.
- Meyers, P.A., 2003. Applications of organic geochemistry to paleolimnological reconstructions: A summary of examples from the Laurentian Great Lakes. *Organic Geochemistry* 34, 261–289.
- Milton, D.J., Dube, A., Sengupta, S.S., 1975. Deposition of ejecta at Lonar crater. *Meteoritics* 10, 456–457.

- Misra, V.N., 2001. Prehistoric human colonization of India. *Journal of Biosciences* 26, 491–531.
- Molnar, P., England, P., Martinrod, J., 1993. Mantle dynamics, uplift of the Tibetan Plateau, and the Indian monsoon. *Reviews of Geophysics* 31, 357–396.
- Mooley, D.A., Parthasarathy, B., 1982. Fluctuations in the deficiency of the summer monsoon over India, and their effect on economy. *Archives for Meteorology, Geophysics and Bioclimatology* 30, 383–398.
- Morrill, C., Overpeck, J.T., Cole, J.E., 2003. A synthesis of abrupt changes in the Asian summer monsoon since the last deglaciation. *Holocene* 13, 465–476.
- Moy, C.M., Seltzer, G.O., Rodbell, D.T., Anderson, D.M., 2002. Variability of El Niño/southern oscillation activity at millennial timescales during the Holocene epoch. *Nature* 420, 162–165.
- Nandy, N., Deo, V., 1961. Origin of Lonar Lake and its salinity. *TISCO Technical Journal of the Tata iron and steel company Ltd. India* 8, 1–2.
- Nayar, T.S., 1990. *Pollen Flora of Maharashtra State India*. Today and Tomorrows Publishers, New Delhi, 157 pp.
- Neff, U., Burns, S.J., Mangini, A., Mudelsee, M., Fleitmann, D., Matter, A., 2001. Strong coherence between solar variability and the monsoon in Oman between 9 and 6 ka ago. *Nature* 411, 290–293.
- Newton, A., Thunell, R., Stott, L., 2011. Changes in the Indonesian throughflow during the past 2000 yr. *Geology* 39, 63–66.
- Ourisson, G., Rohmer, M., Poralla, K., 1987. Prokaryotic hopanoids and other polyprenoid sterol surrogates. *Annual Review of Microbiology* 41, 310–333.
- Overpeck, J.T., Anderson, D.M., Trumbore, S., Prell, W.L., 1996. The southwest monsoon over the last 18,000 years. *Climate Dynamics* 12, 213–225.
- Polanski, S., Fallah, B., Befort, D.J., Prasad, S., Cubasch, U., in press. Regional moisture change over India during the past Millennium: A comparison of multi-proxy reconstructions and climate model simulations. *Global and Planetary Change*, doi: 10.1016/j.gloplacha.2014.08.016.
- Ponton, C., Giosan, L., Eglinton, T.I., Fuller, D.Q., Johnson, J.E., Kumar, P., Collett T.S., 2012. Holocene aridification of India. *Geophysical Research Letters* 39, 1–6.
- Possehl, G.L., 1999. *Indus Age: The Beginning*. Oxford and IBH Publishing Company, New Delhi.

- Prahl, F.G., Hayes, J.M., Xie, T-M., 1992. Diploptene: an indicator of terrigenous organic carbon in Washington coastal sediments. *Limnology and Oceanography* 37, 1290–1300.
- Prasad, S., Kusumgar, S., Gupta, S.K., 1997. A mid-late Holocene record of palaeoclimatic changes from Nal Sarovar: a palaeodesert margin lake in western India. *Journal of Quaternary Science* 12, 153–159.
- Prasad, S., Negendank, J.F.W., 2004. Holocene palaeoclimate in the Saharo-Arabian Desert. In: Fischer, H., Kumke, T., Lohmann, G., Flöser, G., Miller, H., von Storch, H., Negendank, J.F.W. (Eds.), *The Climate in Historical Times: Towards a Synthesis of Holocene Proxy Data and Climate Models*. Springer, Berlin, pp. 209–228.
- Prasad, S., Enzel, Y., 2006. Holocene palaeoclimates of India. *Quaternary Research* 66, 442–453.
- Prasad, S., Anoop, A., Riedel, N., Sarkar, S., Menzel, P., Basavaiah, N., Krishnan, R., Fuller, D., Plessen, B., Gaye, B., Röhl, U., Wilkes, H., Sachse, D., Sawant, R., Wiesner, M.G., Stebich, M., 2014. Prolonged monsoon droughts and links to Indo-Pacific warm pool: A Holocene record from Lonar Lake, central India. *Earth and Planetary Sciences Letters* 391, 171–182.
- Prell, W.L., 1984a. Monsoonal climate of the Arabian Sea during the Late Quaternary: a response to changing solar radiation. In: Berger, A. L., Imbrie, J., Hays, J., Kukla, G., Saltzman, B. (Eds.), *Milankovitch and Climate*. D. Riedel, Hingham, pp. 349–366.
- Prell, W.L., 1984b. Variation of monsoonal upwelling: a response to changing solar radiation. In: Hansen, J., T. Takahashi, T. (Eds.), *Climate Processes and Climate Sensitivity*, AGU, pp. 48–57.
- Prell, W.L., Van Campo, E., 1986. Coherent response of Arabian Sea upwelling and pollen transport to late Quaternary monsoonal winds. *Nature* 323, 526–528.
- Prell, W.L., Kutzbach, J.E., 1987. Monsoon variability over the past 150,000 years. *Journal of Geophysical Research* 92 (D7), 8411–8425.
- Prell, W.L., Kutzbach, J.E., 1992. Sensitivity of the Indian monsoon to forcing parameters and implications for its evolution. *Nature* 360, 647–653.
- Prell, W.L., Murray, D.W., Clemens, S.C., Anderson, D.M., 1992. Evolution and variability of the Indian Ocean summer monsoon: evidence from the western Arabian Sea drilling program. In: Duncan, R. A., Rea, D. K., Kidd, R. B., von Rad, U., Weissel, J. K. (Eds.), *The Indian Ocean: A Synthesis of Results from the Ocean Drilling Program*. Geophysical Monograph, American Geophysical Union, Washington, DC, 70, pp. 447–469.

- Prell, W.L., Kutzbach, J.E., 1997. The impact of Tibetan-Himalayan elevation on the sensitivity of the monsoon climate system to changes in solar radiation. In: Ruddiman, W. F. (Ed.), *Tectonic Uplift and Climate Change*. Plenum Press, New York, pp. 171–201.
- Quamar, M.F., Chauhan, M.S., 2012. Late Quaternary vegetation, climate as well as lake-level changes and human occupation from Nitaya area in Hoshangabad District, southwestern Madhya Pradesh (India), based on pollen evidence. *Quaternary International* 263, 104–113.
- Rach, O., Brauer, A., Wilkes, H., Sachse, D., 2014. Delayed hydrological response to Greenland cooling at the onset of the Younger Dryas in western Europe. *Nature Geoscience* 7, 109–112.
- Rajeevan, M., Sridhar, L., 2008. Inter-annual relationship between Atlantic sea surface temperature anomalies and Indian summer monsoon. *Geophysical Research Letters* 35, L21704, pp. 7.
- Rein, B., Lückge, A., Reinhard, L., Sirocko, F., Wolf, A., Dullo, W.C., 2005. El Niño variability of Peru during the last 20,000 years. *Paleoceanography* 20, PA4003, pp. 17.
- Rohmer, M., Bouvier-Nave, P., Ourisson, G., 1984. Distribution of hopanoid triterpenes in prokaryotes. *Journal of General Microbiology* 130, 1137–1150.
- Romero-Viana, L., Kienel, U., Sachse, D., 2012. Lipid biomarker signatures in a hypersaline lake on Isabel Island (Eastern Pacific) as a proxy for past rainfall anomaly (1942–2006 AD). *Palaeogeography, Palaeoclimatology, Palaeoecology* 350, 49–61.
- Rommerskirchen, F., Plader, A., Eglinton, G., Chikaraishi, Y., Rullkötter, J., 2006. Chemotaxonomic significance of distribution and stable carbon isotopic composition of long-chain alkanes and alkan-1-ols in C₄ grass waxes. *Organic Geochemistry* 37, 1303–1332.
- Rosa-Putra, S., Nalin, R., Domenach, A-M., Rohmer, M., 2001. Novel hopanoids from *Frankia* spp. and related soil bacteria Squalene cyclization and significance of geological biomarkers revisited. *European Journal of Biochemistry* 268, 4300–4306.
- Rozanski, K., Araguas-Araguas, L., Gonfiantini, R., 1993. Isotopic patterns in modern global precipitation. In: *Climate Change in Continental Isotopic Record*, Swart, P.K., Lohman, K.L., McKenzie, J.A., Savin, S. (Eds.), *Geophysical Monograph* 78, 1–37.
- Sachs, J.P., 2014. Hydrogen Isotope Signatures in the Lipids of Phytoplankton. In: Holland H.D. and Turekian K.K. (Eds.) *Treatise on Geochemistry*, Second Edition, Oxford: Elsevier, 12, pp. 79–94.

- Sachse, D., Radke, J., Gleixner, G., 2006. δD values of individual *n*-alkanes from terrestrial plants along a climatic gradient - Implications for the sedimentary biomarker record. *Organic Geochemistry* 37, 469–483.
- Sachse, D., Sachs, J.P., 2008. Inverse relationship between D/H fractionation in cyanobacterial lipids and salinity in Christmas Island saline ponds. *Geochimica et Cosmochimica Acta* 72, 793–806.
- Sachse, D., Billault, I., Bowen, G.J., Chikaraishi, Y., Dawson, T.E., Feakins, S.J., Freeman, K.H., Magill, C.R., McInerney, F.A., van der Meer, M.T.J., Polissar, P., Robins, R., Sachs, J.P., Schmidt, H.-L., Sessions, A.L., White, J.W.C., West, J.B., Kahmen, A., 2012. Molecular paleohydrology: interpreting the hydrogen-isotopic composition of lipid biomarkers from photosynthesizing organisms. *Annual Reviews of Earth and Planetary Sciences* 40, 221–249.
- Saji, N.H., Goswami, B.N., Vinayachandran, P.N., Yamagata, T., 1999. A dipole in the tropical Indian Ocean. *Nature* 401, 360–363.
- Sarkar, A., Ramesh, R., Somayajulu, B.L.K., Agnihotri, R., Jull, A.J.T., Burr, G.S., 2000. High resolution Holocene monsoon record from the eastern Arabian Sea. *Earth and Planetary Science Letters* 177, 209–218.
- Sarkar, S., Wilkes, H., Prasad, S., Brauer, A., Riedel, N., Stebich, M., Basavaiah, N., Sachse, D., 2014. Spatial heterogeneity in lipid biomarker distributions in the catchment and sediments of a crater lake in central India. *Organic Geochemistry* 66, 125–136.
- Schefuß, E., Ratmeyer, V., Stuut, J.B.W., Jansen, J.H.F., Sinninghe Damsté, J.S., 2003. Carbon isotope analyses of *n*-alkanes in dust from the lower atmosphere over the central eastern Atlantic. *Geochimica et Cosmochimica Acta* 67, 1757–1767.
- Schelske, C.L., Hodell, D.A., 1991. Recent changes in productivity and climate of Lake Ontario detected by isotope analysis of sediments. *Limnology Oceanography* 36, 961–975.
- Schulz, H., von Rad, U., Erlenkeuser, H., 1998. Correlation between Arabian Sea and Greenland climate oscillations of the past 110,000 years. *Nature* 393, 54–57.
- Schwark, L., Zink, K., Lechterbeck, J., 2002. Reconstruction of postglacial to early Holocene vegetation history in terrestrial Central Europe via cuticular lipid biomarkers and pollen records from lake sediments. *Geology* 30, 463–466.
- Sengupta, D., Bhandari, N., Watanabe, S., 1997. Formation age of Lonar Meteor Crater, India. *Revista de Física Aplicada e Instrumentacao* 12, 1–7.

- Sengupta, S., Sarkar, A., 2006. Stable isotope evidence of dual (Arabian and Bay of Bengal) vapour sources in monsoonal precipitation over north India. *Earth and Planetary Science Letters* 250, 511–521.
- Shukla, J., Mintz, Y., 1982. Influence of land-surface evapotranspiration on the earth's climate. *Science* 215, 1498–1501.
- Singh, G., Joshi, R.D., Chopra, S.K., Singh, A.B., 1974. Late Quaternary history of vegetation and climate of the Rajasthan desert, India. *Philosophical Transactions of the Royal Society of London B* 267, 467–501.
- Sinha, A., Cannariato, K.G., Stott, L.D., Cheng, H., Edwards, R.L., Yadava, M.G., Ramesh, R., Singh, I.B., 2007. A 900-year (600 to 1500 A.D.) record of the Indian summer monsoon precipitation from the core monsoon zone of India. *Geophysical Research Letters* 34, L16707, pp. 5.
- Sinha, A., Stott, L., Berkelhammer, M., Cheng, H., Edwards, R.L., Buckley, B., Aldenderfer, M., Mudelsee, M., 2011. A global context for megadroughts in monsoon Asia during the past millennium. *Quaternary Science Review* 30, 47–62.
- Sinninghe Damsté, J.S., Kenig, F., Koopmans, M.P., Koster, J., Schouten, S., Hayes, J.M., de Leeuw, J.W., 1995. Evidence for gammacerane as an indicator of water column stratification. *Geochimica et Cosmochimica Acta* 59, 1895–1900.
- Sinninghe Damsté, J.S., Verschuren, D., Ossebaar, J., Blokker, J., van Houten, R., van der Meer, M.T.J., Plessen, B., Schouten, S., 2011. A 25,000-year record of climate-induced changes in lowland vegetation of eastern equatorial Africa revealed by the stable carbon-isotopic composition of fossil plant leaf waxes. *Earth and Planetary Science Letters* 302, 236–246.
- Sirocko, F., Sarnthein, M., Erlenkeuser, H., Lange, H., Arnold, M., Duplessy, J.C., 1993. Century scale events in monsoonal climate over the past 24,000 years. *Nature* 364, 322–324.
- Sirocko, F., Garbe-Schönberg, D., McIntyre, A., Molino, B., 1996. Teleconnections between the subtropical monsoons and high latitude climates during the last deglaciation. *Science* 272, 526–529.
- Smith, F.A., Freeman, K.H., 2006. Influence of physiology and climate on δD of leaf wax *n*-alkanes from C_3 and C_4 grasses. *Geochimica et Cosmochimica Acta* 70, 1172–1187.
- Sontakke, N.A., Singh, N., Singh, H.N., 2008. Instrumental period rainfall series of the Indian region (AD 1813–2005): revised reconstruction, update and analysis. *The Holocene* 18, 1055–1066.

- Spötl, C., Vennemann, T.W., 2003. Continuous-flow IRMS analysis of carbonate minerals. *Rapid Communications in Mass Spectrometry* 17, 1004–1006.
- Staubwasser, M., Sirocko, F., Grootes, P., Segl, M., 2003. Climate change at the 4.2 ka BP termination of the Indus valley civilization and Holocene south Asian monsoon variability. *Geophysical Research Letters* 30, 1425, pp. 4.
- Stockmarr, J., 1971. Tablets with spores used in absolute pollen analysis. *Pollen Spores* 13, 615–621.
- Stott, L.K., Cannariato, K., Thunell, R., Haug, G.H., Koutavas, A., Lund, S., 2004. Decline in surface temperature and salinity in the western tropical Pacific Ocean in the Holocene epoch. *Nature* 431, 56–59.
- Stuiver, M., 1975. Climate versus changes in ^{13}C content of the organic component of lake sediments during the late Quaternary. *Quaternary Research* 5, 251–262.
- Stuiver, M., Reimer, P.J., Bard, E., Beck, J.W., Burr, G.S., Hughen, K.A., Kromer, B., McCormac, G., Van Der Plicht, J., Spurk, M., 1998. INTCAL98 radiocarbon age calibration, 24,000–0 cal BP. *Radiocarbon* 40, 1041–1083.
- Surakasi, V.P., Antony, C.P., Sharma, S., Patole, M.S., Shouche, Y.S., 2010. Temporal bacterial diversity and detection of putative methanotrophs in surface mats of Lonar crater lake. *Journal of Basic Microbiology* 50, 465–474.
- Swapna, P., Krishnan, R., Wallace, J.M., in press. Indian Ocean and monsoon coupled interactions in a warming environment. *Climate Dynamics* 42, 2439–2454.
- Swart, P.K., 1983. Carbon and oxygen isotope fractionation in scleractinian corals: a review. *Earth-Science Reviews* 19, 51–80.
- Talbot, M.R., 1990. A review of the palaeohydrological interpretation of carbon and oxygen isotopic ratios in primary lacustrine carbonates. *Chemical Geology: Isotope Geoscience Section* 80, 261–279.
- Talbot, M.R., Laerdal, T., 2000. The Late Pleistocene-Holocene palaeolimnology of Lake Victoria, East Africa, based upon elemental and isotopic analyses of sedimentary organic matter. *Journal of Paleolimnology* 23, 141–164.
- Ten Haven, H.L., Rohmer, M., Rullkotter, J., Bissere, P., 1989. Tetrahymanol, the most likely precursor of gammacerane, occurs ubiquitously in marine sediments. *Geochimica et Cosmochimica Acta* 53, 3073–3079.
- Thiel, V., Jenisch, A., Landmann, G., Reimer, A., Michaelis, W., 1997. Unusual distributions of long-chain alkenones and tetrahymanol from the highly

- alkaline Lake Van, Turkey. *Geochimica et Cosmochimica Acta* 61, 2053–2064.
- Thompson, L.G., Yao, T., Mosley-Thompson, E., Davis, M.E., Henderson, K.A., Lin, P.N., 2000. High-resolution millennial record of the South Asian monsoon from Himalayan ice cores. *Science* 289, 1916–1919.
- Thompson, L.G., Mosley-Thompson, E., Davis, M.E., Henderson, K.A., Brecher, H.H., Zagorodnov, V.S., Mashiotta, T.A., Lin, P.N., Mikhalevko, V.N., Hardy, D.R., Beer, J., 2002. Kilimanjaro ice core records: evidence of Holocene climate change in tropical Africa. *Science* 298, 589–593.
- Tierney, J.E., Russell, J.M., Huang, Y.S., Damste, J.S.S., Hopmans, E.C., Cohen, A.S., 2008. Northern hemisphere controls on tropical southeast African climate during the past 60,000 years. *Science* 322, 252–255.
- Tipple, B.J., Pagani, M., 2010. A 35 Myr North American leaf-wax compound-specific carbon and hydrogen isotope record: implications for C₄ grasslands and hydrologic cycle dynamics. *Earth and Planetary Science Letters* 299, 250–262.
- Tipple, B.J., Pagani, M., 2012. Environmental control on eastern broadleaf forest species' leaf wax distributions and D/H ratios. *Geochimica et Cosmochimica Acta* 111, 64–77.
- Tissot, C., Chikhi, H., Nayar, T.S., 1994. Pollen of wet evergreen forest of the Western Ghats, India. French Institute of Pondicherry, Pondicherry.
- Toth, L.T., Aronson, R.B., Vollmer, S.V., Hobbs, J.W., Urrego, D.H., Cheng, H., Enochs, I.C., Combsch, D.J., van Woesik, R., Macintyre, I.G., 2012. ENSO drove 2500-year collapse of eastern Pacific coral reefs. *Science* 337, 81–84.
- Trauth, M.H., Maslin, M.A., Deino, A., Strecker, M.R., 2005. Late Cenozoic moisture history of East Africa. *Science* 309, 2051–2053.
- Uemura, H., Ishiwatari, R., 1995. Identification of unusual 17 β (H)-moret-22(29)-ene in lake sediments. *Organic Geochemistry* 23, 675–680.
- Ummenhofer, C.C., Sengupta, A., Li, Y., Taschetto, A.S., England, M.H., 2011. Multi-decadal modulation of the El Niño-Indian monsoon relationship by Indian Ocean variability. *Environmental Research Letters* 6, 1–8.
- Vellore, R.K., Krishnan, R., Pendharkar, J., Choudhury, A.D., Sabin, T.P., 2014. On anomalous precipitation enhancement over the Himalayan foothills during monsoon breaks. *Climate Dynamics*, DOI: 10.1007/s00382-013-2024-1.
- Venkatesan, M.I., 1989. Tetrahymanol: Its widespread occurrence and geochemical significance. *Geochimica et Cosmochimica Acta* 53, 3095–3101.

- Venkatesan, M.I., Ruth, E., Kaplan, I.R., 1990. Triterpenols from sediments of Santa Monica Basin, Southern California Bight, U.S.A. *Organic Geochemistry* 16, 1015–1024.
- Vishnu-Mittre, 1975. The archaeobotanical and palynological evidence for the early origin of agriculture in South and Southeast Asia. In: Arnott, M.L. (Ed.), *Gastronomy. The Anthropology of Food and Food Habits*. Mouton Publishers, Paris, The Hague, pp. 13–21.
- Wang, B., An, S., 2002. A mechanism for decadal changes of ENSO behavior: roles of background wind changes. *Climate Dynamics* 18, 475–486.
- Wang, J., Zhu, L., Nishimura, M., Nakamura, T., Ju, J., Xie, M., Takahiro, W., Testsuya, M., 2009. Spatial variability and correlation of environmental proxies during the past 18,000 years among multiple cores from Lake Pumoyum Co, Tibet, China. *Journal of Paleolimnology* 42, 303–315.
- Wang, P., Clemens, S., Beaufort, L., Braconnot, P., Ganssen, G., Jian, Z., Kershaw, P., Sarnthein, M., 2005. Evolution and variability of the Asian monsoon system: state of the art and outstanding issues. *Quaternary Science Reviews* 24, 595–629.
- Wang, Y.J., Cheng, H., Edwards, R.L., An, Z.S., Wu, J.Y., Shen, C.-C., Dorale, J.A., 2001. A high-resolution absolute-dated late Pleistocene monsoon record from Hulu Cave, China. *Science* 294, 2345–2348.
- Wang, Y.J., Cheng, H., Edwards, R.L., He, Y.Q., Kong, X.G., An, Z.S., Wu, J.Y., Kelly, M.J., Dykoski, C.A., Li, X.D., 2005. The Holocene Asian Monsoon: Links to solar changes and North Atlantic climate. *Science* 308, 854–857.
- Wang, Y., Liu, X., Herzsuh, U., 2010. Asynchronous evolution of the Indian and East Asian Summer Monsoon indicated by Holocene moisture patterns in monsoonal central Asia. *Earth-Science Reviews* 103, 135–153.
- Wasson, R.J., Smith, G.I., Agrawal D.P., 1984. Late Quaternary sediments, minerals, and inferred geochemical history of Didwana lake, Thar desert India. *Palaeogeography, Palaeoclimatology, Palaeoecology* 46, 345–372.
- Webster, P.J., Magana, V.O., Palmer, T.N., Shukla, J., Tomas, R.A., Yanai, M., Yasunari, T., 1998. Monsoons: Processes, predictability and prospects for prediction. *Journal of Geophysical Research* 103, 14451–14510.
- Wohlfarth, B., Wichuratree, K., Inthongkaew, S., Fritz, S.C., Blaauw, M., Reimer, P.J., Chabangborn, A., Löwemark, L., Chawchai, S., 2012. Holocene environmental changes in northeast Thailand as reconstructed from a tropical wetland. *Global Planetary Change* 92–93, 148–161.

- Xu, H., Ai, L., Tan, L., An, Z., 2006. Stable isotopes in bulk carbonates and organic matter in recent sediments of Lake Qinghai and their climatic implications. *Chemical Geology* 235, 262–275.
- Xu, Y., Jaffé, R., 2008. Biomarker-based paleo-record of environmental change for an eutrophic, tropical freshwater lake, Lake Valencia, Venezuela. *Journal of Paleolimnology* 40, 179–194.
- Xu, Y., Jaffé, R., 2009. Geochemical record of anthropogenic impacts on Lake Valencia, Venezuela. *Applied Geochemistry* 24, 411–418.
- Yadava, M.G., Ramesh, R., Pant, G.B., 2004. Past monsoon rainfall variations in peninsular India recorded in a 331-year-old speleothem. *Holocene* 14, 517–524.
- Yancheva, G., Nowaczyk, N.R., Mingram, J., Dulski, P., Schettler, G., Negendank, J.F.W., Liu, J., Sigman, D.M., Peterson, L.C., Haug, G.H., 2007. Influence of the intertropical convergence zone on the East Asian monsoon. *Nature* 445, 74–77.
- Zander, J.M., Caspi, E., Pandey, G.N., Mitra, C.R., 1969. The presence of tetrahymanol in *Oleandra wallichii*. *Phytochemistry* 8, 2265–2267.
- Zhang, R., Delworth, T.L., 2006. Impact of Atlantic multidecadal oscillations on India/Sahel rainfall and Atlantic hurricanes. *Geophysical Research Letters* 33, L17712, pp. 1–5.

List of Figures and Tables

Fig. 1.1.	Climatological land surface rainfall for GPCP5 ^a data set (Becker et al., 2013) from 1901-2009 (mm/day; shaded colours) and lower tropospheric wind vectors at 850 hPa for ERA-Interim reanalysis data set (Dee et al., 2011) from 1989-2011 for summer (JJAS ^b) (left) and winter (DJF ^c) (right) monsoon. White circles mark the location of Lonar Lake.	2
Fig. 1.2.	Compilation of Holocene ISM variability from ISM domain. A: Locations of the records, B: Records: a. Jung et al., 2004; b. Gupta et al., 2003; c. Fleitmann et al., 2003; d. Sarkar et al., 2000; e. Prasad and Enzel, 2006; f. Demske et al., 2009; g. Berkelhammer et al., 2012; h. Ponton et al., 2012.	7
Fig. 1.3.	Plot of $\delta^{18}\text{O}$ versus rainfall for Sagar, Madhya Pradesh (modified after Kumar et al., 2010).	11
Fig. 1.4.	Location of Lonar Lake (red circle) in the ‘monsoon zone’ (Gadgil, 2003) marked by the blue dashed line. Envelopes in dark and light blue represent storm-tracks from Bay of Bengal (BoB) in monsoon and post monsoon, respectively; the smaller arrow represents the Arabian Sea (AS) branch (modified after Sengupta and Sarkar, 2006). Modern seawater $\delta^{18}\text{O}$ values are indicated for Arabian Sea and Bay of Bengal (from Kumar et al., 2010).	11
Fig. 1.5.	Four day backwards trajectories for air parcels during selected rainfall events affecting Lonar (asterisk) during the monsoon (ISM, 11.6.13), post monsoon (11.11.10), pre monsoon (19.4.13) and winter monsoon (23.1.13) seasons, calculated using an ensemble (24 members) of the Air Resources Lab Hysplit Program, to represent moisture source for the region.	12
Fig. 2.1.	Schematic workflow used for lipid biomarker and stable isotope analysis.	17
Fig. 3.1.	Location of Lonar Lake; map of Lonar crater lake showing sampling locations of floating mat, benthic mat and surface sediment samples.	23
Fig. 3.2.	(a) Map of Lonar Lake showing crater vegetation belts and ACL (in oblique numbers) in surface sediment samples. (b) Leaf wax <i>n</i> -alkane composition [both concentration of individual <i>n</i> -alkanes and distribution (ACL)] in representative vegetation samples from in trees and grasses (name in green).	25
Fig. 3.3.	Map of Lonar Lake showing distribution of all major biomarkers in lake sediments ($\mu\text{g/g}$ dry sediment).	30
Fig. 3.4.	Long chain <i>n</i> -alkane composition [both concentration of individual <i>n</i> -alkanes and distribution (ACL)] in surface sediment samples.	31
Fig. 3.5.	Comparison of composition of long chain <i>n</i> -alkanes in nearshore samples and samples away from the shore.	31
Fig. 3.6.	Major lipid biomarker composition of floating and benthic mat samples.	32

Fig. 3.7.	Comparison of <i>n</i> -alkane composition [both concentration of total long chain <i>n</i> -alkanes and distribution (ACL)] with box and whisker plots, for (a) vegetation samples (b) surface sediment samples. The plots show upper and lower quartiles (boxes), and whiskers extended to extreme data points. They also show median (horizontal lines) and mean (diamond) and the data points (filled squares).	33
Fig. 4.1.	Location of Lonar crater lake in the ‘monsoon zone’ (Gadgil, 2003) marked by the blue dashed line. Envelopes in dark and light blue represent storm-tracks from Bay of Bengal (BOB) in monsoon and post-monsoon, respectively; the smaller arrow represents the Arabian Sea (AS) branch (modified after Sengupta and Sarkar, 2006). Modern seawater $\delta^{18}\text{O}$ values are indicated for Arabian Sea and Bay of Bengal (from Kumar et al., 2010).	41
Fig. 4.2.	Flux of major biomarkers and their stable isotopic composition ($\delta^{13}\text{C}$, δD) at Lonar Lake during the Holocene, along with other proxies (pollen and Al). a. abundance (%) of pollen from grasses, b. abundance (%) of pollen from aquatic plants, c. flux of leaf wax <i>n</i> -alkanes, d. ACL, e. $\delta^{13}\text{C}$ of long chain <i>n</i> -alkanes, f. δD of long chain <i>n</i> -alkanes and $\delta\text{D}_{\text{wax}}$, g. flux of Al (normal counts); boxes represent zones where evaporites (gaylussite crystals) were found (modified from Prasad et al., 2014), h. flux of <i>n</i> -C ₁₇ , i. $\delta^{13}\text{C}$ and δD of <i>n</i> -C ₁₇ , j. flux of total tetrahymanol (tnol), k. $\delta^{13}\text{C}$ and δD of tetrahymanol (tnol). Unit for fluxes of all biomarkers is $\mu\text{g/g}$ dry sediment/year.	48
Fig. 4.3.	(a) Monthly rainfall and $\delta\text{D}_{\text{rain}}$ variability at Sagar from 2003 to 2005 (left panel) and four day backwards trajectories for air parcels during selected rainfall events affecting Sagar (asterisk) during Monsoon (3 right panels), calculated using an ensemble (24 members) of the Air Resources Lab Hysplit Program, to represent moisture source for the region.	55
Fig. 4.4.	Holocene ISM variability from ISM domain. Locations of the records (inset), records: Current study, Fleitmann et al., 2003, Berkelhammer et al., 2012.	55
Fig. 5.1.	(a) Location of sites discussed in the text-1: $\delta^{18}\text{O}$ from Oman Stalagmite (Fleitmann et al., 2003); 2: Marine core with catchment in Godavari delta (Ponton et al., 2012); 3: Lonar Lake (our study); 4: $\delta^{18}\text{O}$ from Mawmluh cave stalagmite (Berkelhammer et al., 2012); 5: Hyongong peat (Hong et al., 2003). (b) Geology of the Lonar Lake (after Maloof et al., 2009) and position of the core.	60
Fig. 5.2.	(a) Lonar litholog. Two prominent evaporite gaylussite horizons indicate drier conditions. Symbols adjacent to the lithology indicate the position of dated samples: blue circles: terrestrial fragments, yellow circles: bulk organic matter, and brown circles: dated gaylussite. (b) Age model of composite Lonar profile, derived from the P_Sequence depositional model implemented in OxCal 4.1 (Bronk Ramsey, 1999, 2008). The coloured shading represents the 2σ probability range. Individual AMS ^{14}C dates obtained from bulk organic matter, terrestrial fragments, and gaylussite crystal are displayed as calibrated 2σ probability functions. (c) Correlation using marker layers. (d) Evaporitic gaylussite crystal.	62
Fig. 5.3.	Results of multiproxy investigations on the 10 m long Lonar core. In the first column (dotted grey box) are shown the prominent chalcolithic cultural periods (Kayatha, Savalda, Malwa and Jorwe) (Misra, 2001) detected in this region. Arrow with (*) indicates adoption of low rainfall crop patterns, and arrow with (**) indicates decadal scale drought induced famines. The Al (total counts) have been normalised with respect to sedimentation rate.	66

Fig. 5.4.	Simplified pollen diagram for the Lonar Lake sediment sequence. The colours in the far right column have the same implications for climate as in Fig. 5.3. Arrows indicate the major transition points in the catchment vegetation.	68
Fig. 5.5.	Comparison of Holocene reconstructions of the ISM. Location of sites is shown in Fig. 5.1a. The colour bars have the same interpretation as in Fig. 5.3. (a) Oxygen isotope record from Oman (Fleitmann et al., 2003). The light grey bar shows the range of modern stalagmite. (b) Carbon isotope data from biomarkers (C ₂₈) derived from the Godavari catchment (Ponton et al., 2012). (c) Oxygen isotope record from NE India (Berkelhammer et al., 2012). (d) Carbon isotopic composition from Hyongyang peat, eastern Tibet (Hong et al., 2003). (e) ENSO reconstruction from Laguna Pallacocha, Ecuador (Moy et al., 2002). (f) Percentage of sand in a core from El Junco Lake, San Cristobal, Galápagos (Conroy et al., 2008). (g) A 10-year running mean of the relative percentage of lithic sediments in a deep-sea core off the coast of Peru (Rein et al., 2005). (h) The $\Delta^{14}\text{C}$ record from tree rings which largely reflects changes in solar activity (Stuiver et al., 1998). Single point arrows indicate direction of increase/decrease while double pointed arrow indicates no major change.	73
Fig. 5.6.	SST anomalies in the IPWP calculated with respect to averaged SST over last 2 cal ka during PD1 (a), in the less saline interval (D-D) sandwiched between the two PD (b), and PD2 (c). See text for references. Only records covering all the three time slices are shown. Red circles and blue circles indicate warmer and cooler SST anomalies respectively. (For interpretation of the references to colour in this figure legend, the reader is referred to the web version of this article.)	75
Tab. A.1.	Species (if available, indent., not identified), concentration of <i>n</i> -alkanes ($\mu\text{g/g}$ dry leaf) and ACL (C ₂₃ to C ₃₅) of Lonar crater modern vegetation.	79
Tab. A.2.	Mat and water samples with concentration of compounds ($\mu\text{g/g}$ dry mat and $\mu\text{g/l}$ water respectively) from Lonar crater lake.	80
Tab. A.3.	Surface sediment samples with location, concentration of compounds ($\mu\text{g/g}$ dry sediment) and ACL (C ₂₅ to C ₃₅) from Lonar crater lake.	81
Tab. B.1.	Fluxes for aquatic biomarkers in $\mu\text{g/g}$ dry sediment/year.	82

List of Publications

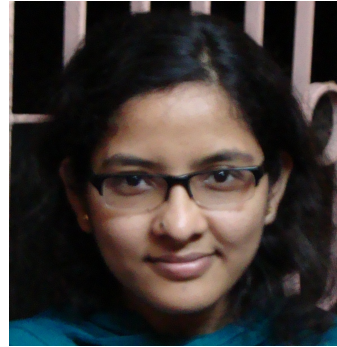
- **Sarkar, S.**, Wilkes, H., Prasad, S., Brauer, A., Riedel, N., Stebich, M., Basavaiah, N., Sachse, D., 2014. Spatial heterogeneity of lipid biomarker distributions in the catchment and sediments of a crater lake in central India. *Organic Geochemistry* 66, 125–136 (own contribution ca. 80%).
 - *Field work and obtaining of samples (Lonar, India: 04/2010 and 02/2011)*
 - *Processing and analyzing of samples in lab (lipid biomarker analysis)*
 - *Data interpretation*
 - *Preparation of manuscript (text, figures and tables)*

- **Sarkar, S.**, Prasad, S., Wilkes, H., Riedel, N., Stebich, M., Basavaiah, N., Sachse, D., 2014. Monsoon source shifts during the drying mid-Holocene: biomarker isotope based evidence from the core ‘monsoon zone’ (CMZ) of India (submitted to *Quaternary Science Reviews*; own contribution: ca. 80%).
 - *Processing and analyzing of samples in lab (lipid biomarker and stable isotope analysis)*
 - *Data interpretation*
 - *Preparation of manuscript (text, figures and table)*

- Prasad, S., Anoop, A., Riedel, N., **Sarkar, S.**, Menzel, P., Basavaiah, N., Krishnan, R., Fuller, D., Plessen, B., Gaye, B., Röhl, U., Wilkes, H., Sachse, D., Sawant, R., Wiesner, B., Stebich, M., 2014. Prolonged monsoon droughts and links to Indo-Pacific warm pool: a Holocene record from Lonar Lake, Central India. *Earth and Planetary Science Letters* 391, 171–182 (own contribution: ca. 30%).
 - *Processing and analyzing of samples in lab*
 - *Partly data interpretation*

CURRICULUM VITAE

Saswati Sarkar



Personal information

Date of birth	19.03.1984
Place of birth	Kolkata, India
Marital status	married
Profession	Geologist (Master of Science)
Contact	Inselhof 7, 14478 Potsdam, Germany
Phone	+ 49 331 88 72 860 + 49 176 31 38 25 42
Email	saswatiitb@gmail.com

Experiences

Professional career

Since 02/2009

PhD student at Institute of Earth and Environmental Sciences, University of Potsdam (supervision: Dr. Dirk Sachse)

PhD Thesis:

“Holocene Variations in the Strength of the Indian Monsoon System: A Combined Biomarker and Stable Isotope Approach”

Member in the DFG Graduate School GRK 1364/1: “Shaping Earth's Surface in a Variable Environment - Interactions between tectonics, climate and biosphere in the African-Asian monsoonal region”, University of Potsdam

Internships

05/2007

UCIL, Turamdih Underground and Banduhurang Opencast (Uranium) Mines, India: Undergone a 20 days training in both underground and opencast uranium mines to study the geological, exploratory and production mining aspects. Detailed study of the mine planning, mining method, geotechnical aspects, processing techniques and also waste disposal and environmental management

Education

University

07/2006 – 06/2008 **Master of Science (two years course) in Applied Geology (CPI: 9.41/10) at Indian Institute of Technology (IIT) Bombay, India**

Master Thesis:

Sarkar, S. (2008): Study of Oligocene Foraminifera from Western Kutch, India.

06/2003 – 06/2006 **Bachelor of Science (three years course) with Honours in Geology (63.62%; First class above 60%) at Presidency College (under the University of Calcutta), India**

School

03/1990 – 03/2002 **Bagbazar Multipurpose Girls High School, Kolkata, India**

Languages

Bengali	first language
English and Hindi	proficient
German	basic level A2 GER

IT Skills

Operating systems	Windows 9x/2000/XP/7, MacOS
Data processing and	
Data visualization	ArcGIS, Matlab, SPSS, Adobe Illustrator CS4 and CS5, GC-MS and GC-IRMS
Office Programs	Microsoft Office, Open Office

Empirical Methods

Field work	Organic geochemical sampling in lake environment
Lab work	Lipid biomarker analysis (extraction, separation and quantification)

Field experiences

04/2010 and 02/2011	Organic geochemical sampling at Lonar crater lake, Maharashtra, India
12/2007	Studying metasedimentary and metabasic rocks of the Delhi Supergroup near Sirohi district Rajasthan and Ambaji, Gujarat, India. Responsible for lithological and structural mapping in the area, study of structural features, petrography, interpretation of structural history and determination of rock mechanic parameters
12/2005	Mapping of underground mine in Pachekhani, Rangpo Sikkim and visit to opencast coal mines of Ramnagar Colliery and coal beneficiation plant, Maithon, West Bengal, India
12/2004	Structural and lithological mapping of regional folds of an area south of Mahagiri Quartzite, Orissa, India

01/2004 Reconnaissance studies on lithology, igneous and primary sedimentary structures in and around Ghatshila, West Bengal, India

Advanced Training and Certificates

02/2011 ECOLMAS Organic Geochemistry Course, Texel, Netherlands
10/2010 Quaternary Paleoclimate course, Free University Berlin, Germany

International Conferences and Workshops (Attended)

01/2013 Indo-German-Workshop, GFZ Potsdam, Germany
07/2011 INQUA, Bern, Switzerland (Poster)
05/2010 EGU, Vienna, Austria (Poster)
08 – 09/2009 Himalaya Field School, Himachal Pradesh, India

Conferences and Workshops (Contribution)

Prasad, S., Anoop, A., Riedel, N., Sarkar, S., Menzel, P., Basavaiah, N., Krishnan, R., Plessen, B., Gaye, B., Röhl, U., Wilkes, H., Sachse, D., Wiesner, M. G., Stebich, M., (2014): ENSO and Indian Megadroughts – was there a fluctuating link during the Holocene? Department of Ecology, French Institute of Pondicherry, 9 May 2014, Pondicherry, India (Lecture)

Sarkar, S., Wilkes, H., Prasad, S., Brauer, A., Basavaiah, N., Strecker, M. R., **Sachse, D.**, (2012): Biomarker evidence for increasing aridity in south-central India over the Holocene. AGU Fall Meeting 2012, 3-7 December, San Francisco, USA (Talk)

Sarkar, S., Wilkes, H., Prasad, S., Brauer, A., Basavaiah, N., Strecker, M. R., **Sachse, D.**, (2012): Biomarker evidence for increasing aridity in central India over the Holocene. International Paleolimnology Symposium 2012, 21-24 August, Glasgow, UK (Poster)

Sarkar, S., Wilkes, H., Prasad, S., Brauer, A., Basavaiah, N., Strecker, M. R., Sachse, D., (2011): Biomarker evidence for increasing aridity in central India over the Holocene. INQUA 2011, 21-27 July, Bern, Switzerland (Poster)

Sarkar, S., Wilkes, H., Prasad, S., Brauer, A., Basavaiah, N., Strecker, M. R., Sachse, D., (2011): Centennial scale fluctuations during the late Holocene transition to aridity at Lonar Lake, central India – evidence from lipid biomarkers and compound-specific carbon isotope analysis. HIMPAC Kick-off-meeting, 27-29 June 2011, Potsdam, Germany (Talk and Poster)

Sarkar, S., Sachse, D., Wilkes, H., Prasad, S., Brauer, A., Strecker, M. R., Basavaiah, N., (2010): Evaluation of the potential of organic geochemical proxies from lake sediments of central India to reconstruct the monsoon variability during Holocene. EGU Spring Meeting 2010, 2-7 May, Vienna, Austria (Poster)

Sarkar, S., Sachse, D., Wilkes, H., Prasad, S., Brauer, A., Strecker, M. R., (2009): Holocene variations in the strength of the SW Indian monsoon system: A combined sedimentological, biomarker and stable isotope approach. Annual Graduate School Workshop “Earth Surface Processes”, 10 July 2009, Potsdam, Germany (Talk)

Teaching Experiences

SS 2013

Seminar “Biogeochemistry”, Institute of Earth and Environmental Sciences, University of Potsdam

Awards

Recipient of the DFG funded PhD scholarship within the Graduate School 1364/1, University of Potsdam

Ranked 1st in the class (M.Sc. Applied Geology, IIT Bombay, India)

Ranked All India 7th in the Graduate Aptitude Test in Engineering for M.Tech in IITs (GATE 2008)

Ranked All India 21st in the Joint Admission Test for M.Sc. in IITs (JAM 2006)

Selbstständigkeitserklärung

Ich erkläre hiermit, dass ich die vorliegende Dissertation selbstständig verfasst habe und versichere darüber hinaus, dass zu dessen Anfertigung nur die angegebenen Quellen und Hilfsmittel verwendet wurden.

Ferner bestätige ich, dass diese Arbeit an keiner anderen Hochschule eingereicht wurde.

Potsdam, 26. August 2014

(Saswati Sarkar)